REPORT DOCUMENTATION PAGE

Form Approved OMB No. 074-0188

1. AGENCY USE ONLY (Leave blank)	2. REPORT DATE ~~1996~~ 2-96	3. REPORT TYPE AND DATES COVERED
		Technical report

4. TITLE AND SUBTITLE

Variablilty of the Arctic Basin Oceanographic Fields

5. FUNDING NUMBERS

N/A

6. AUTHOR(S)

K.D. Sabinin

7. PERFORMING ORGANIZATION NAME(S) AND ADDRESS(ES)

Marine Science Corporation

8. PERFORMING ORGANIZATION REPORT NUMBER

N/A

9. SPONSORING / MONITORING AGENCY NAME(S) AND ADDRESS(ES)

SERDP
901 North Stuart St. Suite 303
Arlington, VA 22203

10. SPONSORING / MONITORING AGENCY REPORT NUMBER

N/A

11. SUPPLEMENTARY NOTES

Paper published by the Marine Science Corporation, Februaury, 1996. This work was supported in part by SERDP.

12a. DISTRIBUTION / AVAILABILITY STATEMENT

Approved for public release: distribution is unlimited

12b. DISTRIBUTION CODE

A

13. ABSTRACT ***(Maximum 200 Words)***

This report is in two parts - an experimental one and a theoretical one. The experimental part, written by K.D. Sabinin and V.T. Sokolov, with assistance from P.N. Golovin, V. Yu. Karpy, and N.V. Lebedev, is devoted to a description of the oceanographic fields in the Arctic Basin and the variability of these fields, in 1973-1979, using data of oceanographic surveys in the High-latitudinal Expeditions "Sever." Special attention was paid to Atlantic Water in the Arctic Ocean which seems to be the main source of information in acoustic monitoring of the ocean, in the framework of the Arctic-ATOC program.

The theoretical part of the report written by A.S. Sarkisyan and N.G. Iakovlev deals with numerical modeling of the present state of the Arctic Ocean thermohaline structure and circulation, as well as with changes in the thermohaline fields which may take place in the ocean after a 100% increase of carbon dioxide levels in the atmosphere.

14. SUBJECT TERMS

SERDP, Arctic Basin, Oceanographic fields, Arctic-ATOC program

15. NUMBER OF PAGES

33

16. PRICE CODE N/A

17. SECURITY CLASSIFICATION OF REPORT	18. SECURITY CLASSIFICATION OF THIS PAGE	19. SECURITY CLASSIFICATION OF ABSTRACT	20. LIMITATION OF ABSTRACT
unclass.	unclass.	unclass.	UL

NSN 7540-01-280-5500

Standard Form 298 (Rev. 2-89)
Prescribed by ANSI Std. Z39-18
298-102

MARINE SCIENCE INTERNATIONAL CORPORATION

VARIABILITY OF THE ARCTIC BASIN OCEANOGRAPHIC FIELDS

K.D. Sabinin

Sabinin, K.D., et al. *"Variability of the Arctic Basin Oceanographic Fields."* Marine Science International Corporation, February 1996.

MARINE SCIENCE INTERNATIONAL CORPORATION

VARIABILITY OF THE ARCTIC BASIN OCEANOGRAPHIC FIELDS

Final Report

INTRODUCTION

This report consists of two parts - an experimental one and a theoretical one. The experimental part, written by K.D. Sabinin and V.T. Sokolov, with assistance from P.N. Golovin, V.Yu. Karpy and N.V. Lebedev, is devoted to a description of the oceanographic fields in the Arctic Basin and the variability of these fields, in 1973-1979, using the data of oceanographic surveys in the High-latitudinal Expeditions "Sever". Special attention was paid to Atlantic Water in the Arctic Ocean which seems to be the main source of information in acoustic monitoring of the ocean, in the framework of the Arctic-ATOC program.

The theoretical part of the report written by A.S. Sarkisyan and N.G. Iakovlev deals with numerical modeling of the present state of the Arctic Ocean thermohaline structure and circulation, as well as with changes in the thermohaline fields which may take place in the ocean after a 100% increase of carbon dioxide levels in the atmosphere (commonly called the "CO2 doubling" scenario).

The Introduction and Conclusion of the report were written by K.D. Sabinin.

PART 1. ANALYSIS OF EXPERIMENTAL DATA ON THE ARCTIC BASIN OCEANOGRAPHIC FIELDS

1. Oceanographic regions of the Arctic Basin.

The main distinguishing feature of the Arctic Basin is the year-round presence of multiyear ice which covers up to 95% of its area in the wintertime. The ice cover has a great influence on the hydrological regime of the Arctic Basin. However, the formation of the spatial structure of the fields of oceanic properties in the Arctic Basin, is largely affected by Atlantic, Pacific and river waters. The zones of interaction between these waters and Arctic water are characterized by increased spatial-temporal variability of the main hydrological and hydrophysical characteristics in the winter season: water temperature, salinity, density and sound velocity.

The principles for division into geographical regions and characterization of vertical profiles of the main hydrological and hydrophysical elements, were outlined in the previous work (14). A description of typical features of the winter hydrological regime of the delineated natural hydrological regions for addressing the objectives of acoustic monitoring in the Arctic Ocean was, also, provided. The present work contains a chart of the natural hydrological regions (see Fig. 1), as well as a List of these regions:

- region 1 - the region of Spitsbergen and Fram strait (S):
- region 2 - the region of the Franz-Josef-Land (FJL);
- region 3 - the region of Severnaya Zemlya (SZ);
- region 4 - the Pole-Siberian region (PS);
- region 5 - the Pole-Canadian region (PC);
- region 6 - the region of the Canadian Abyssal Plain (CP);
- region 7 - the region of the Beaufort Sea (BS).

In considering Fig. 1, special attention should be given to the fact that in the real ocean the boundaries of the natural hydrological regions are not clearly defined. Thus, transient oceanographic structures can, obviously, be observed. As a result, the presented boundaries are to some extent of a conventional character. However, as shown by the variability

analysis below, they are quite reliable in separating regions with different types of vertical oceanographic structures.

2. Variability of the Arctic Basin oceanographic fields in 1973-1979.

The division of the Arctic Basin (AB) into regions, according to the characteristic types of vertical profiles of hydrological and hydrophysical characteristics, and determination of the approximate boundaries of these regions (within the framework of acoustic monitoring studies of the AB), allow a differentiating approach to the analysis of the vertical structure of the characteristics and study of their variability within the regions delineated.

The advantage of the differentiated approach over the integral one is that for a more representative and qualitative analysis of the variability of acoustic characteristics in the water column, in a specific region, it is important not only to know the integral characteristics of temperature and salinity in the natural hydrological layers (mean in the layer), but also to determine the vertical profiles of these characteristics in the natural hydrological layers themselves, and the variability range of temperature, salinity and sound velocity at each of the standard levels. Thus, for purposes of large-scale acoustic tomography of the AB and subsequent reconstruction of specific oceanographic conditions, it is important to know a-priori mean vertical distributions of temperature, salinity and the corresponding mean vertical distribution of the sound velocity in natural hydrological regions, as well as the limits of variability of these characteristics. Mean profiles are also necessary for investigation of the interannual variability of the characteristic vertical profiles of temperature, salinity and sound velocity in any of the hydrological regions, since only by comparing the actual profiles with mean profiles, can the temporary variability be correctly assessed.

Mean profiles for all seven natural hydrological regions of the AB were based on the seven most representative large-scale surveys of the AB in the 1970s (1973-1979) which will be be used as our reference point, in this case. Thus, we selected all oceanographic stations for all of the years that were within the specific natural hydrological region with

conventional boundaries shown in Fig. 1. Then, sound velocities were calculated for each separate oceanographic station at each level based on the actual temperature and salinity values. After that, mean temperature, salinity and sound velocity were determined at each of the standard levels: 5, 10, 25, 50, 75, 100, 150, 200, 250, 300, 400, 500, 750, 1000, 1250, 1500, 2000, 2500, 3000, 3500, 4000, 4500. In addition, simultaneously, maximum and minimum values of these characteristics at all levels which provide some understanding of the extreme variability of the oceanographic and hydrophysical characteristics,were selected for each specific level within the given region. In addition, root-mean-square deviations of temperature, salinity and sound velocity were calculated based on a seven-year sampling for each of the regions at each standard level. They enable us to assess the probability of the extreme variability of these characteristics at each level. Mean profiles of temperature, salinity, sound velocity and their extreme departures at each of the levels are presented for all of the natural hydrological regions in Figs. 2-8. These figures also present T,S -diagrams based on mean temperature and salinity values at each standard level which contain additional information on mean vertical distribution of the water masses within the hydrological region, and the extent of their transformation.

Statistical T,S-diagrams (see Figs.9-15) were also plotted for the regions delineated on the basis of all oceanographic stations within the region over the period 1973 to 1979. They allow estimation of the variability of mean T,S-diagrams and indicate to what extent sampling of stations for the natural hydrological regions identified, is representative. A combined analysis of mean profiles of hydrological and hydrophysical characteristics, their extreme values, mean and statistical T,S-diagrams in each separate hydrological region allows us to reach a sufficiently full understanding of the character, features and range of both the vertical and the horizontal variability of these characteristics.

As is immediately apparent from the analysis, the variability of the sound velocity is affected mainly by the temperature variability (see Figs. 2-8). The largest variability of all the characteristics is observed in the upper layer - up to 500 m (Figs. 2-8). The only exception are regions 4 and 5 (Pole-Siberian and Pole-Canadian) where a significant variability in the near-bottom temperature is observed (Figs.5,6). This is related to the fact that a detailed regioning partition of the near-bottom layer within the Amerasian and Eurasian sub-basins of the Arctic Basin cannot be made such as was done for the surface and deep layers. Bottom water, filling deep-sea zones of the sub-basins, varies little, both in terms of space and

time. Regions 4 and 5 are the transitions from the Eurasian to the Amerasian sub-basin, which are separated by the Lomonosov Ridge. Therefore, during a detailed regioning within the sub-basins, using typical profiles of the hydrological characteristics in the surface and deep layers, stations on different sides of the Lomonosov Ridge where bottom water temperature is known to differ by 0.2-0.32 °C, are assigned to these regions. In connection with this, the variability in temperature (and hence, in the sound velocity) in the near-bottom layer is so large in regions 4 and 5, compared to other regions. (see Fig. 2, 3, 4, 7, 8). This situation is caused by the specifics of regional partitioning, unsuitable for the near-bottom layer in regions 4 and 5, rather than by the actual variability. Thus, for the transition regions 4 and 5, mean profiles will be representative only down to depths of 1000-1500 m (Fig. 5, 6), whereas for the other natural hydrological regions in the Arctic Basin, the background profiles of hydrological and hydrophysical characteristics, as well as mean T,S-diagrams will be representative down to the bottom (Fig. 2, 3, 4, 7, 8).

The largest variability in temperature is observed in the layers of high temperature gradients, primarily related to warm Atlantic Water in the Atlantic sector and to Pacific water in the Pacific sector (Figs. 2-8). In the regions of Spitsbergen, FJL and Severnaya Zemlya (Figs 2, 3 and 4) in the Eurasian sub-basin the largest temperature variability is observed in the layer of the main thermocline and in the Atlantic Water layer (Figs. 2-4). This is also evident in statistical T,S -diagrams (Figs. 9- 11). In the continental slope areas in these regions (for example, in the FJL region - see Fig. 3) the extreme variability of temperature can reach 3 - 3.5 °C (Fig. 3). This is related to the mesoscale outflow processes of cold winter shelf water along the continental slope, where they lie under warm Atlantic Water. These processes make a significant contribution to the large-scale spatial variability of the thermohaline fields in the Eurasian sub-basin.

With spreading in the AB, the temperature of Atlantic Water decreases (see Fig. 2-15). The thickness of the main thermocline is reduced and, hence, the variability of temperature is, also, reduced in the central regions of the Arctic Basin: Pole-Canadian, Pole-Siberian, in the region of the Canadian abyssal plain and in the Beaufort Sea (see Figs. 5-8, 12-15). An interesting feature of the statistical T,S-diagrams in the Pole regions 4 and 5 (see Figs. 12-13) is the manifestation of occasional penetration of Pacific water to these regions. It is well seen that over the whole of the period 1973 to 1977 only at 3-4 stations in the Pole-Siberian region is there a second temperature peak connected with Pacific water, although it is much

more close to the Bering Strait through which the Pacific water flows, than to the Pole-Canadian region where such stations are considerably greater in number (see Fig. 13). This indicates that Pacific water flows into the Pole-Canadian region more frequently, passing through the regions of the Canadian abyssal plain and the Beaufort Sea.

Regions 6 and 7 are characterized by significant variability in the layer of Pacific water. This is reflected in extreme profiles of both temperature and salinity (see Figs. 7 and 8) and, especially, in statistical T,S-diagrams (see Figs. 14, 15). The Beaufort Sea region differs (Fig. 15) from that of the Canadian abyssal plain (Fig. 14) in even larger variability in the surface layer, which is related to the fact that region 7 covers the area of the continental slope of the Beaufort Sea and the area of the flaw polynya, where in wintertime the mesoscale processes connected with intense ice formation and convective mixing occur, and which have a decisive influence on the formation and transformation of thermohaline fields in this region. In addition, the main inflow of Pacific water is observed in the region of the continental slope of the Beaufort Sea, therefore it has the largest variability which is manifested, mainly, in strong vertical temperature anomalies (see Fig. 15). In the Atlantic Water layer in both regions (6 and 7) the variability in temperature and salinity is not large (see Figs. 7, 8, 14, 15). In the near-bottom and the upper quasi-homogeneous layers in all of the natural hydrological regions, the temperature variability is insignificant and does not exceed 0.05-0.07 °C (Figs.2-8).

The variability of salinity, unlike temperature variability, has maximum values in the upper 100-m layer and is related to the halocline (Figs. 2-15). Near Spitsbergen and FJL (regions 1 and 2) where the variability is least, it can excee 1‰, although in other regions it can be even more (Figs.4-8). This is connected with the fact that in the regions of Spitsbergen and FJL surface water is less freshened and most close in salinity to Atlantic Water. However, in these regions and in the boundary areas, separate stations can be sufficiently freshened, which is apparent from the statistical T,S-diagrams (Figs. 9, 10). This is attributed to the penetration of comparatively strongly freshened winter surface water to the areas of Spitsbergen, and FJL, from the Pole regions 4 and 5.

It is known that surface water over much of the AB is strongly freshened. Freshening occurs in the summertime, but is also observed in winter, related to different factors, such as: melting of drifting ice, ice shelves, icebergs and fresh water inflow from rivers. On the

whole, the intensity of the influence of different factors in the AB, resulting in freshening, varies in different regions and is one of the principles for regional division. With depth, the variability of salinity sharply decreases, although in the upper portion of Atlantic Water in the Eurasian sub-basin in the layer of 100-350 m it is still significant reaching 0.1-0.2 ‰ (Figs. 2-6, 9-14). However, in the continental slope region (for example, in the FJL region - Fig. 3) the extreme variability of salinity (as well as of temperature) in the upper portion of the Atlantic Water layer (200-400 m) can be very large and reach 1.0 ‰. As mentioned earlier, this is related to intense mesoscale processes in the continental area. Hence, separate stations can strongly differ both in temperature and salinity in this layer compared to the nearby oceanographic stations occupied in the deep-sea zone of the natural hydrological region. Such an extreme variability in temperature and salinity naturally affects the extreme variability of the sound velocity which is also large in the upper Atlantic Water layer at the continental slope, reaching 15-20 m/s (Fig. 3).

In the Amerasian sub-basin in regions 6 and 7 the variability of salinity in the 150-250 m layer is also sufficiently large (Figs.7-8). It turns out that in the main thermocline associated with Atlantic Water significant salinity variability is also observed, which can be easily seen if mean and statistical T,S-diagrams are analyzed jointly (see Figs. 7, 8, 14, 15). Below 500 m - in the lower portion of the Atlantic Water layer and in the near-bottom layer - the variability of salinity is relatively small everywhere (Figs.2-15).

Maximum variability of the sound velocity is observed in the regions of Spitsbergen and FJL in the main thermocline layer (60-300 m) governed by Atlantic Water (Figs.2, 3) Below, in the Atlantic Water layer down to a depth of 1000 m, the variability in the sound velocity dramatically decreases to 0.1-0.2 m/s (Figs 2, 3). With the spreading of Atlantic Water in the AB, it is cooled, the thickness of the main thermocline decreases, therefore, there is a decrease in the variability of the sound velocity. In the Amerasian sub-basin there is a second peak in the variability of the sound velocity in the 50-100 m layer connected with the thermocline governed by Pacific water, which in the Beaufort Sea even exceeds the peak in the variability of the sound velocity connected with the thermocline governed by Atlantic Water (Fig. 8). Below 1000 m in the regions of Spitsbergen and FJL and below 500 m in other hydrological regions, the variability of the sound velocity is relatively small (Figs. 2-8).

3. Variability of Atlantic Water parameters in the Arctic Basin

3.1 Introduction

Deep Atlantic Water in the Arctic Basin is one of the main climate-forming factors in the Northern Polar Area. It plays a significant role in the formation of the large-scale oceanographic structure of the Arctic Basin and in the heat balance of the Arctic (4, 5, 6, 7, 9). The influence of Atlantic Water on the regime of the Arctic Basin has been investigated by many authors (1-9, 12). There were hypotheses and suggestions that the heat flux from the Atlantic Water leads to a change in the total thickness of the ice cover in the Arctic Basin and also contributes to the formation and maintenance of flaw polynyas which play a significant role in sea/air interaction in winter in the Arctic (4, 5, 9). A significant transformation of Atlantic Water in the region of the continental slope (1) to which flaw polynyas in both the Eurasian and the Amerasian sub-basins are linked, also contributes to it (4).

Nansen found (9), that the source of Atlantic Water inflow to the Arctic Basin through Fram strait is the Spitsbergen current, which is a branch of the Norwegian current. This was confirmed by subsequent full-scale studies - the first oceanographic surveys of the entire Arctic Basin in 1955-1956 and further surveys - in 1973-1979, as well as by many theoretical studies for modeling large-scale circulation in the Arctic Ocean (3, 9, 11, 12, 13).

A more detailed study of the mean fields of the parameters of Atlantic Water and its interannual variability, based on the analysis of the charts of the anomalies of these parameters, appears to be of great interest. This study was possible only after careful processing of data from a series of large-scale oceanographic surveys in the Arctic Basin performed during the period 1973-1979.

3.2 Characteristics of Atlantic water parameters in the Arctic Basin

The main distinguishing feature of Atlantic Water flowing through Fram Strait and spreading over the entire Arctic Basin is the positive temperature, unlike the temperatures of surface and bottom waters. Hence, the depth of the 0 °C isotherm was assumed to be a

natural boundary of this water. Mean winter distribution of the upper and lower boundaries (based on the 0 °C isotherm), the Atlantic layer thickness, the temperature maximum in the Atlantic Water core and the depth of its location in the Arctic Basin over the period 1973 to 1979, as well as the annual distribution of the anomalies of these parameters, are presented in Figs. 16-55.

Atlantic Water (AW) flows into the Arctic Basin in the form of an intermediate layer about 550-750 m thick (Fig. 18). At the entrance to the Arctic Basin through Fram Strait the upper boundary of AW is located at a depth of about 70-100 m (Fig. 16), and the lower - at 800-900 m (Fig.17). As is evident from Fig. 16, 19 and 20, the core of AW is located close to the continental slope of Spitsbergen. Such a circulation pattern in this region is confirmed by diagnostic calculations of currents in the Arctic Basin (3). The maximum temperature in the AW core reaches 2-3 °C in Fram Strait, on average (Fig. 19) and the depth of its temperature maximum - only 180-200 m (Fig. 20).

On spreading into the Arctic Basin, the AW layer deepens under cold and freshened surface Arctic water. Thus, in the vicinity of the Lomonosov Ridge the upper boundary is at a depth of 200-220 m, in the region of the Canadian abyssal plain and in the Beaufort Sea is already at a depth of 250-300 m (Fig. 16). The depth of the lower AW boundary behaves slightly differently. In the vicinity of the Lomonosov Ridge the shallowest AW depth is observed to be 700-750 m., whereas in the Amerasian sub-basin it sinks down to a depth of 900 m and even 1000-1100 m - in the region of the Beaufort Sea (Fig. 17). This distribution of mean depth of the lower AW boundary in the Arctic Basin is, of course, reflected in the distribution of the mean AW thickness (Fig. 18). The minimum thickness of AW is observed in the vicinity of the Lomonosov Ridge (450-500 m), whereas in the Amerasian sub-basin the AW thickness increases up to 600-650 m (Fig. 18). In addition to the fact that AW deepens when spreading in the Arctic Basin, it becomes strongly transformed and this is well seen on the charts of the distribution of the mean temperature maximum in the AW core and its depth (Figs. 19,20). As follows from the analysis of these figures, intense AW transformation occurs in the Eurasian sub-basin in the region of the Nansen abyssal plain and the continental slope of Spitsbergen, Franz-Josef-Land and Severnaya Zemlya, where the temperature in the core dramatically drops from 2.0-2.5 °C to 0.8 °C and its depth sharply increases from 260 m to 380-400 m. With further spreading of AW from the Eurasian to the Amerasian sub-basin, its transformation is not large - the maximum temperature of AW

slowly decreases. In the vicinity of the Lomonosov Ridge it drops to 0.7 °C, in the region of the Canadian abyssal plain and the Beaufort Sea it drops to 0.4-0.5 °C (Fig. 19). The depth of the temperature maximum in the AW core also slowly increases to 420-440 m in the vicinity of the Lomonosov Ridge, reaching a depth of 500 m in the Amerasian sub-basin (Fig. 20).

The distribution of mean parameters of AW in the Arctic Basin confirms, on the whole, the winter pattern of mean AW layer currents obtained from diagnostic calculations of the circulation in the Arctic Ocean based on numerical modeling in (3, 12, 13). According to this pattern, two interrelated circulations develop in the Eurasian sub-basin: a cyclonic one with its center in Fram Strait and an anticyclonic one (from updated calculations /3, 12/) with its center in the vicinity of the Lomonosov Ridge. The cyclonic circulation is most intense where the AW enters the Arctic Basin along the continental slope of Spitsbergen and FJL (here, the largest AW transformation takes place (see Fig. 19, 20), and the anticyclonic circulation responsible for the AW transport from the Eurasian to the Amerasian sub-basin is much less pronounced (the AW transformation strongly attenuates (see Fig. 19, 20) (3, 12). According to some estimates, there is one anticyclonic circulation in the AW column (13) in the Amerasian sub-basin, which is in agreement with the mean multiyear distribution of the AW parameters obtained in this study; whereas, according to other calculations (3, 12), no common circulation pattern in the AW layer in the wintertime in this region has been obtained.

In the analysis of the distribution of the mean AW parameters in the Arctic Basin, special attention should be paid to the areas of the continental slope in all regions of the Arctic Basin. All AW parameters experience significant changes in these areas (see Figs. 17-20). Thus, the lower AW boundary, for example, in the region of the continental slope of the FJL and the Chukchi Rise, can vary from 800 m to 200-300 m (Fig. 17), and the AW thickness decreases from 600-700 m to 50-200 m (Fig. 18). Sometimes there is observed a complete disappearance of AW in some regions of the continental slope. As a result, the maximum temperature of AW decreases in the continental slope regions from 0.5 °C to 0.1-0.2 °C in the region of the Chukchi Rise and from 1.7-2.0 °C to 0.7-1.0 °C in the region of Severnaya Zemlya and FJL (see Fig. 19) and its depth decreases, as a rule, from 480 m to 200 m in the region of the Chukchi Rise and from 260 m to 160 in the region of Severnaya Zemlya and FJL (see Fig. 20).

However, study of the AW transformation in the area of the continental slope of the Laptev Sea in the vicinity of Severnaya Zemlya based on data of smaller-scale observations (mesoscale oceanographic polygons) shows that AW in the continental slope area can not only rise, but sink as well (1). This depends on the steepness of the continental slope. It was noted that in the region of a comparatively more gentle slope, the upper AW boundary and the depth of the AW temperature maximum rises (AW "creeps" to the slope), whereas in the region of a steeper continental slope, it is vice versa, a deepening of the upper AW boundary and the depth of the AW core are observed. It is connected with a strong interaction between AW and ambient water when spreading along the continental slope (1). The transformation of AW is manifested in an intense heat redistribution in the water column both below the AW layer and above it, and in the presence of the enhanced fine structure at the continental slope.

The continental slope is a dynamically active zone. Hence, the intense AW transformation in the slope area is caused by various dynamical processes, one of them being intrusions of cold and dense winter shelf water (1). Another cause is an intensification of the AW flow at the slope /3, 12/. In this case, the topography of the continental slope may promote a local hydrodynamical instability of the mean motion which contributes to more intense vertical mixing and transformation of AW.

3.3 Variability of Atlantic water parameters in the Arctic Basin over the period 1973-1979

Let us consider the distributions of anomalies of the upper AW boundary in the Arctic Basin presented in Figs.21-27. The following tendency is apparent in the analysis of these figures: in 1973-1975 (Figs.21-23) the upper AW boundary throughout much of the Arctic Basin is 5-10 m higher than the multiyear mean, although in 1973 and in 1974 in some small regions (the Mendeleyev Ridge, the Nansen abyssal plain) there are local anomalies where the upper AW boundary is 10-20 m lower than the multiyear mean. In 1976 (Fig. 24) it is close to the multiyear mean. In 1977-1979 (Figs.25-27), the upper AW boundary is observed to be 5-10 m lower over much of the Arctic Basin and in some local regions - 15-20 m (the Mendeleyev Ridge, Figs. 25-27). Here again, special attention should be paid to the continental slope areas both in the Eurasian and Amerasian sub-basins. The largest

spatial variability of all mean multiyear parameters of AW (Fig. 16-20), including the upper AW boundary, is observed in these regions (Fig. 16). Hence, the largest anomalies of the upper AW boundary, reaching sometimes -50 to +50 m, are observed in the continental slope regions (see Figs.21-27). It was not possible to reveal any regular pattern regarding the interannual variability in the location and change of the sign of the anomalies in the upper AW boundary in these regions.

The lower AW boundary was determined by means of linear interpolation when the difference in the depth between standard levels was reaching 100-250 m, making the accuracy of its determination not more than +/-50 m. In this connection, the analysis of the distribution of the anomalies of the lower AW boundary over much of the Arctic Basin (especially in its central part) (see Figs 28-34) has not revealed any serious departures from the multiyear mean, except in some local regions: for example, in the region of the Lomonosov Ridge where a mean multiyear rise in the lower AW boundary (see Fig.17) is observed. Throughout much of the Arctic Basin the anomalies of the lower AW boundary are only +50 m... - 50 m. Hence, it was impossible to establish any typical features in the interannual variability of the lower AW boundary. The largest anomalies in the position of the lower AW boundary, as well as of the upper one - are located in the continental slope area (see Figs.28-34). As mentioned, this is governed by the increased AW transformation in the continental slope region. The value of the rise and fall in the lower AW boundary relative to the multiyear mean, can be +300 to -300 m. In some areas of the continental slope rises and falls in the lower and upper AW boundaries were observed in one and the same year. For example, in the region of the Chukchi Rise in 1973, 1975, 1977 and 1979 (see Figs. 28, 30, 32, 34) or in the region of Severnaya Zemlya in 1973 and 1976 (see Figs.28,31). Different deformation of the upper and lower AW boundaries in the region of the continental slope is related (as suggested earlier) to: the different steepness of the slope, the local topographic features of the continental slope and the intensity of the different dynamical processes in the slope area.

Although the mean multiyear distribution of the AW thickness (Fig. 18) in the Arctic Basin repeats to a greater extent, the mean multiyear distribution of the AW lower boundary (Fig. 17), still the tendency of the interannual variability of the distribution of the anomalies in the AW thickness over 1973 to 1979 (see Figs.35-41) is more like that of the distribution of the anomalies of the AW upper boundary (see Figs.21-27). Thus, in 1973-1975 (see

Figs.35-37) a small (~ 50 m) increase in the AW thickness, as well as the rise in the upper AW boundary was observed over much of the Arctic Basin (see Figs.21-23). In 1976 and 1977 (see Figs.38, 39) it is close to the multiyear mean, probably, except in the Nansen abyssal plain, where the AW thickness was still 50-100 m in excess of the multiyear mean. The year 1978 greatly differs from the preceding years (see Fig.40), in that a significant decrease of 100-150 m in the AW thickness is observed over much of the Arctic Basin, and in the Nansen abyssal plain the AW thickness was even 250-400 m less than the multiyear mean. However, already in 1979, the AW thickness is close to the multiyear mean or slightly greater (see Fig. 41). In the areas of the continental slope, as in the case of the lower AW boundary, the largest AW thickness anomalies are observed. The sign of the anomaly of the AW thickness is governed by the sign of the anomaly of the lower AW boundary (see Figs.28-34 and Figs.35-41).

In addition to thickness, the interannual thermal variability of AW in the Arctic Basin is characterized by the maximum temperature in the AW core. The largest variability of the AW maximum temperature is observed in the Nansen abyssal plain (see Figs.49-55). This is related to the fact that the most intense transformation of AW occurs in this region as it penetrates the Arctic Basin, as is seen from mean distribution of the maximum temperature of AW (Fig. 19). The value of the maximum temperature anomalies in the Nansen abyssal plain can reach +0.3.. -0.3 °C, whereas in the remainder of the Arctic Basin they do not exceed +0.05 ...-0.05 °C (see Figs.49-55). It seems possible to predict the thermal state of AW and correctly assess the interannual variability of this state, if the anomalies of the AW temperature maximum are analyzed only in the region of Fram Strait and the Nansen abyssal plain. According to some estimates, AW reaches the Canadian abyssal plain in 6 years (8) but from recent, updated estimates this value is 3-4 times greater, 20-25 years /2/. According to the same estimates, AW can reach the central Arctic Basin in only 10-15 years.

Thus, from the above considerations, let us trace the interannual variability of the temperature maximum in the AW core, in the wintertime, in the Nansen abyssal plain. An analysis of Figs.49-55 indicates that there is a two-year cycle in the variability of the anomaly sign of the AW maximum temperature in this region. In 1973 (see Fig. 49) the AW temperature was slightly less than the multiyear mean, while in the following year - above it (see Fig. 50), and so on. In 1976 (see Fig. 52), as in 1977 (see Fig. 53) an increase of 0.15-

0.30 °C in the maximum temperature of AW is observed (especially in the region of Fram strait and Spitsbergen). Then, in 1978 (see Fig. 54) and in 1979 (see Fig. 55) the two-year cycle in the change of the sign of the anomaly of the AW maximum temperature, in the Nansen abyssal plain, is renewed. This analysis suggests that it was not possible to detect a tendency for warming or cooling of AW in the Arctic Basin for estimating climatic variability over such a short time interval (1973-1979).

REFERENCES

1. Golovin P.N. Features of the genesis and transformation of water masses on the continental slope. - Proc. of the AARI, 1993, vol.429, pp.68-75.

2. Dmitriyev N.Ye., Polyakov I.V. On the interlayer of Atlantic Water in the Arctic basin. 1. The Geographical characteristics. - Meteorologiia i Gidrologiia, 1995, No.8, pp.37-42.

3. Dmitriyev N.Ye., Polyakov I.V. On the interlayer of Atlantic Water in the Arctic basin. 2. Circulation. - Meteorologiia i Gidrologiia, 1995, No.9, pp.92-101.

4. Zubov N.N. Ice of the Arctic. - M., Glavsevmorput' Publishers, 1945, 360 p.

5. Nikiforov Ye.G., Shpaikher A.O. Typical features of the formation of large-scale variations of the hydrological regime of the Arctic Ocean. - L., Gidrometeoizdat, 1980, 272 p.

6. Panov V.V., Shpaikher A.O. On the influence of Atlantic Water on some features of the hydrological regime of the Arctic Basin and adjacent seas. - Okeanologiia, 1963, v.iii, No.4, pp.579-590.

7. Panov V.V., Shpaikher A.O. The role of Atlantic Water in the formation of the hydrometeorological regime of the Arctic Seas. - Proc. of the AARI, 1963, v.264, pp.10-14.

8. Timofeyev V.T. Water masses of the Arctic Basin. - M., Gidrometeoizdat, 1960, 190 p.

9. Treshnikov A.F., Baranov G.I. Structure and water circulation of the Arctic Basin. - L., Gidrometeoizdat, 160 p.

10. Isaaks E.H., Srivastava R.M. Applied Geostatistics. - New York: Oxford University Press, 1989, 561 pp.

11. Newton J. L. And Coachman L. K. Atlantic Water Circulation in the Canada Basin. - Arctic, J. of the Arctic Institute of North America, 1974,. 27, No. 4, pp. 297- 303.

12. Polyakov I. V. Baroclinic and barotropic factors in the formation of the Arctic Ocean circulation. - Polar Research.

13. Semtner A. Numerical simulation of the Arctic Ocean circulation. - J. Physical Oceanography, 1976, vol. 6, No. 4, pp. 409 - 425.

14. Sokolov V.T. Subdivision into types and regions, of hydrological water structures in the Arctic Basin. - In: "Climatic variability of the Arctic Ocean", MSIC Techn. Report 1995, pp. 32 - 36.

MARINE SCIENCE INTERNATIONAL CORPORATION

VARIABILITY OF THE ARCTIC BASIN OCEANOGRAPHIC FIELDS

K.D. Sabinin

FIGURES
PART 1

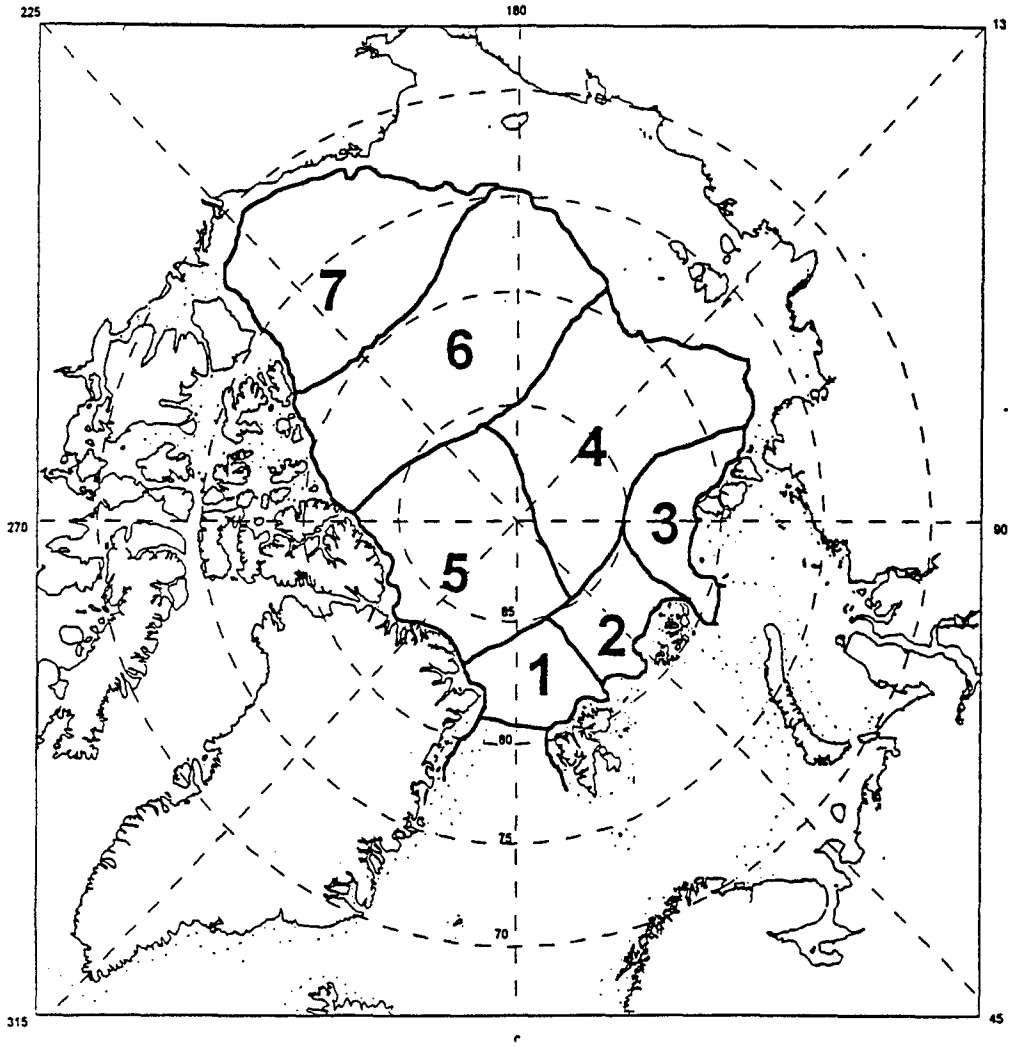

Fig. 1. Natural hydrological regions of the Arctic Basin.

1- region 1 - the region of Spitsbergen and Fram strait (S):

2 - region 2 - the region of the Franz-Josef-Land (FJL);

3 - region 3 - the region of Severnaya Zemlya (SZ);

4 - region 4 - the Pole-Siberian region (PS);

5 - region 5 - the Pole-Canadian region (PC);

6 - region 6 - the region of the Canadian Abyssal Plain (CP);

7 - region 7 - the region of the Beaufort Sea (BS).

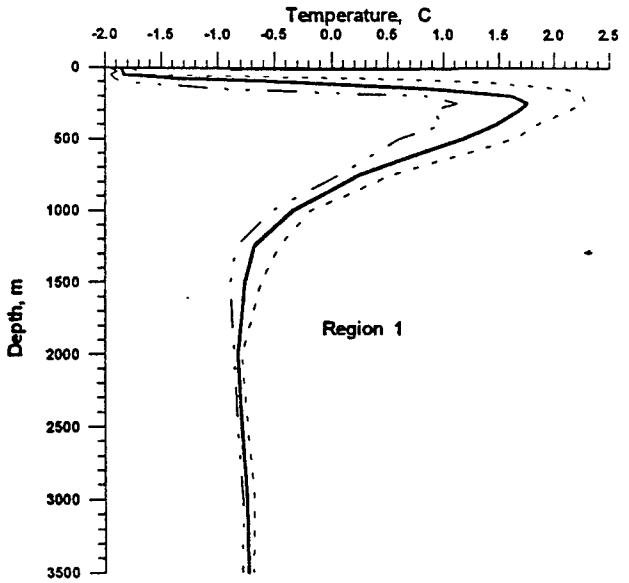

a

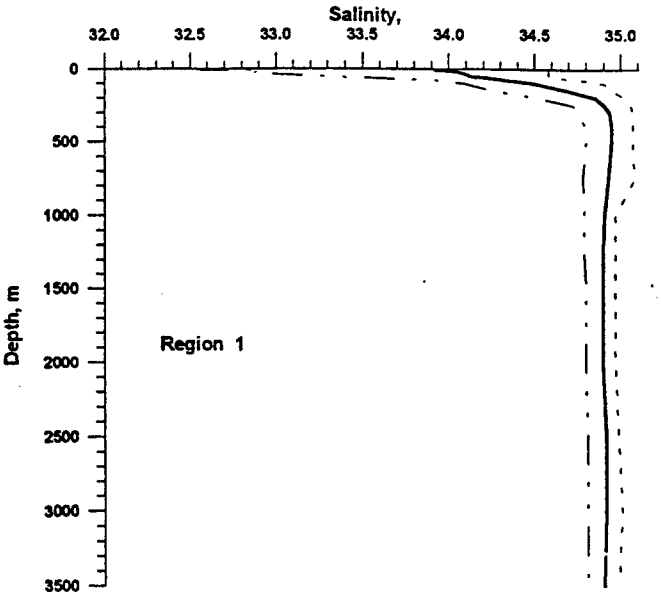

b

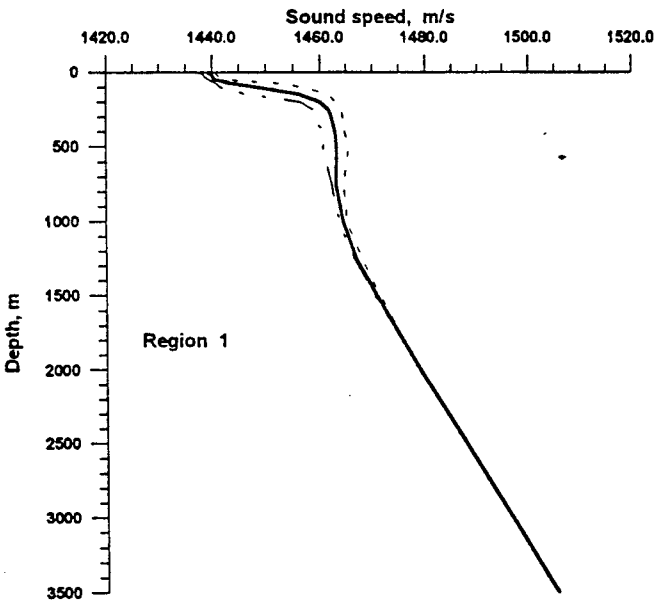

c

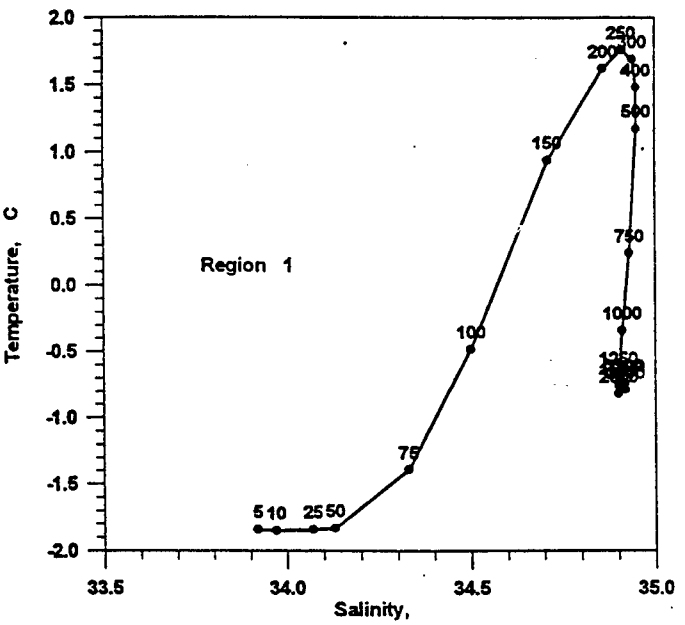

d

Fig. 2. Mean (——) and extreme (maximum ····· , minimum -----) curves for winter values (over the period 1973 - 1979) for region 1:
a - temperature, °C ;
b - salinity, ‰ ;
c - sound velocity, m/s ;
d - T,S - diagram

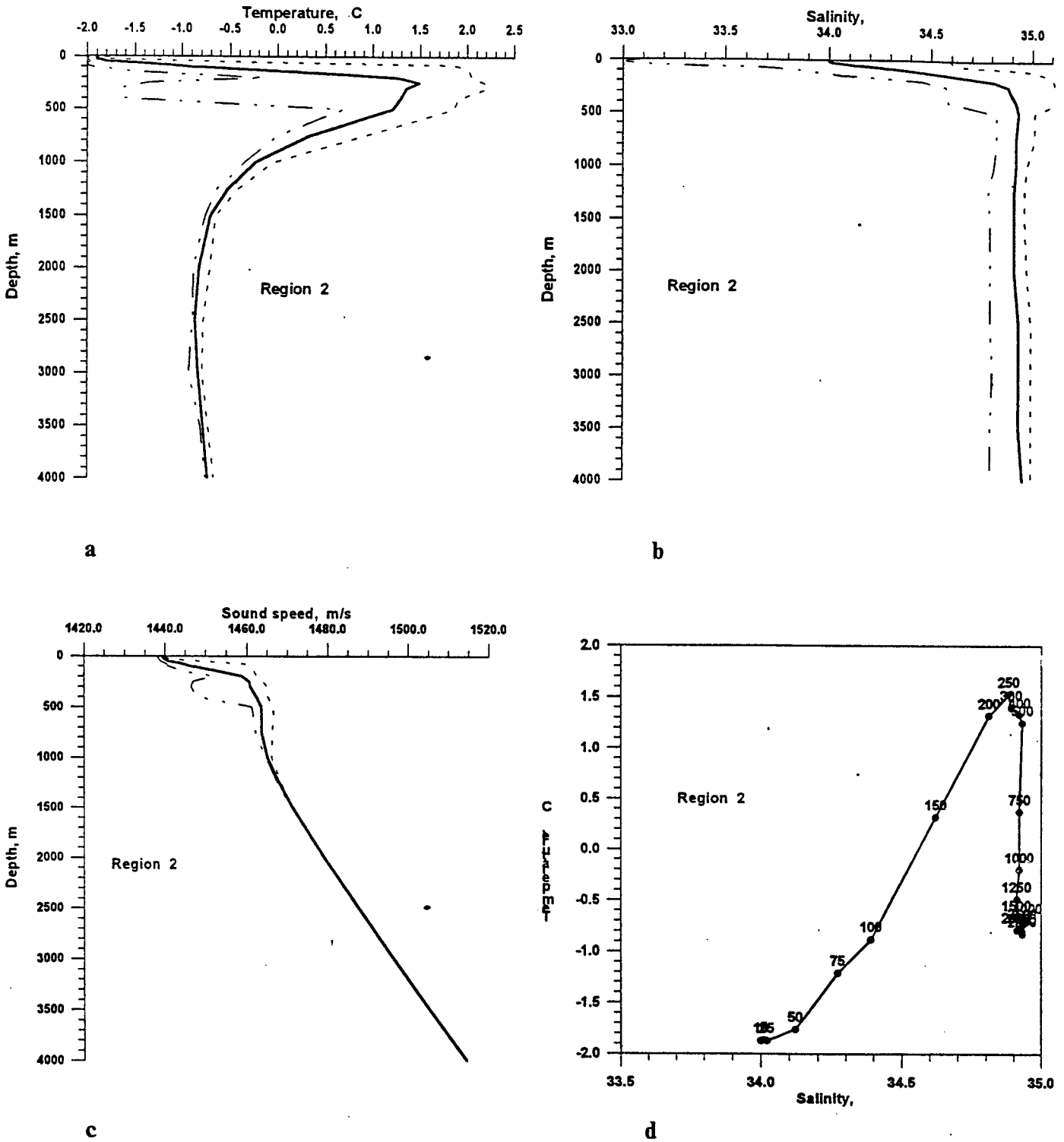

Fig. 3. Mean (——) and extreme (maximum ····· , minimum -----) curves for winter values (over the period 1973 - 1979) for region 2:
a - temperature, °C ;
b - salinity, ‰ ;
c - sound velocity, m/s ;
d - T,S - diagram

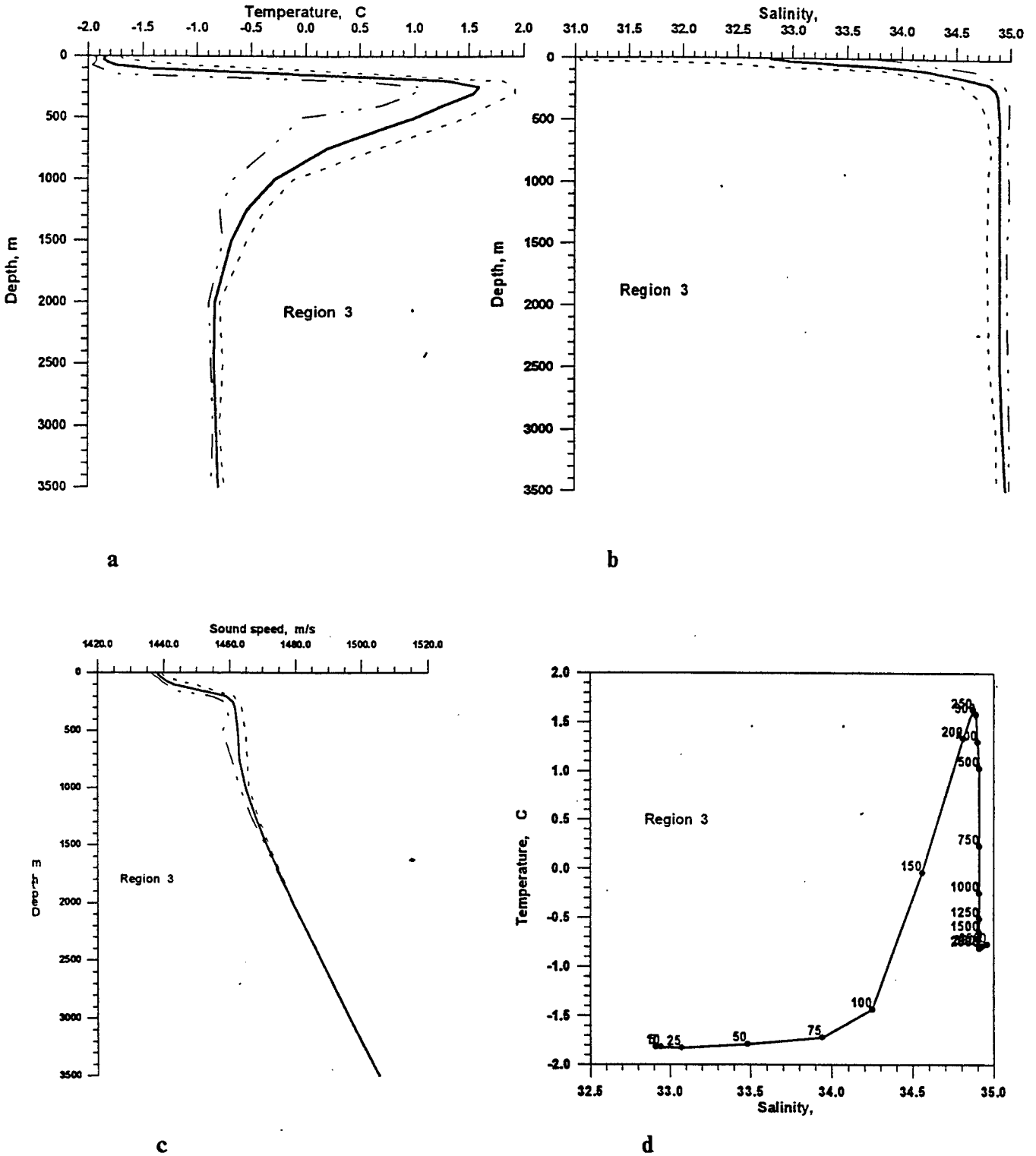

Fig. 4. Mean (——) and extreme (maximum ····· , minimum ------) curves for winter values (over the period 1973 - 1979) for region 3:
a - temperature, °C ;
b - salinity, ‰ ;
c - sound velocity, m/s ;
d - T,S - diagram

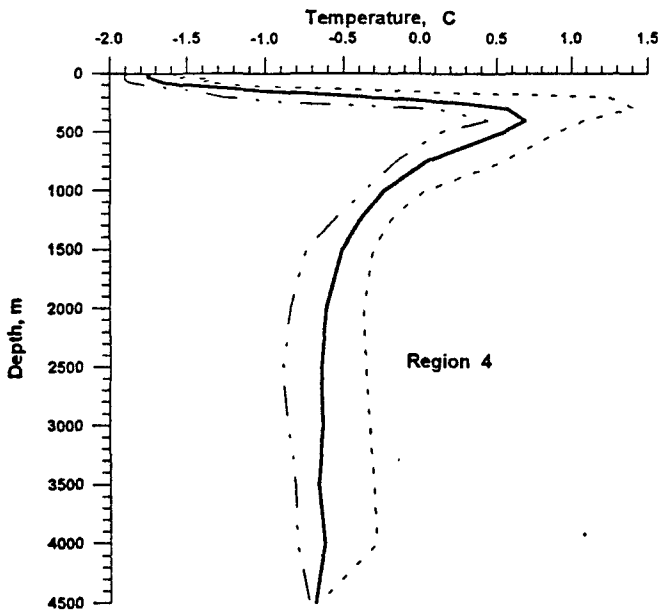

a

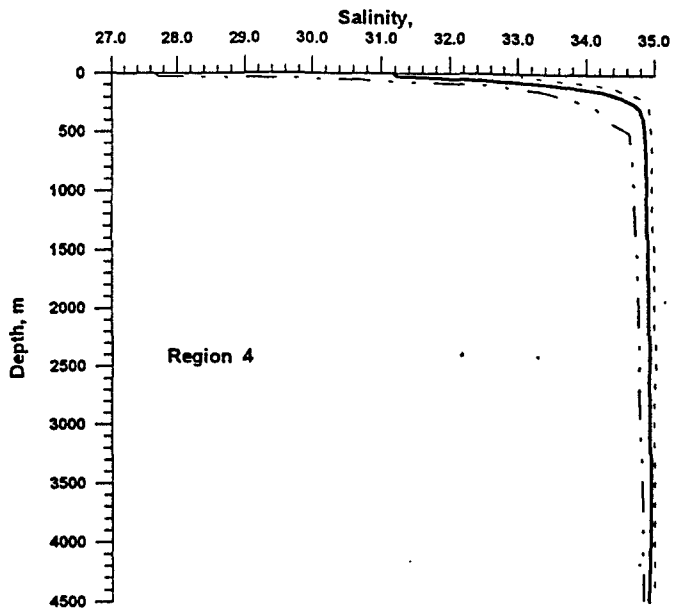

b

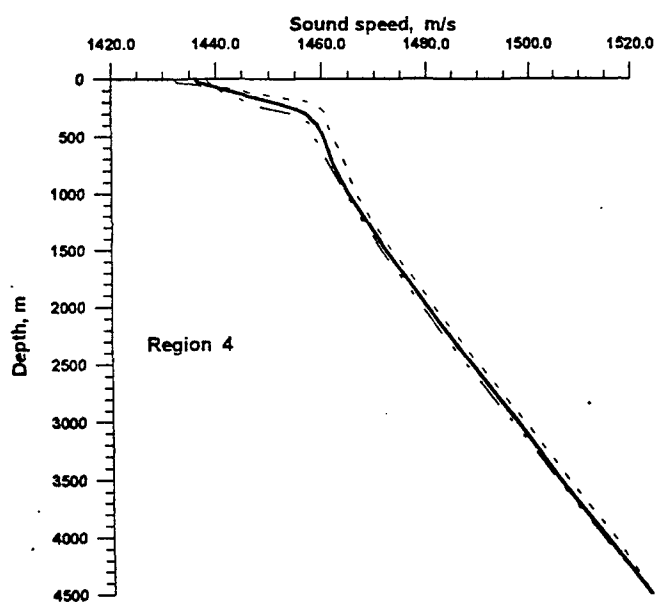

c

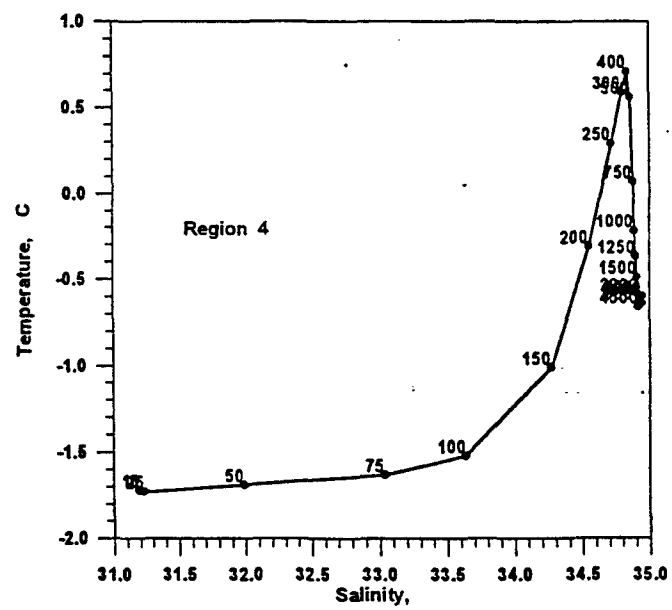

d

Fig. 5. Mean (——) and extreme (maximum ····· , minimum ------) curves for winter values (over the period 1973 - 1979) for region 4:
a - temperature, °C ;
b - salinity, ‰ ;
c - sound velocity, m/s ;
d - T,S - diagram

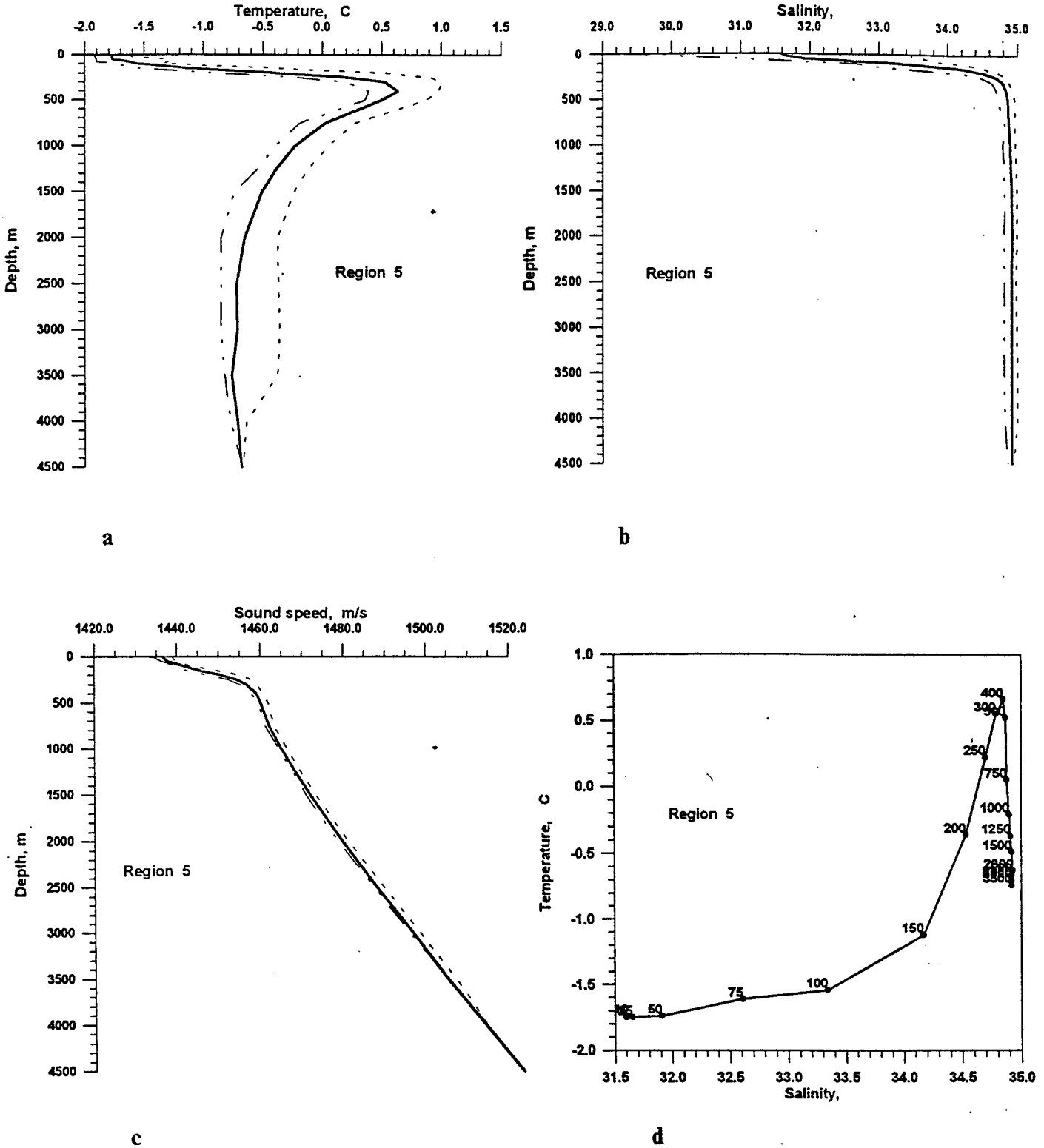

Fig. 6. Mean (——) and extreme (maximum ····· , minimum ------) curves for winter values (over the period 1973 - 1979) for region 5:
a - temperature, °C ;
b - salinity, ‰ ;
c - sound velocity, m/s ;
d - T,S - diagram

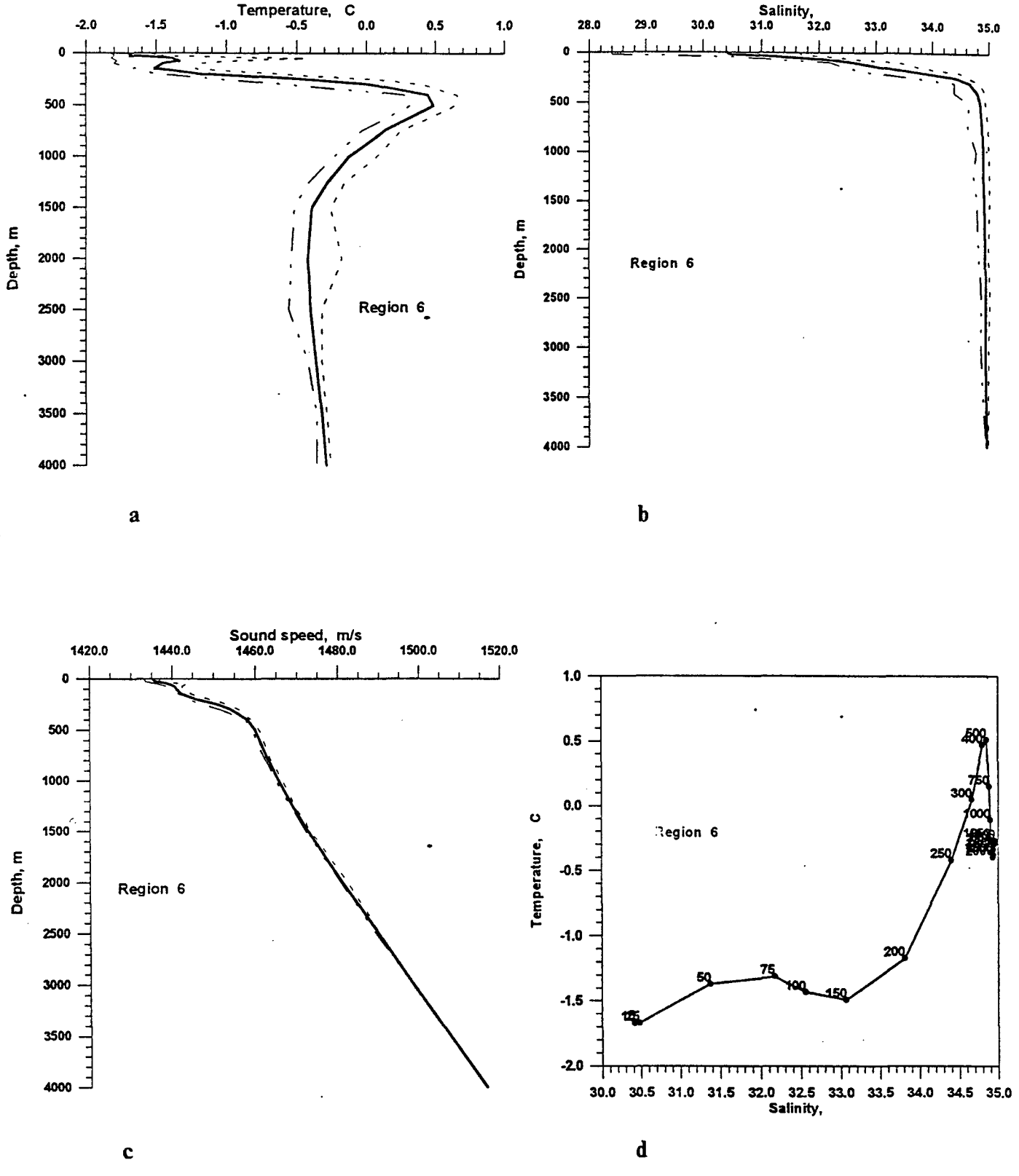

Fig. 7. Mean (——) and extreme (maximum ····· , minimum ------) curves for winter values (over the period 1973 - 1979) for region 6:
a - temperature, °C ;
b - salinity, ‰ ;
c - sound velocity, m/s ;
d - T,S - diagram

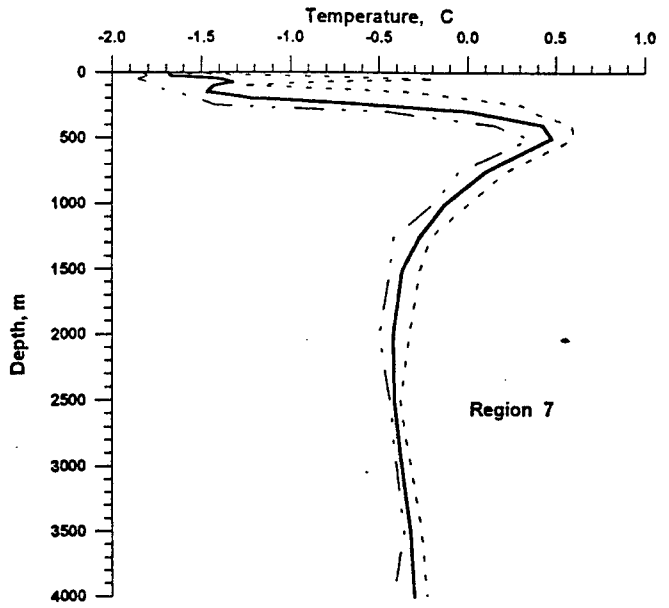

a

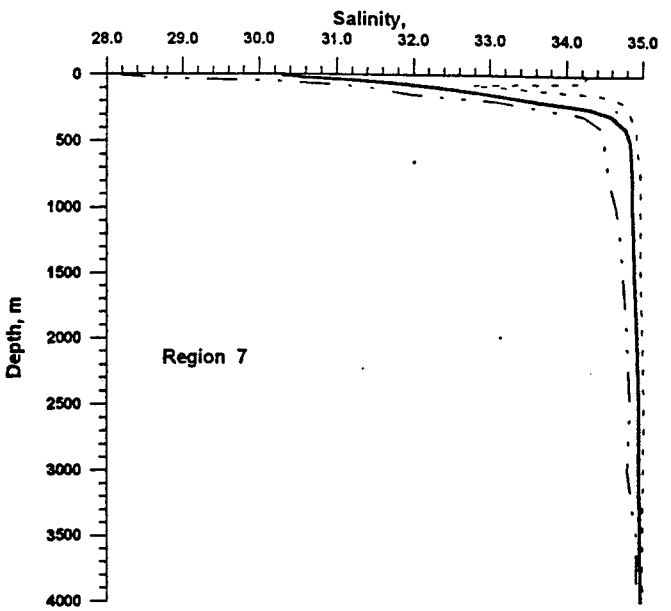

b

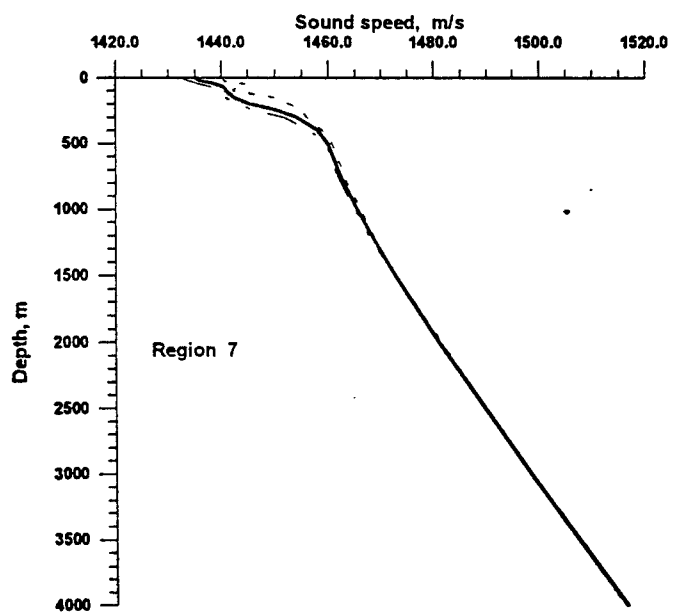

c

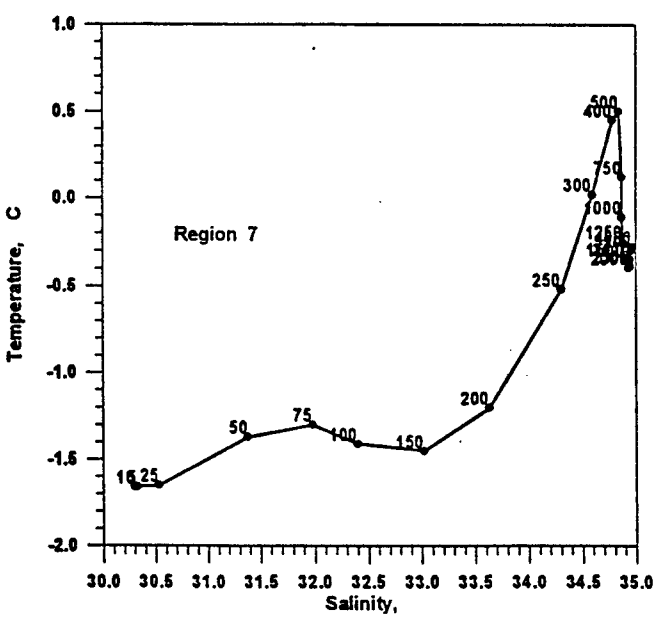

d

Fig. 8. Mean (——) and extreme (maximum ····· , minimum - - - - -) curves for winter values (over the period 1973 - 1979) for region 7:
a - temperature, °C ;
b - salinity, ‰ ;
c - sound velocity, m/s ;
d - T,S - diagram

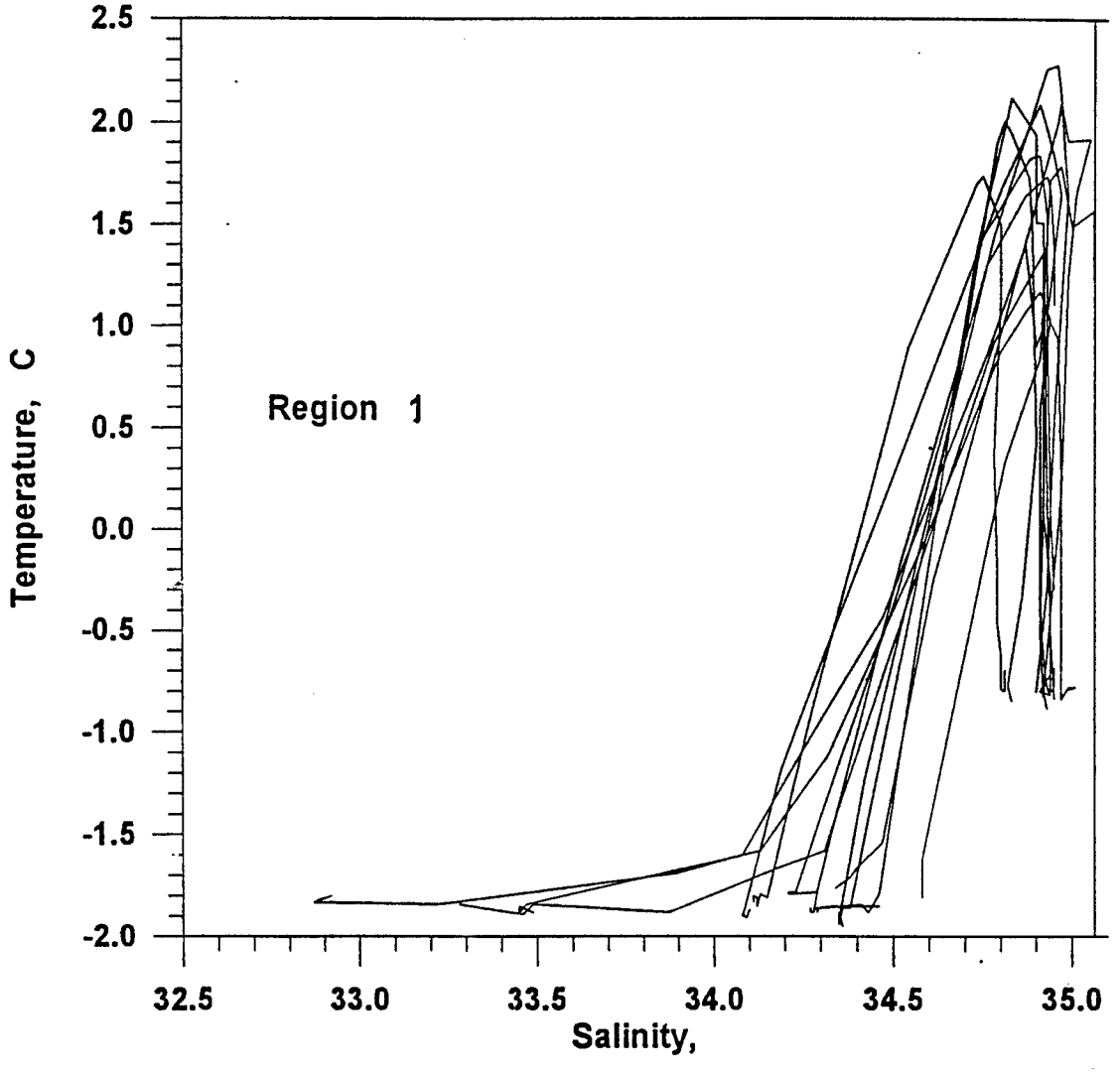

Fig. 9. Statistical T,S - diagram for region 1 (over the period 1973 - 1979).

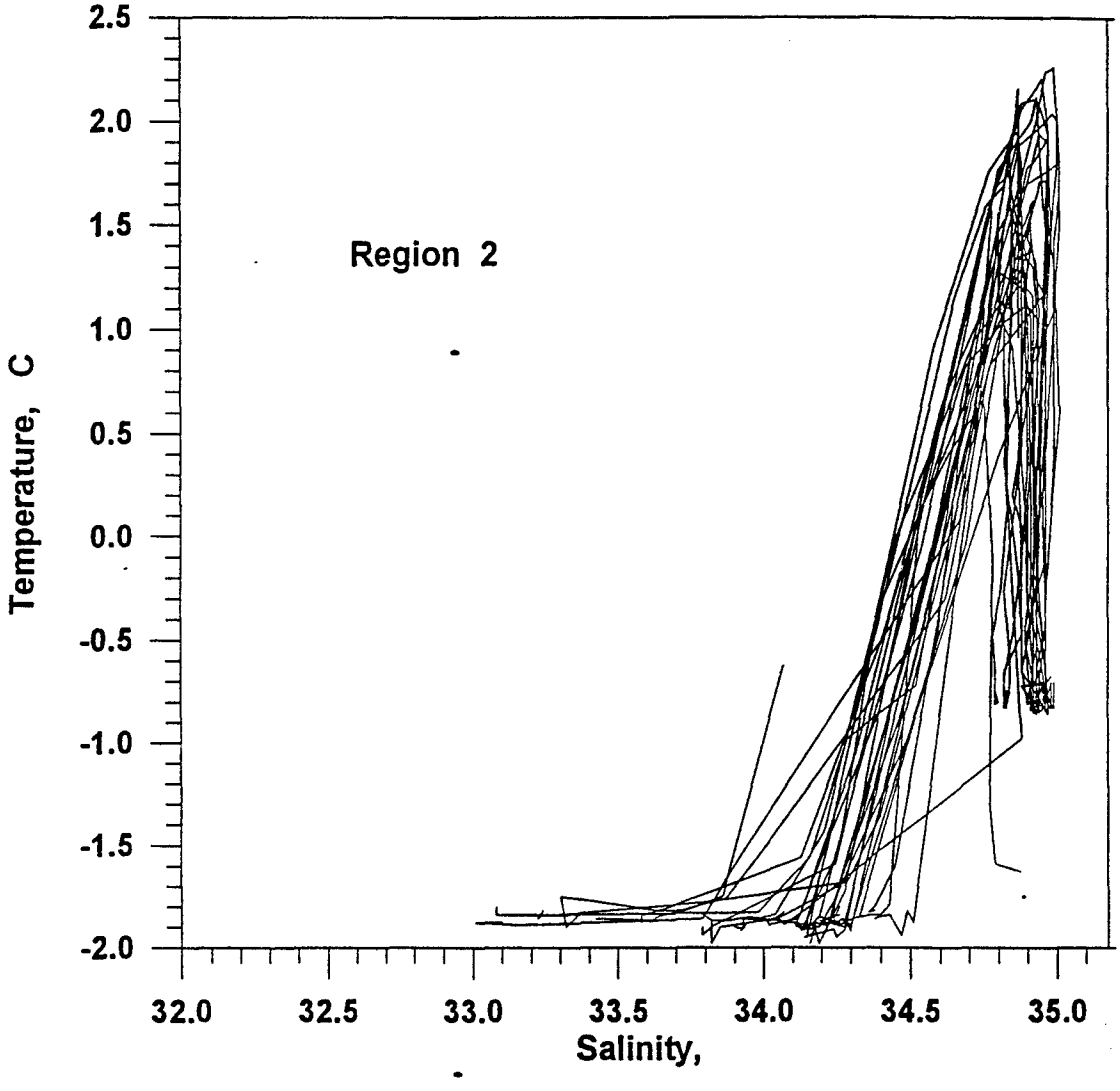

Fig. 10. Statistical T,S - diagram for region 2 (over the period 1973 - 1979).

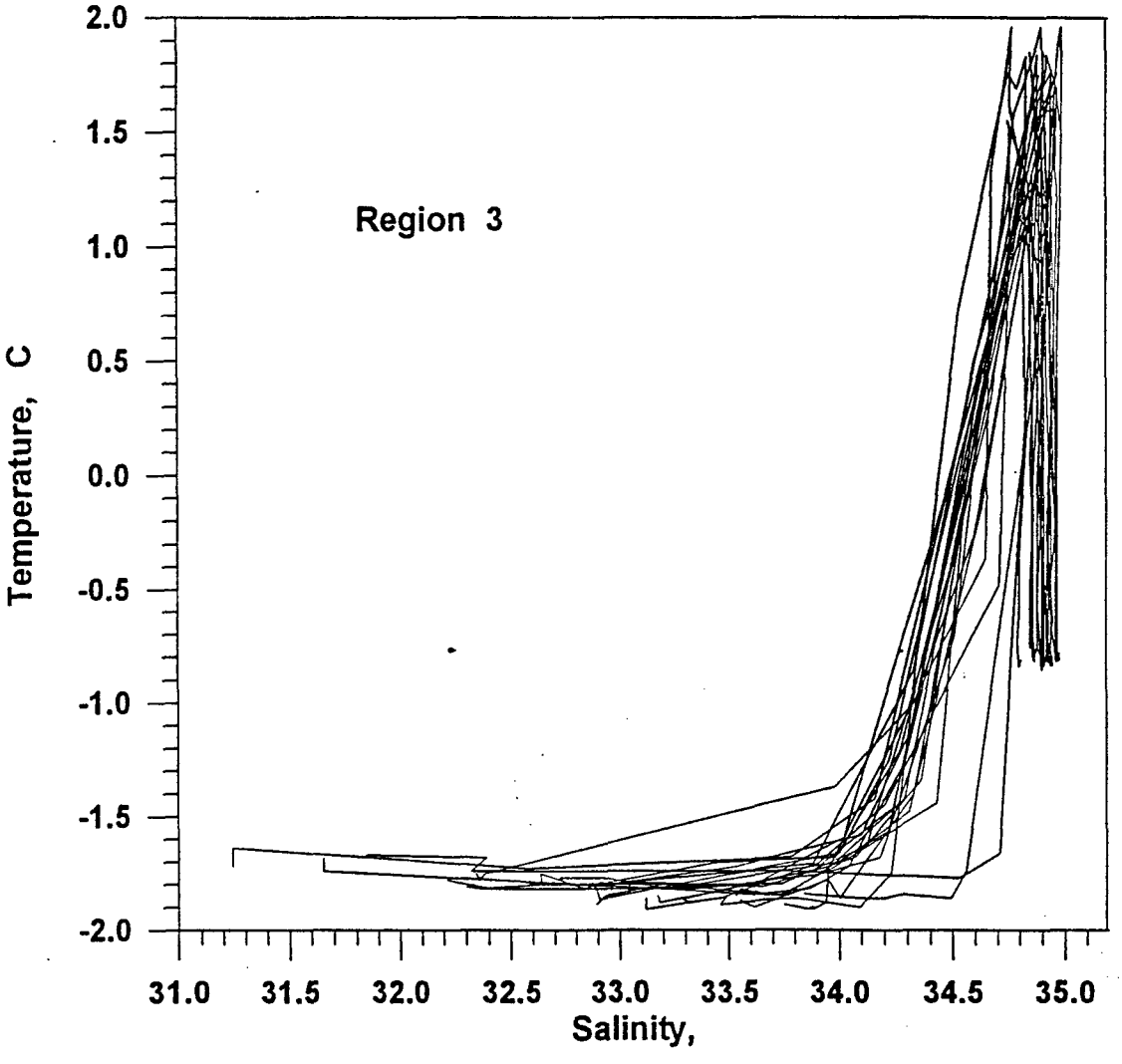

Fig. 11. Statistical T,S - diagram for region 3 (over the period 1973 - 1979).

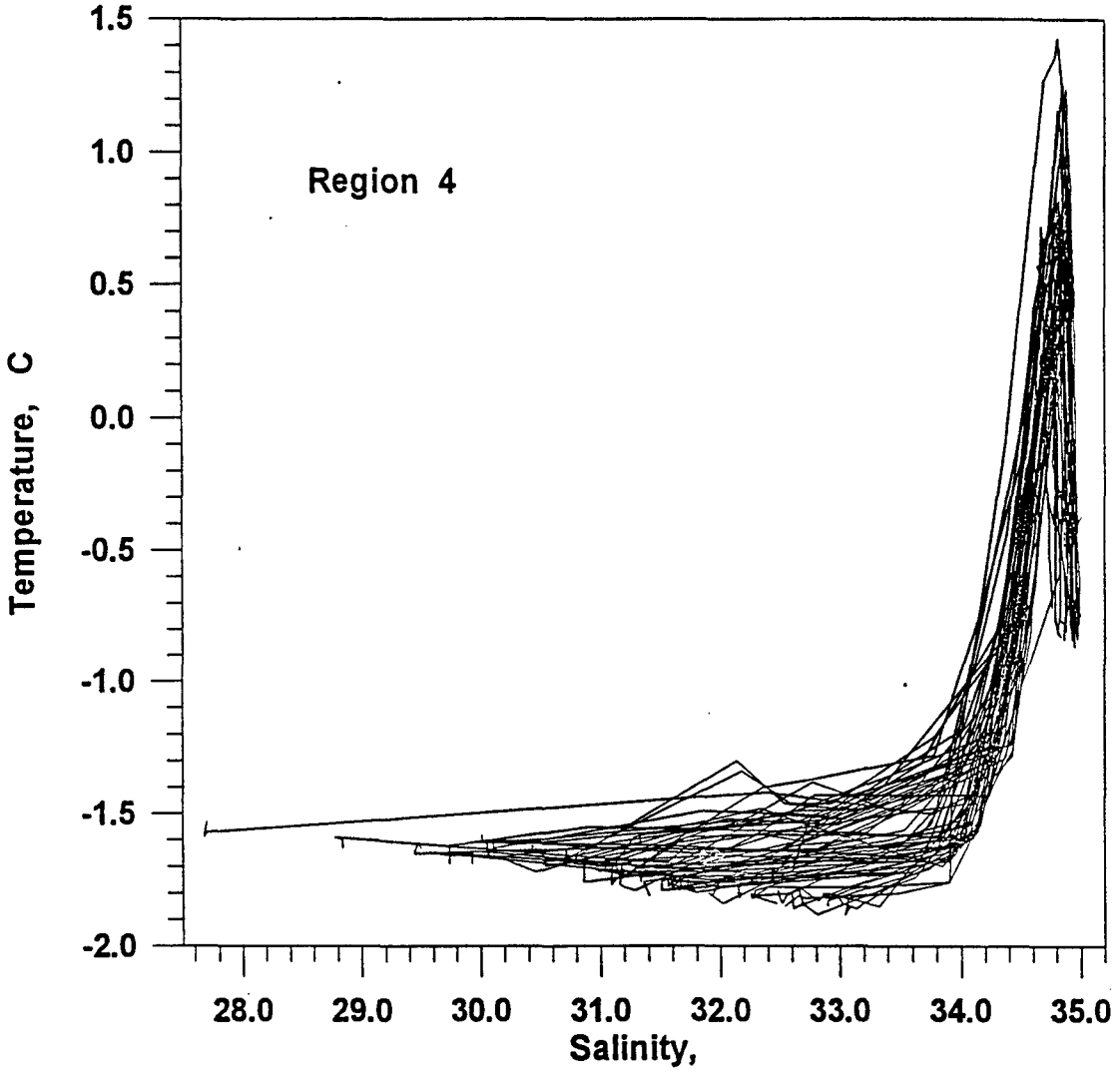

Fig. 12. Statistical T,S - diagram for region 4 (over the period 1973 - 1979).

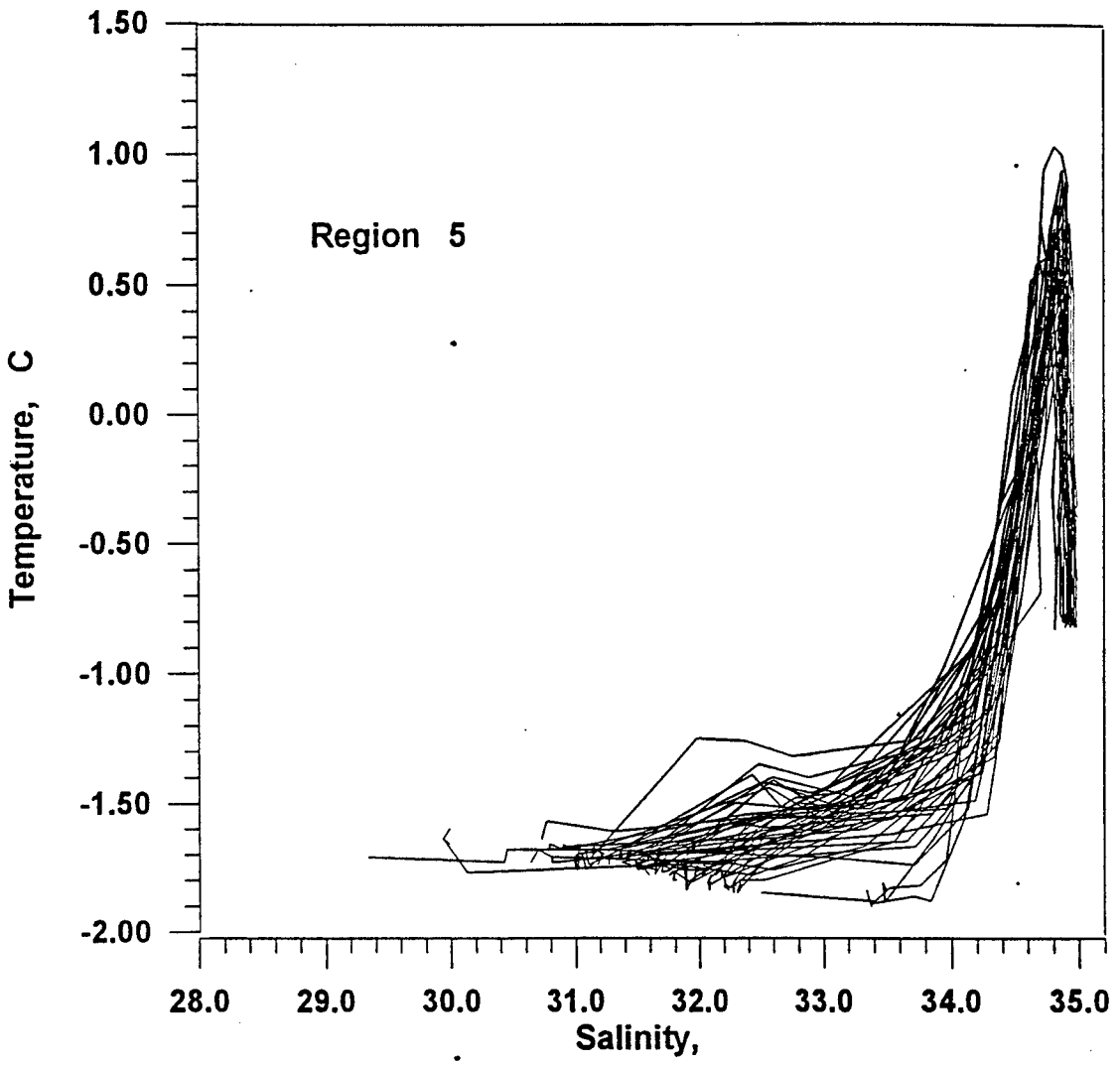

Fig. 13. Statistical T,S - diagram for region 5 (over the period 1973 - 1979).

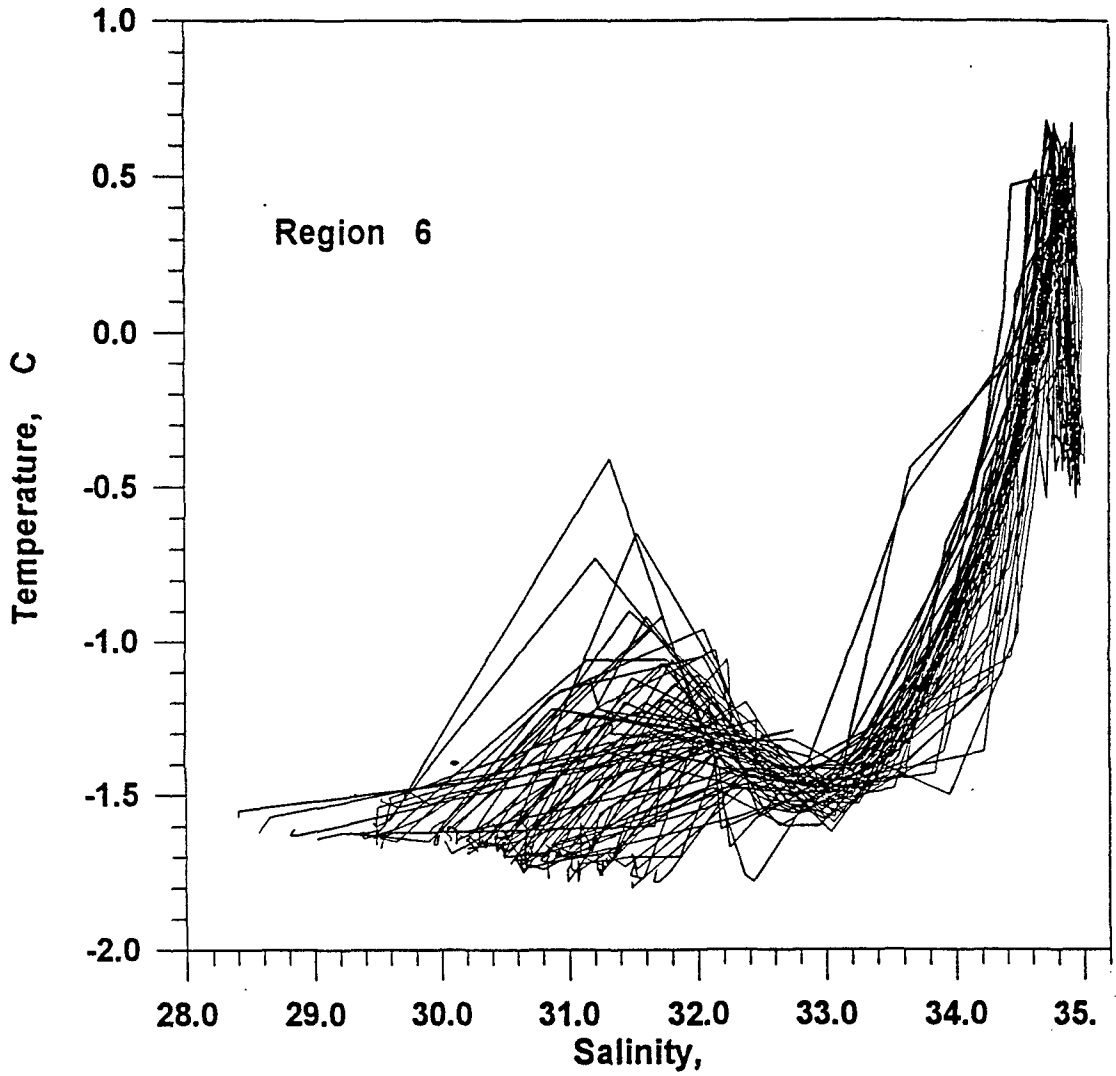

Fig. 14. Statistical T,S - diagram for region 6 (over the period 1973 - 1979).

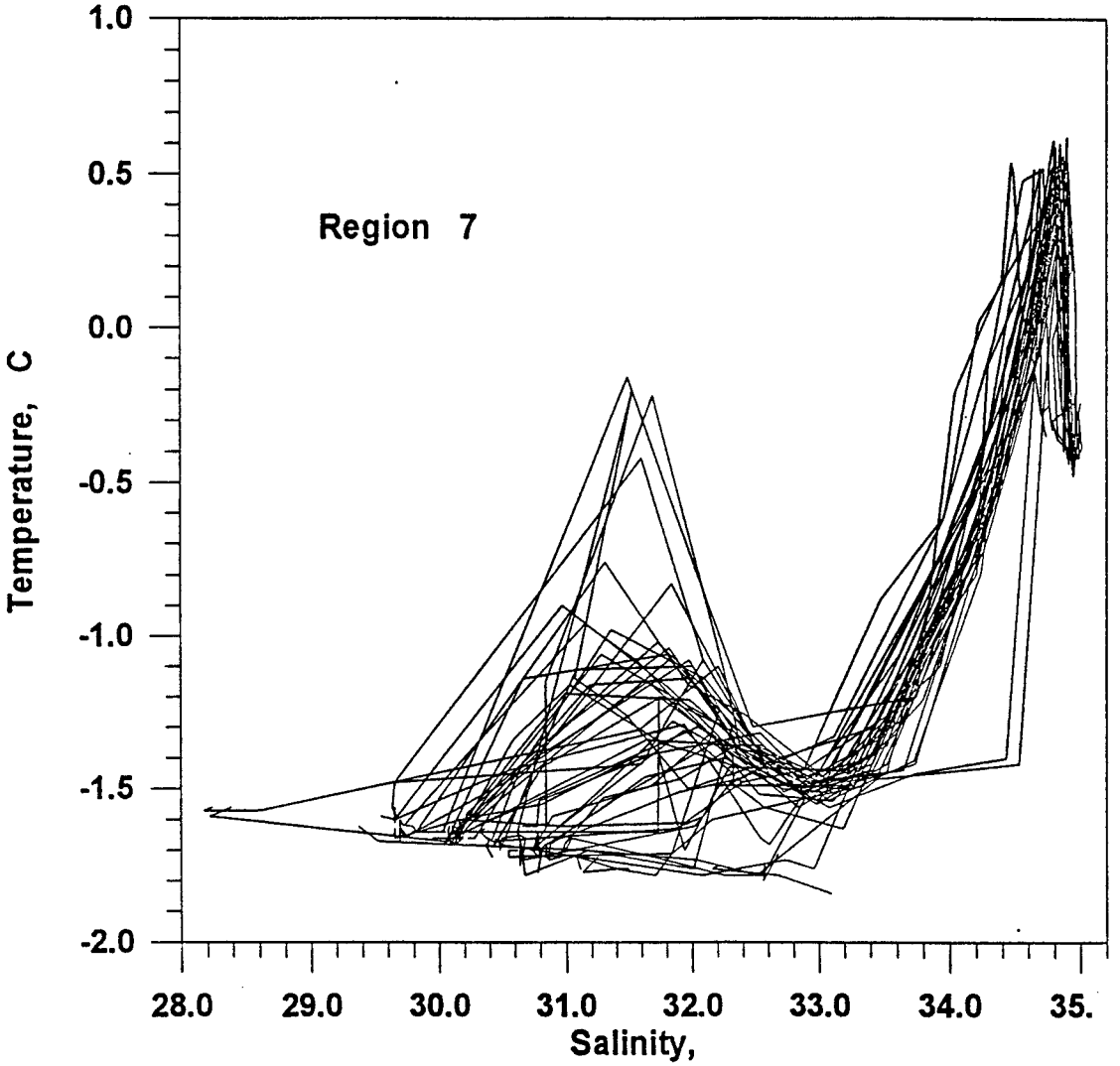

Fig. 15. Statistical T,S - diagram for region 7 (over the period 1973 - 1979).

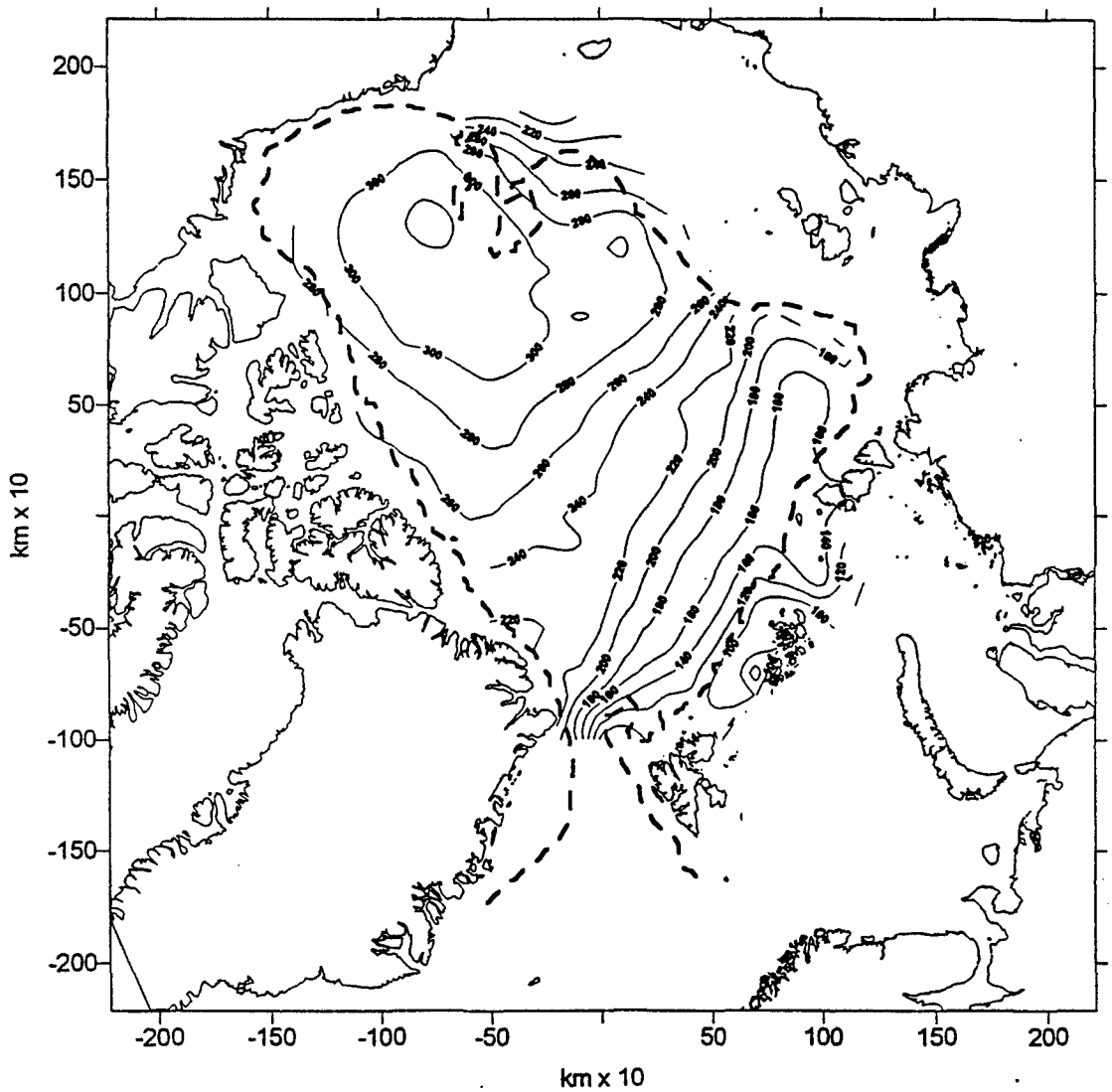

Fig. 16. Mean multiyear (1973-1979) depth of the upper boundary of Atlantic water (based on the 0 C isotherm).

The dashed line denotes the 1000 m isobath.

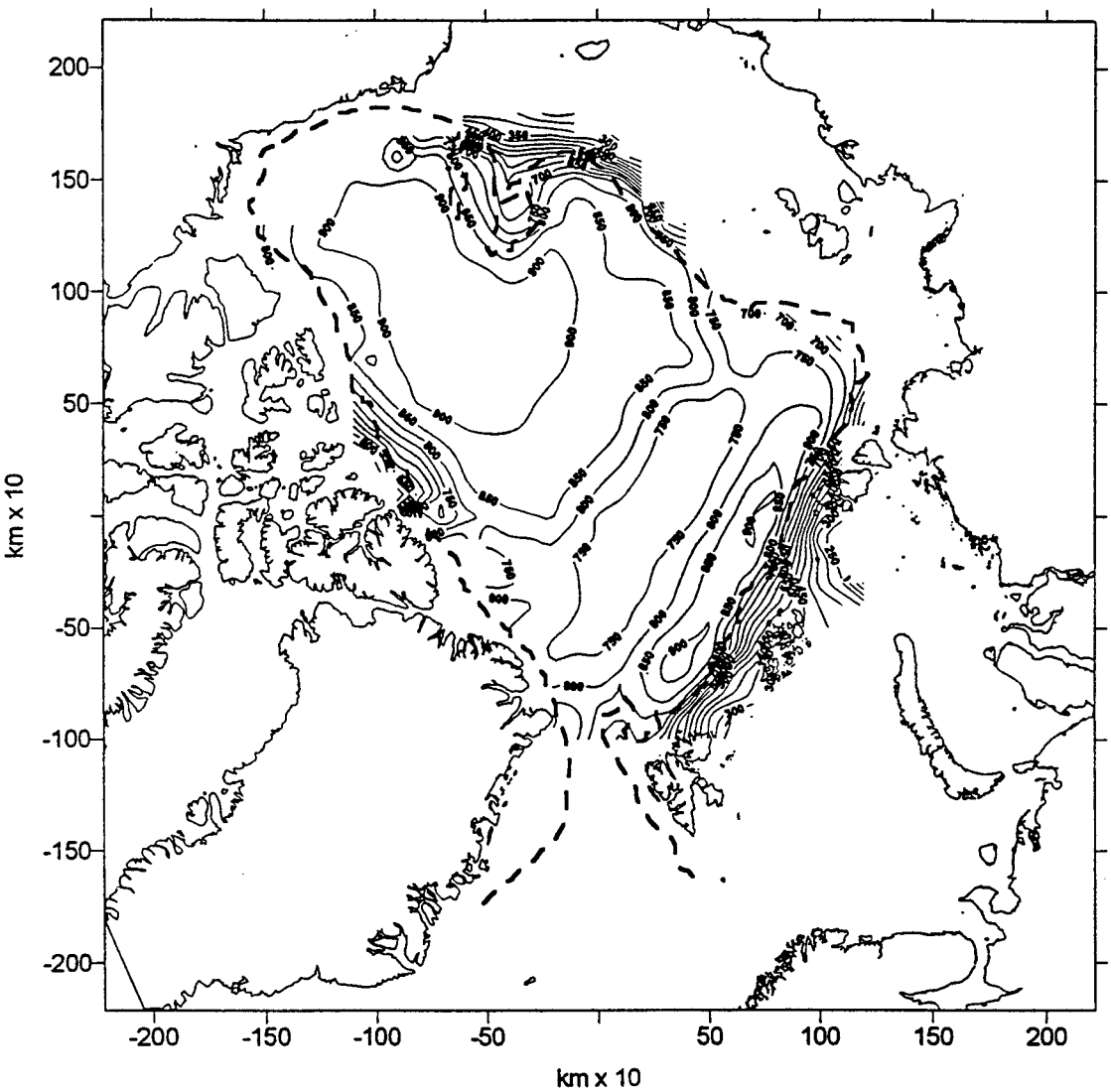

Fig. 17. Mean multiyear (1973-1979) depth of the lower boundary of Atlantic water (based on the 0 C isotherm).

The dashed line denotes the 1000 m isobath.

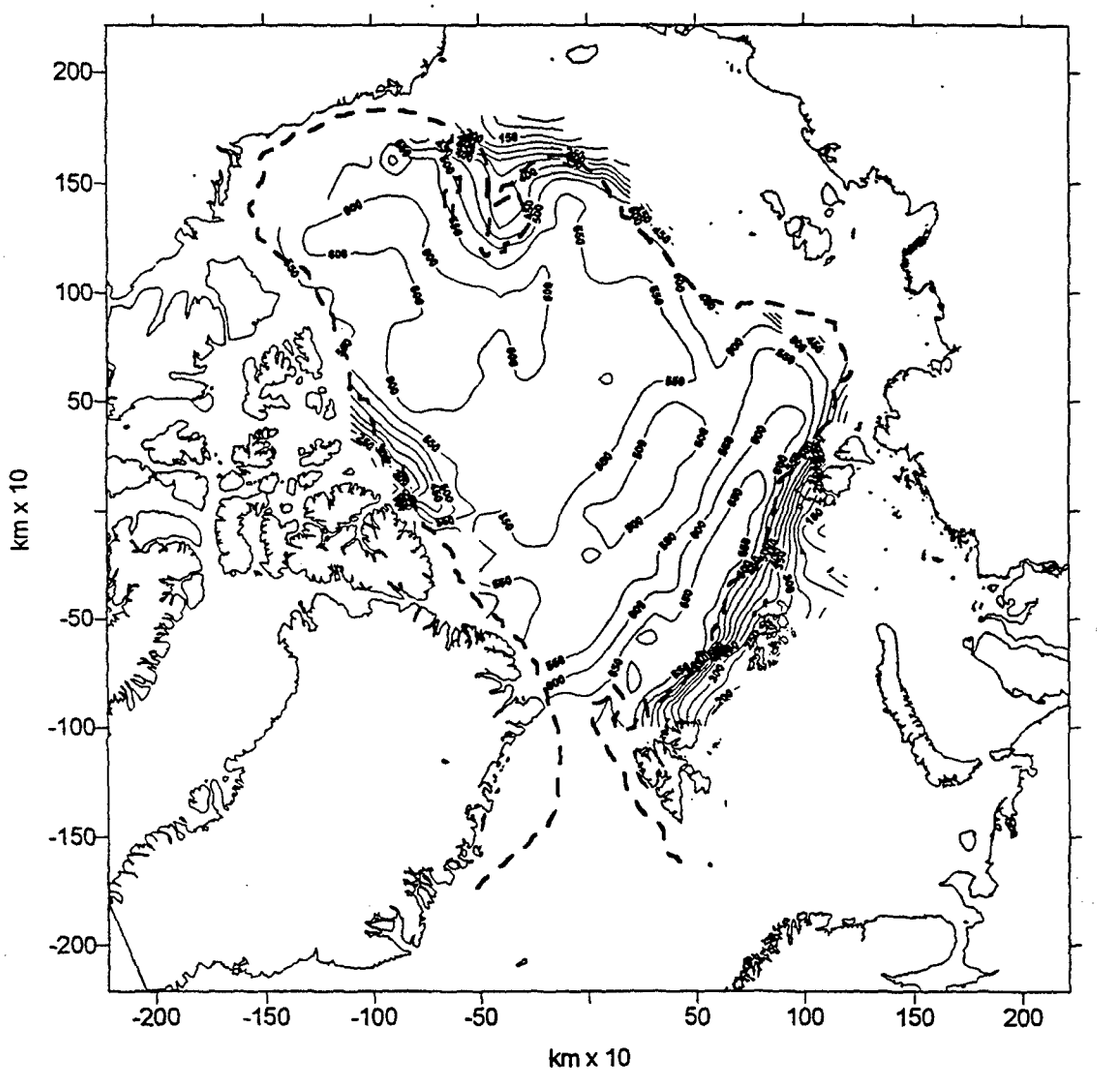

Fig. 18. Mean multiyear (1973-1979) thickness of Atlantic water (based on the 0 C isotherm).

The dashed line denotes the 1000 m isobath.

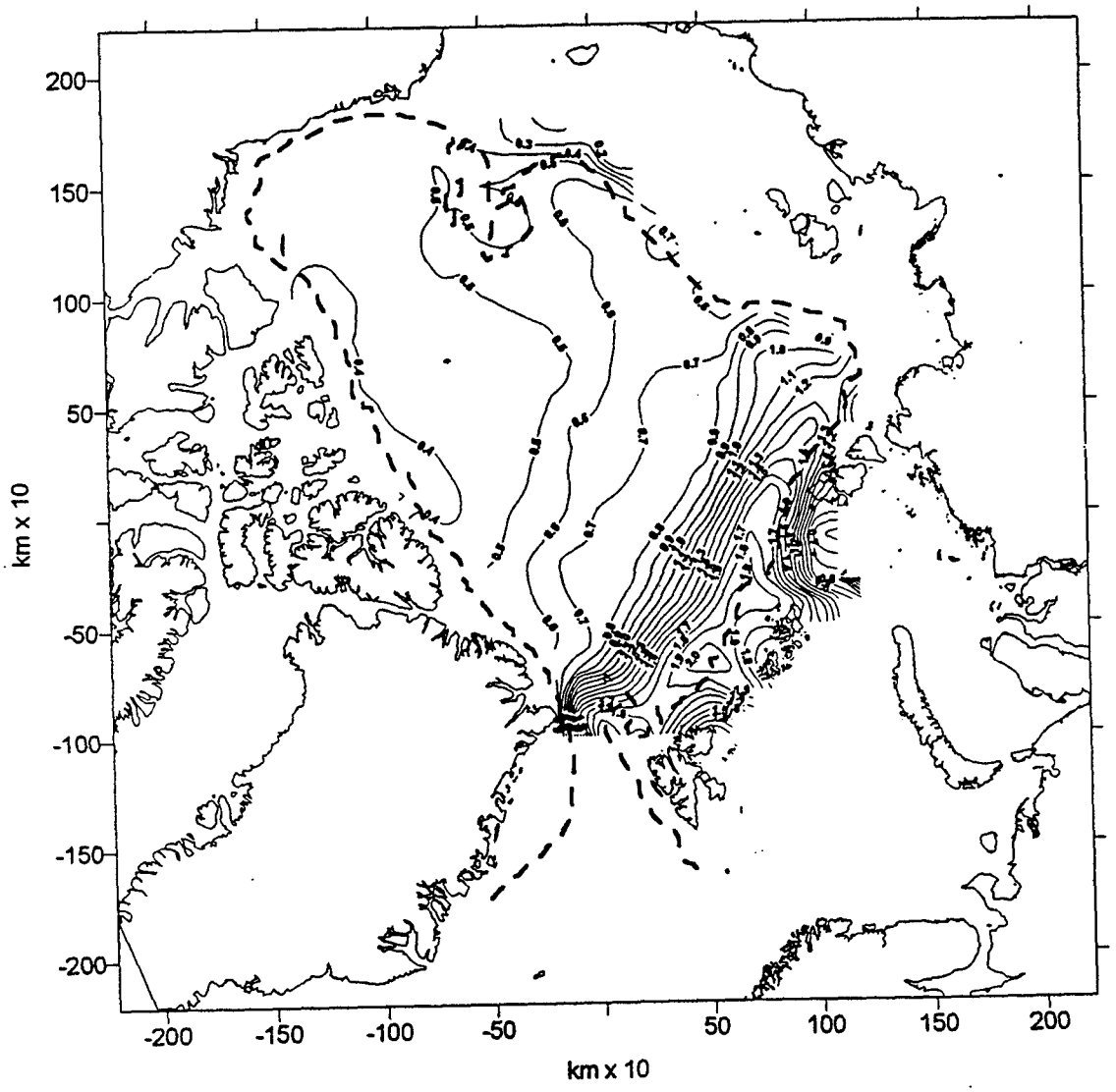

Fig. 19. Mean multiyear (1973-1979) maximum temperature of Atlantic water. The dashed line denotes the 1000 m isobath.

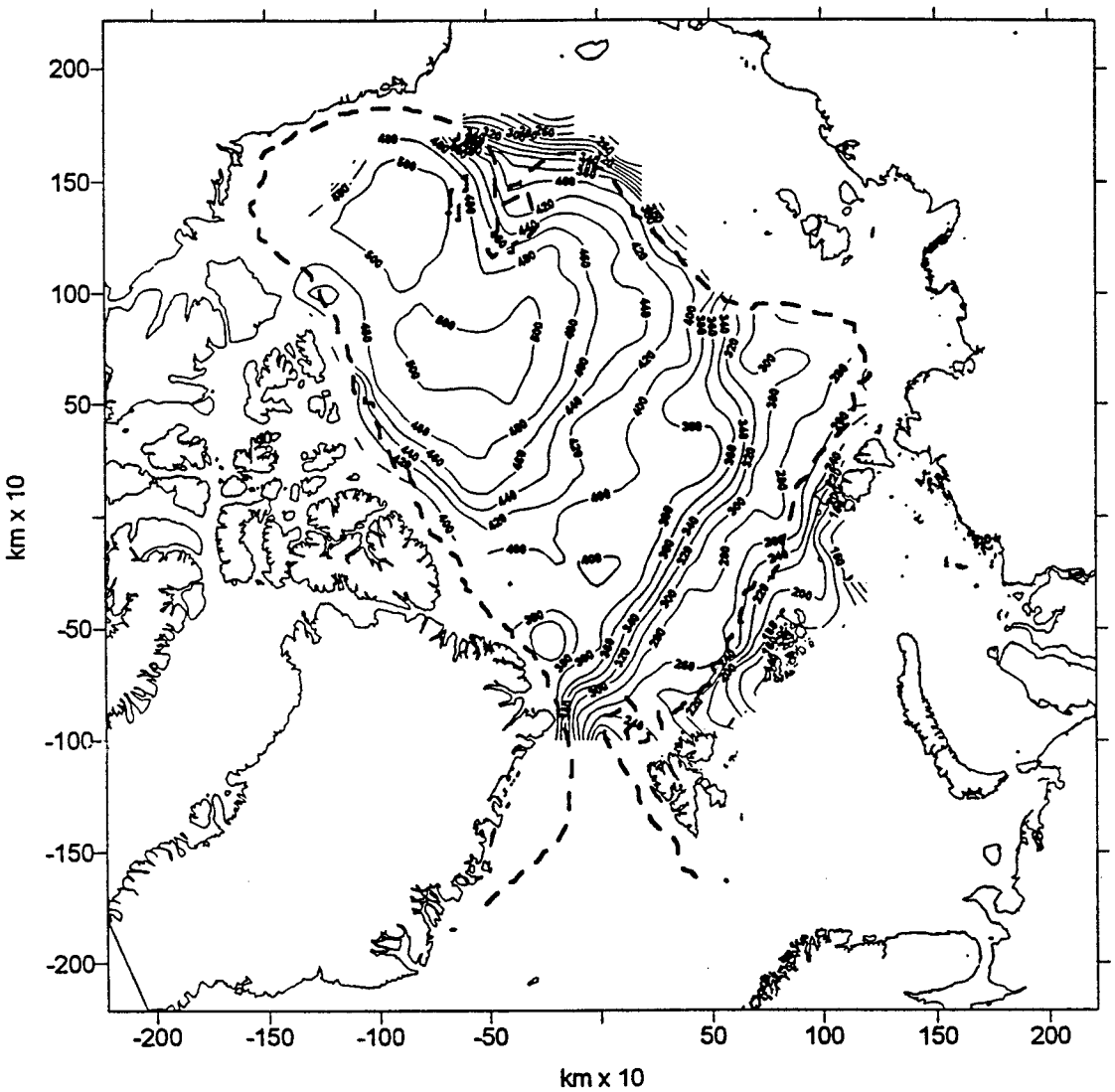

Fig. 20. Mean multiyear (1973-1979) depth of the maximum temperature of Atlantic water.

The dashed line denotes the 1000 m isobath.

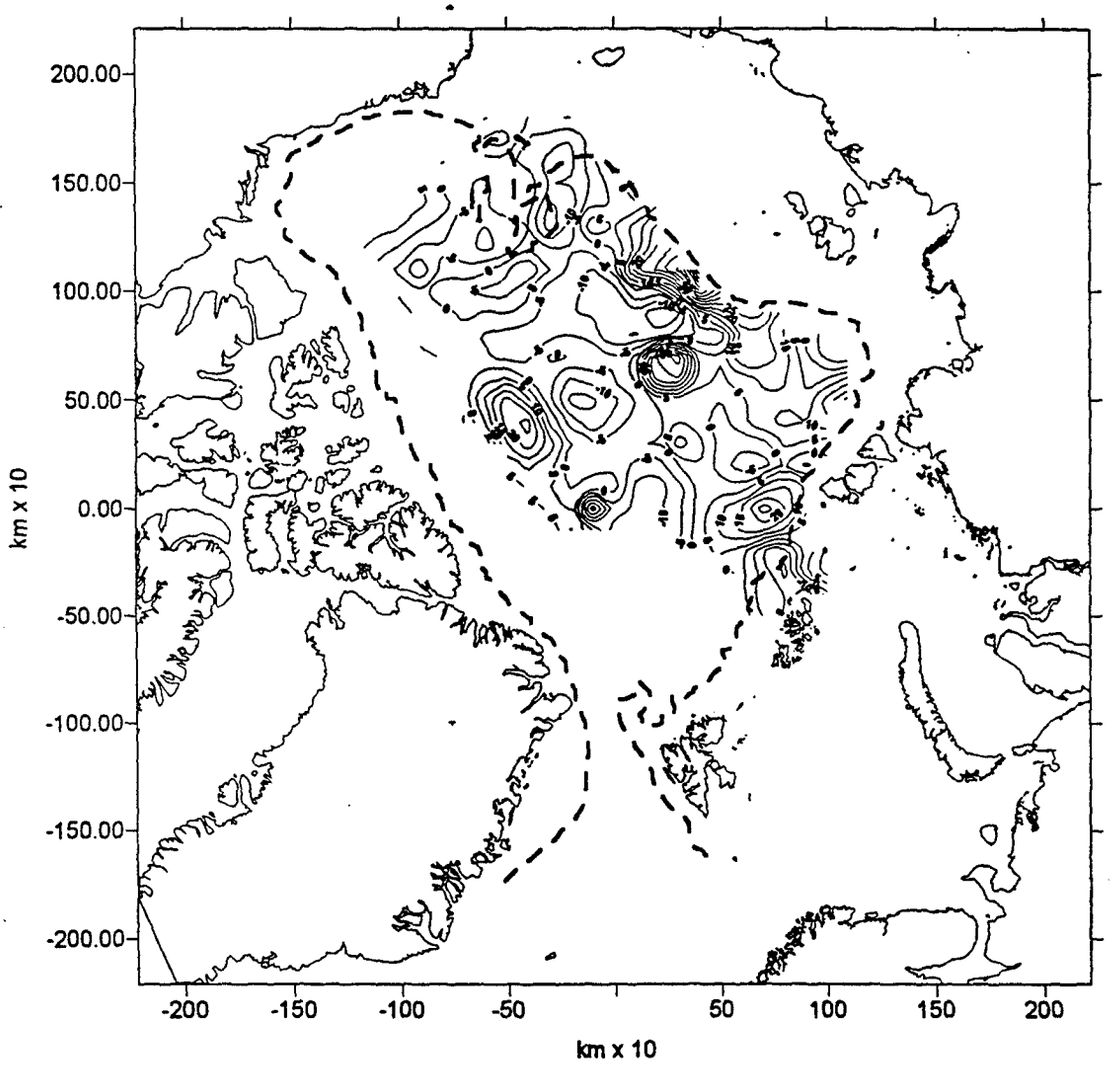

Fig. 21. Anomalies in the depth of the upper boundary of Atlantic water for 1973. The dashed line denotes the 1000 m isobath.

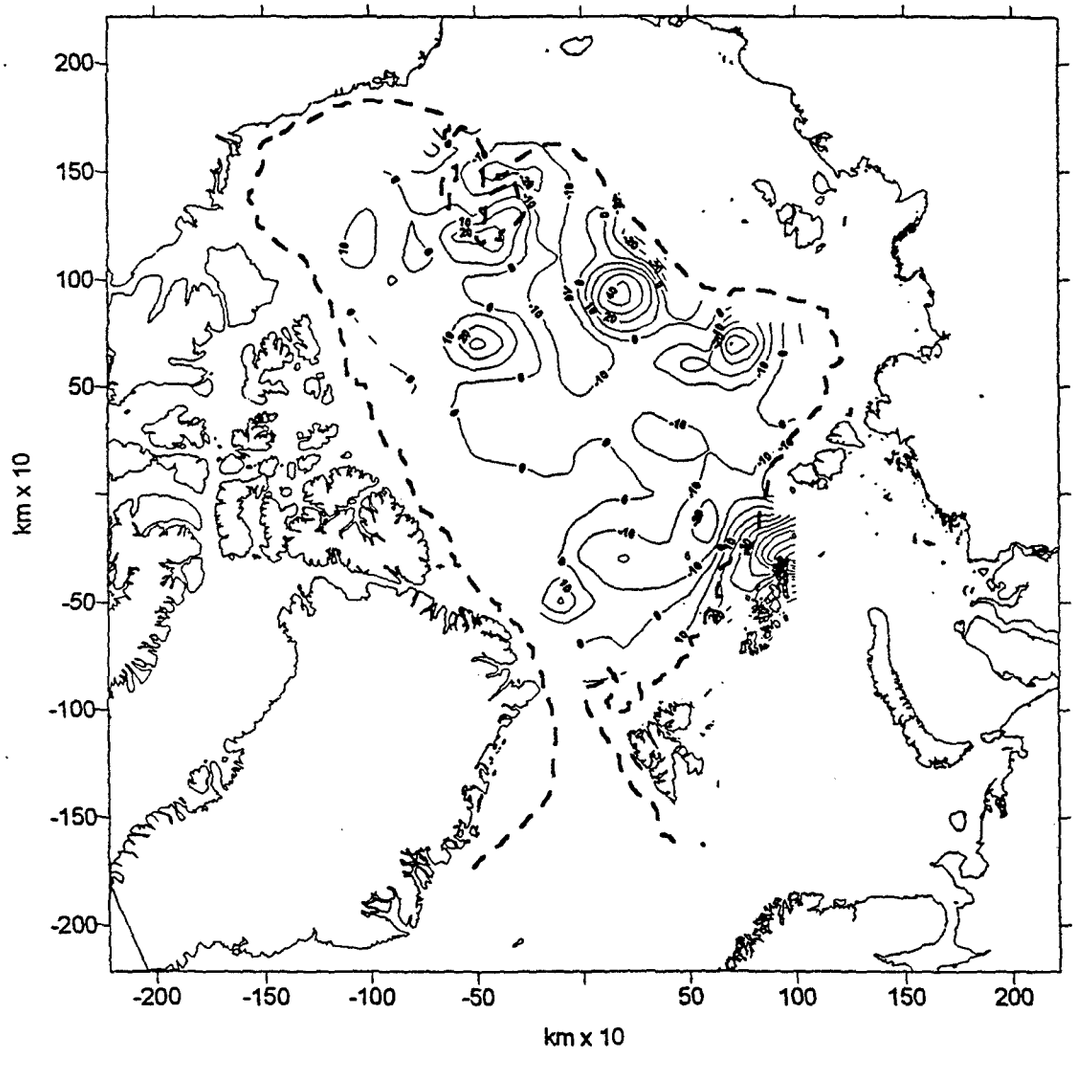

Fig. 22. Anomalies in the depth of the upper boundary of Atlantic water for 1974. The dashed line denotes the 1000 m isobath.

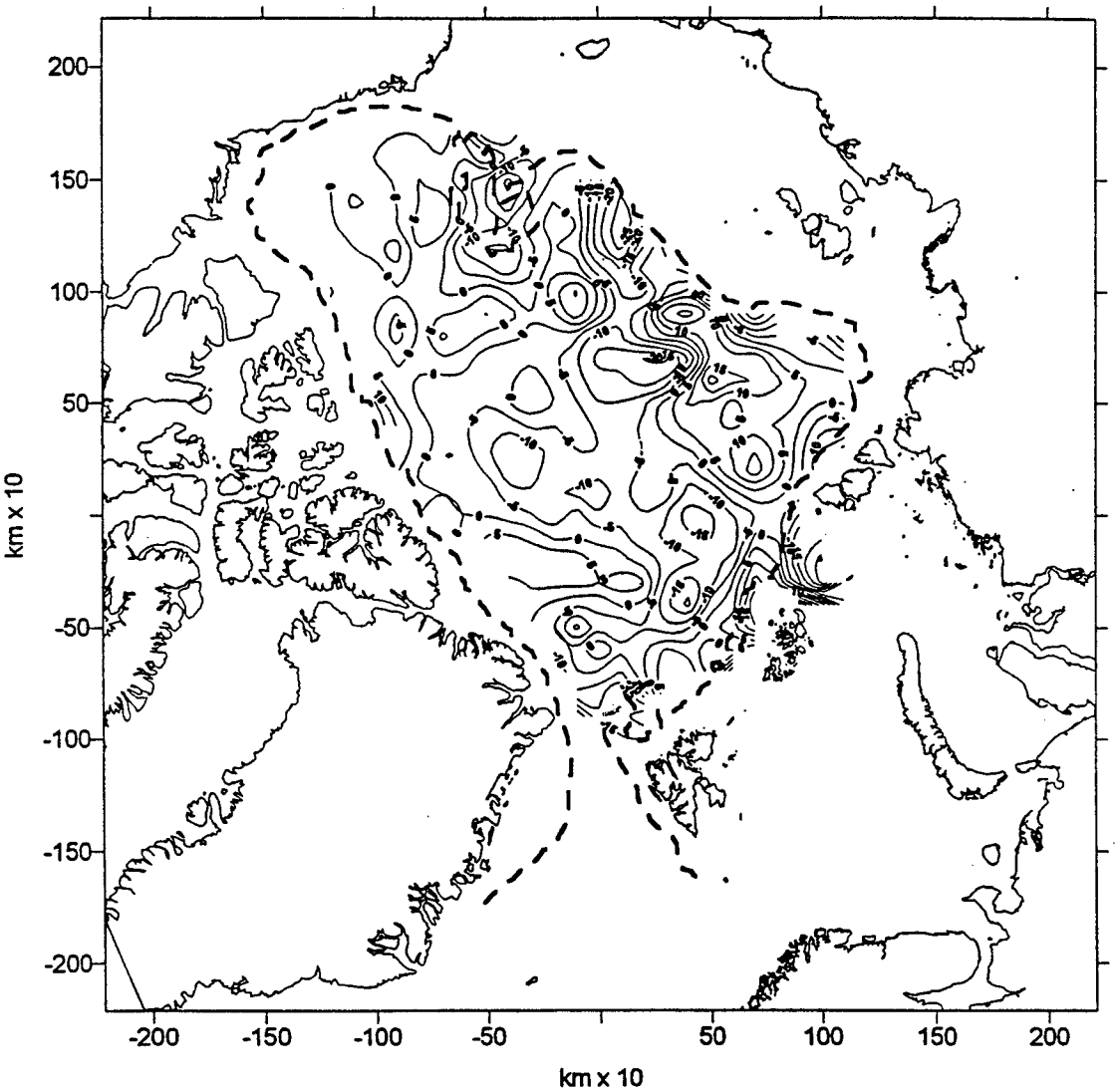

Fig. 23. Anomalies in the depth of the upper boundary of Atlantic water for 1975. The dashed line denotes the 1000 m isobath.

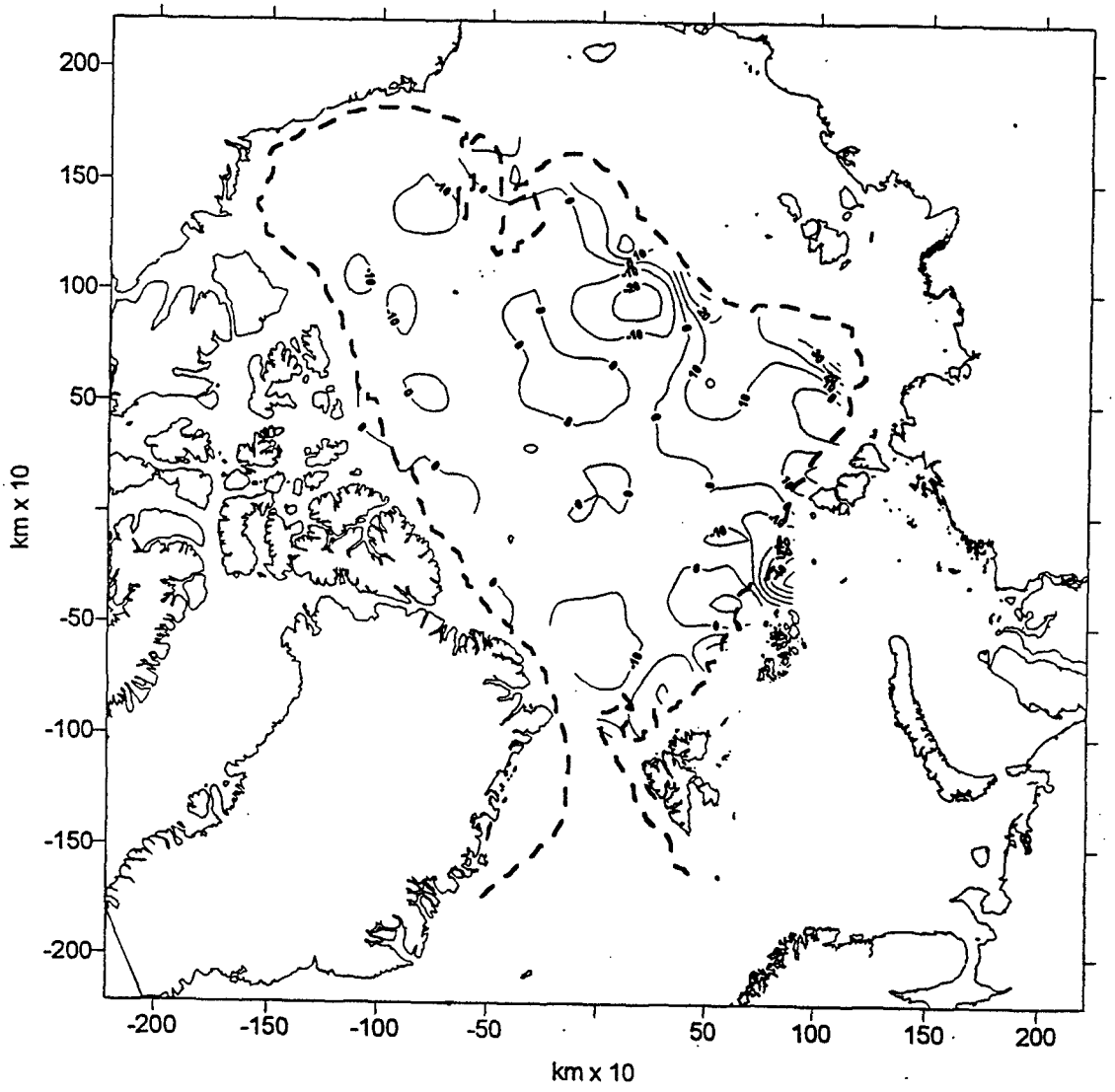

Fig. 24. Anomalies in the depth of the upper boundary of Atlantic water for 1976. The dashed line denotes the 1000 m isobath.

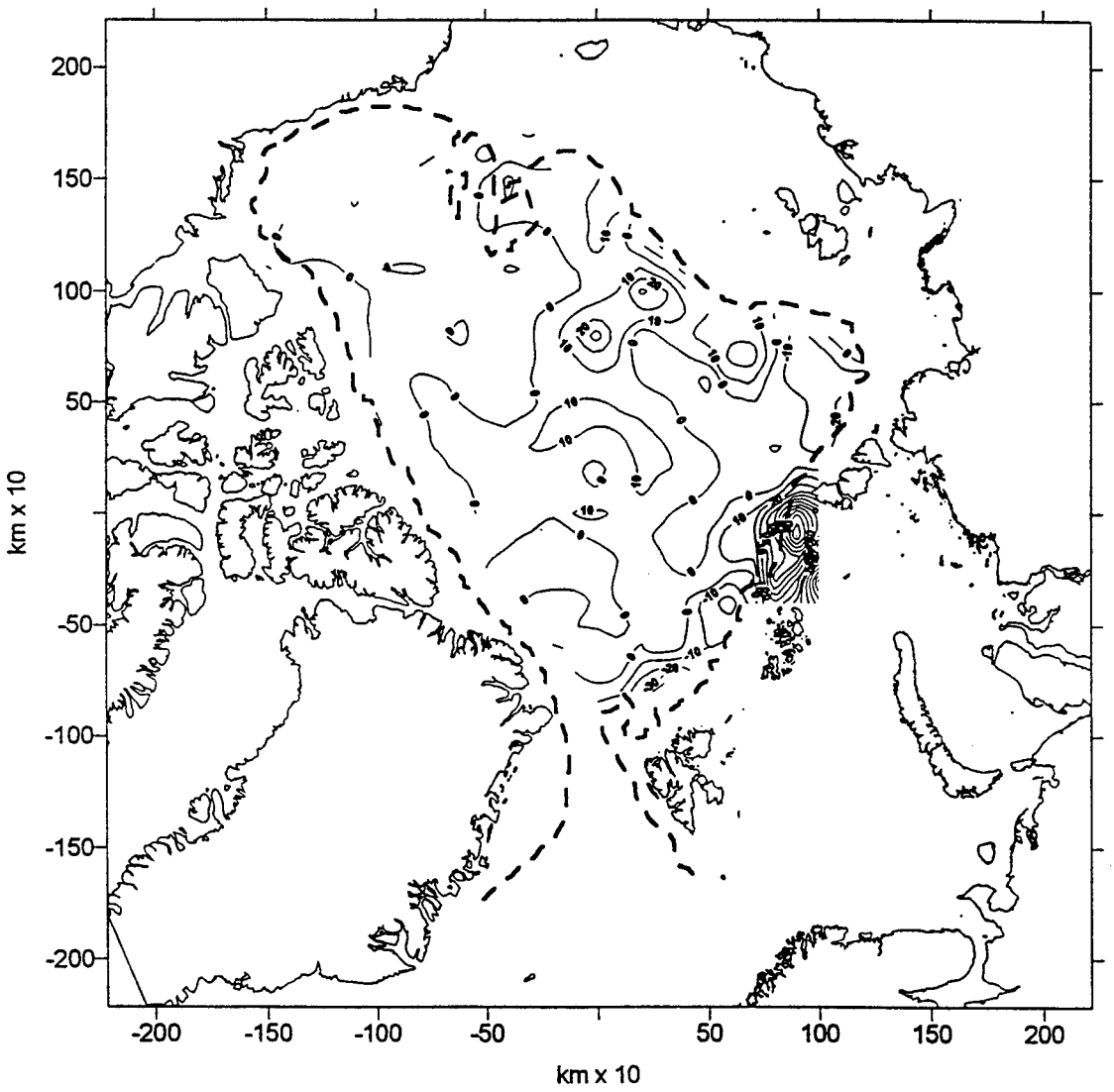

Fig. 25. Anomalies in the depth of the upper boundary of Atlantic water for 1977. The dashed line denotes the 1000 m isobath.

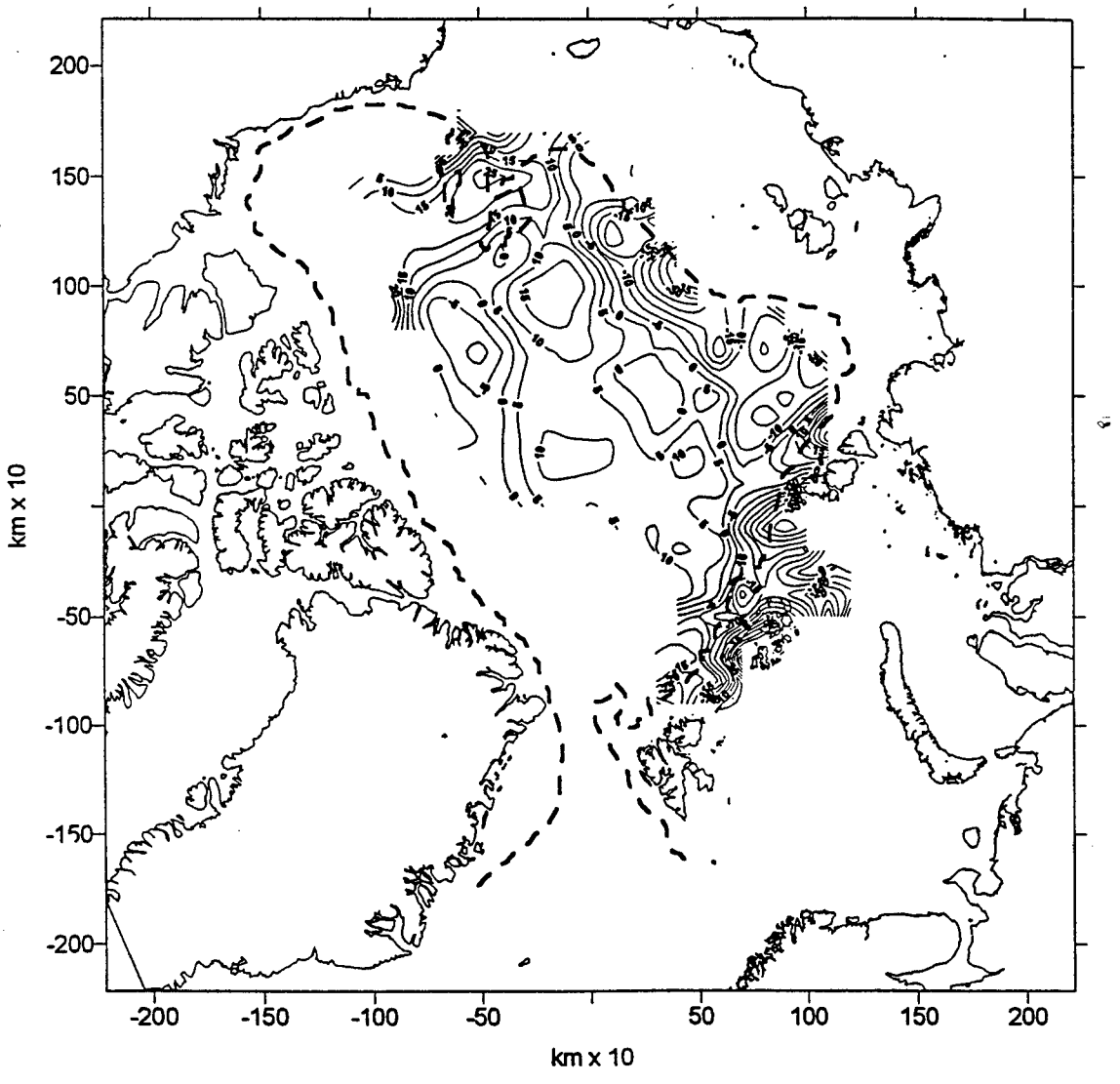

Fig. 26. Anomalies in the depth of the upper boundary of Atlantic water for 1978. The dashed line denotes the 1000 m isobath.

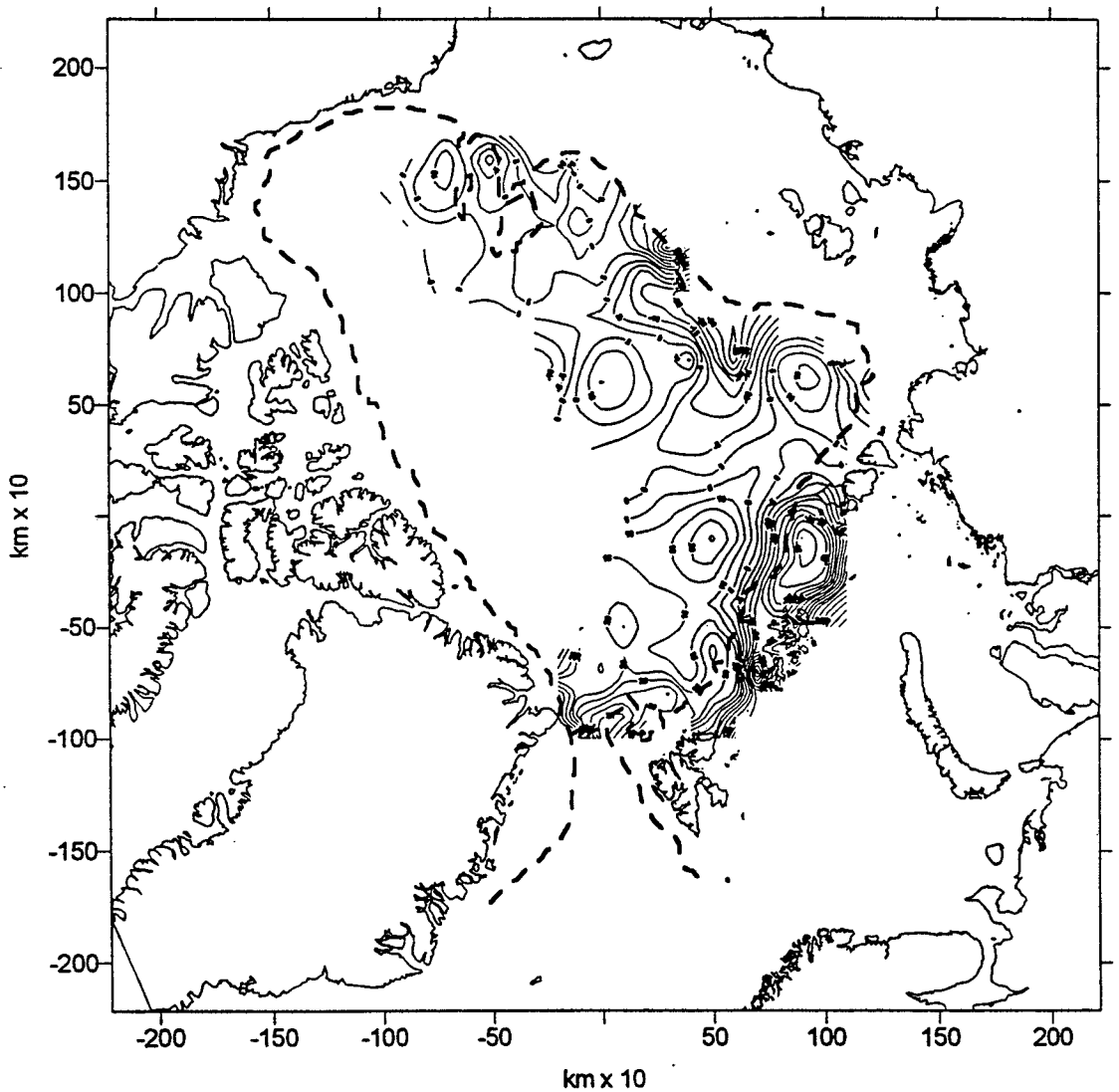

Fig. 27. Anomalies in the depth of the upper boundary of Atlantic water for 1979. The dashed line denotes the 1000 m isobath.

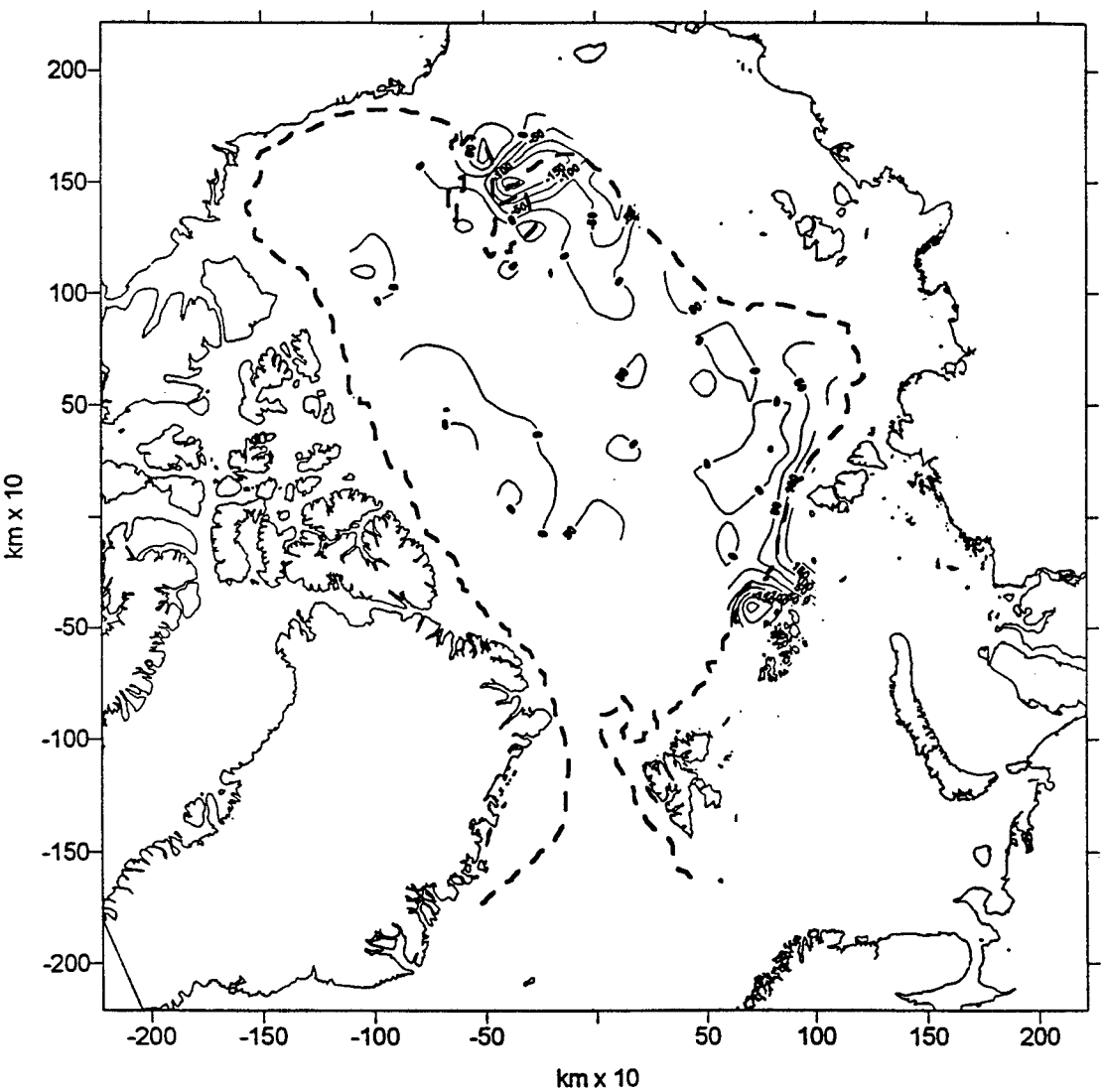

Fig. 28. Anomalies in the depth of the lower boundary of Atlantic water for 1973. The dashed line denotes the 1000 m isobath.

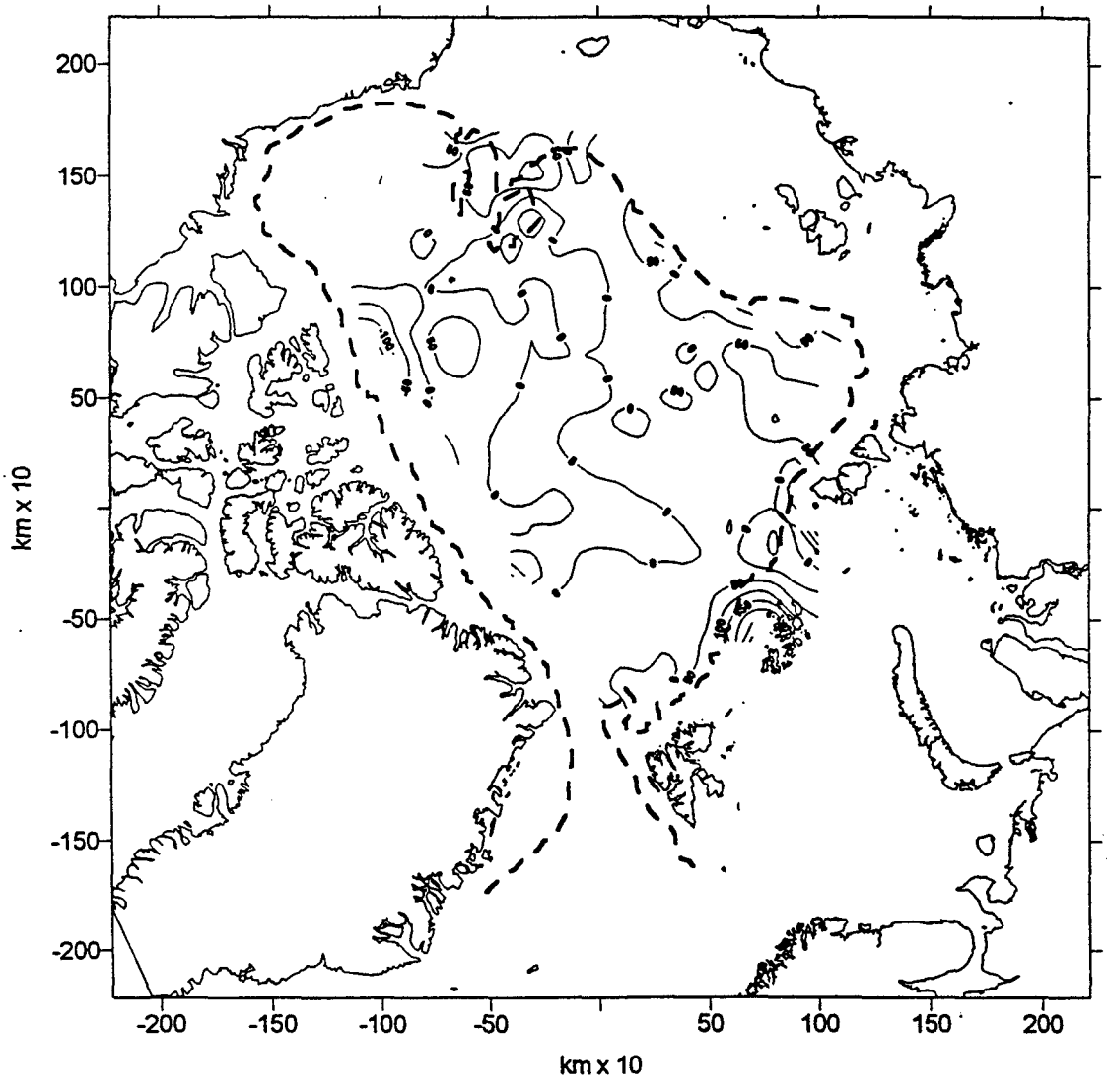

Fig. 29. Anomalies in the depth of the lower boundary of Atlantic water for 1974. The dashed line denotes the 1000 m isobath.

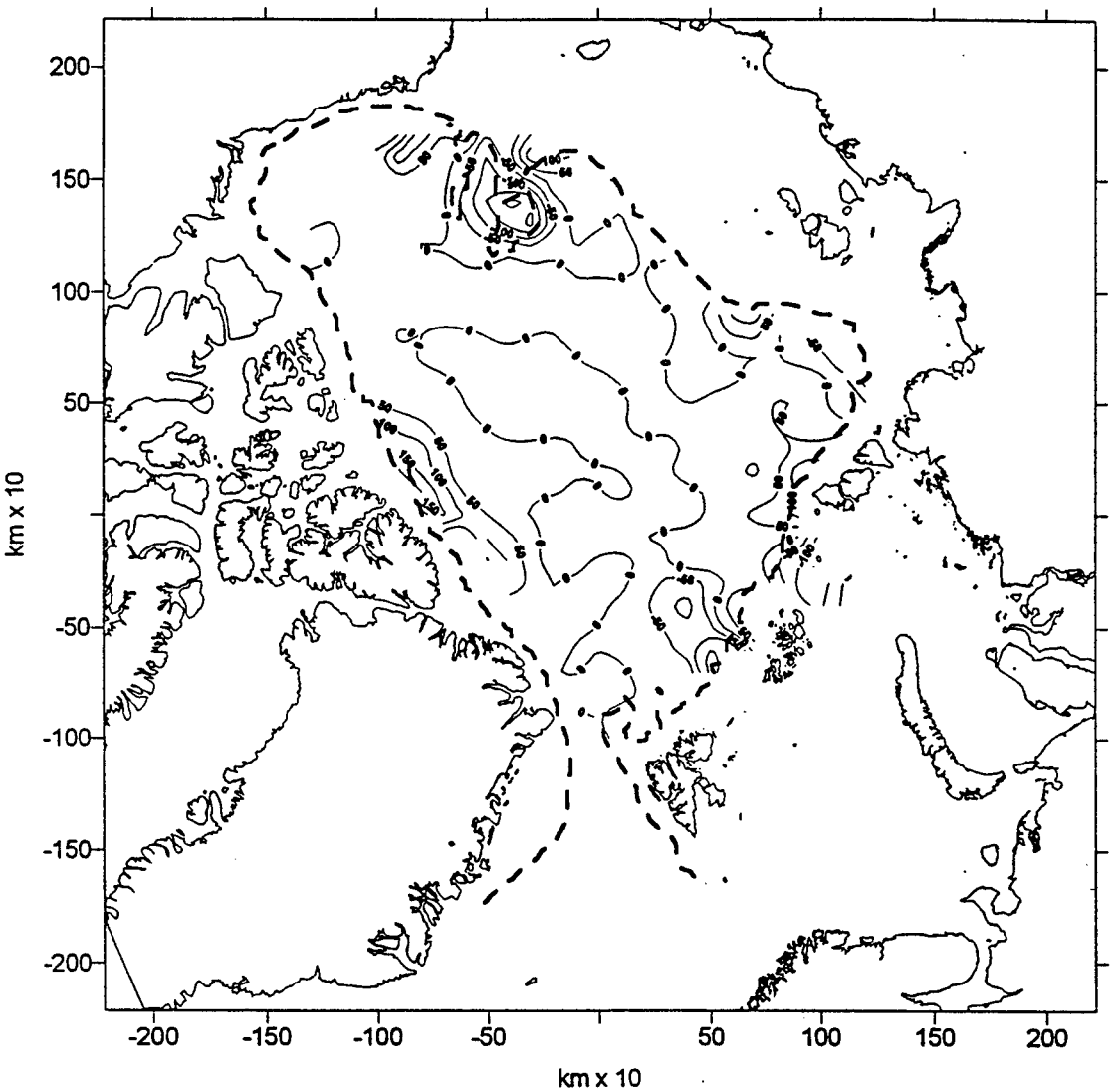

Fig. 30. Anomalies in the depth of the lower boundary of Atlantic water for 1975. The dashed line denotes the 1000 m isobath.

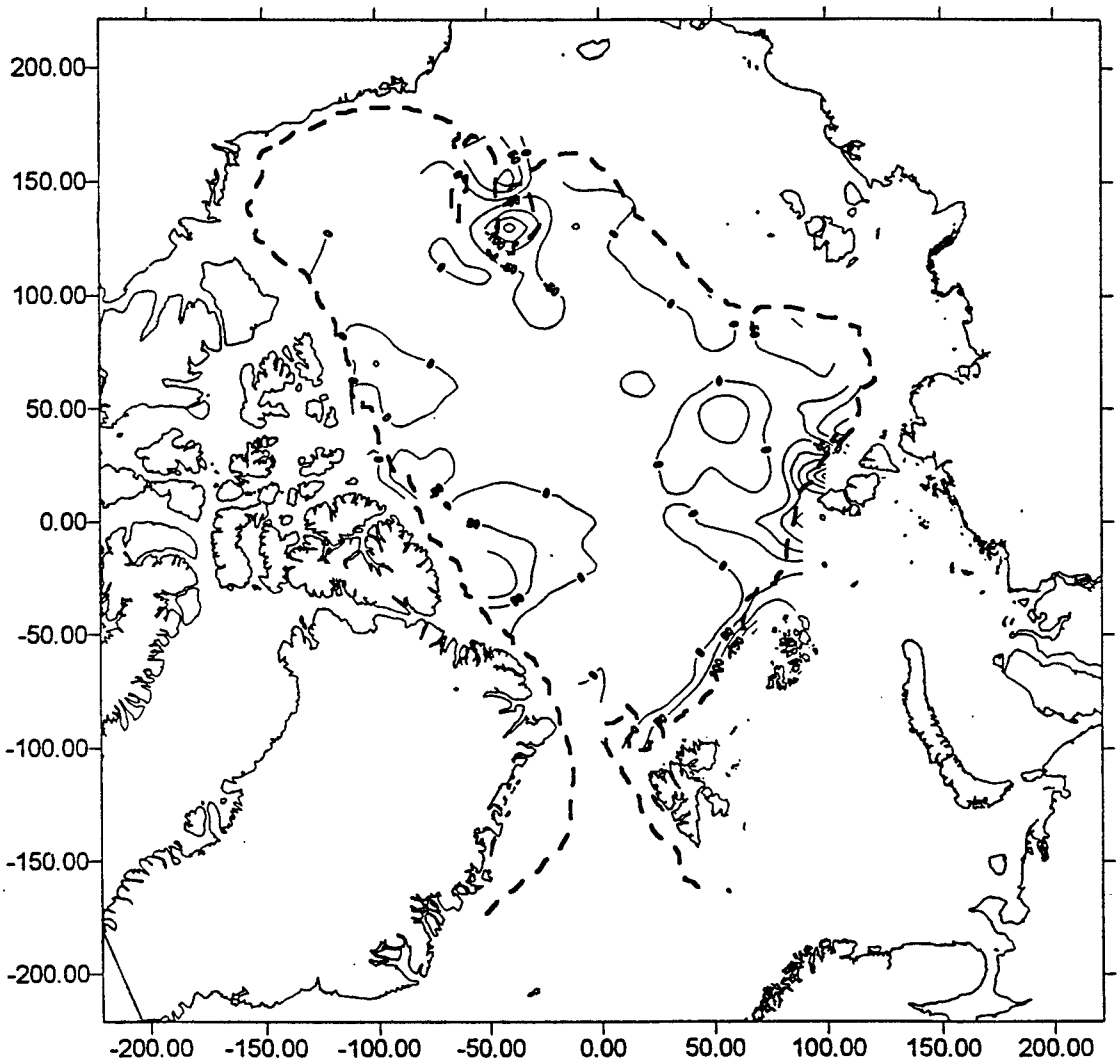

Fig. 31. Anomalies in the depth of the lower boundary of Atlantic water for 1976. The dashed line denotes the 1000 m isobath.

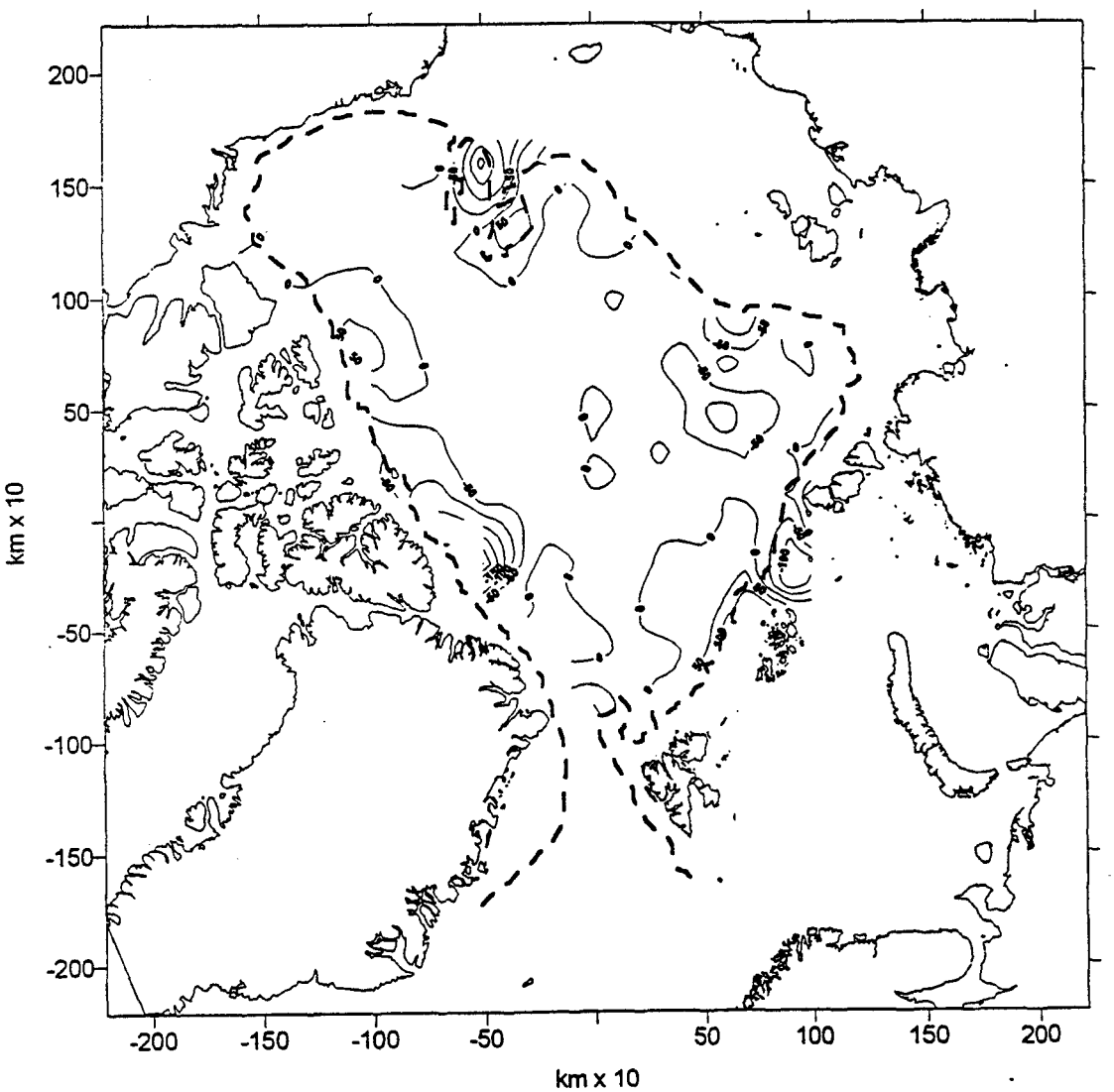

Fig. 32. Anomalies in the depth of the lower boundary of Atlantic water for 1977. The dashed line denotes the 1000 m isobath.

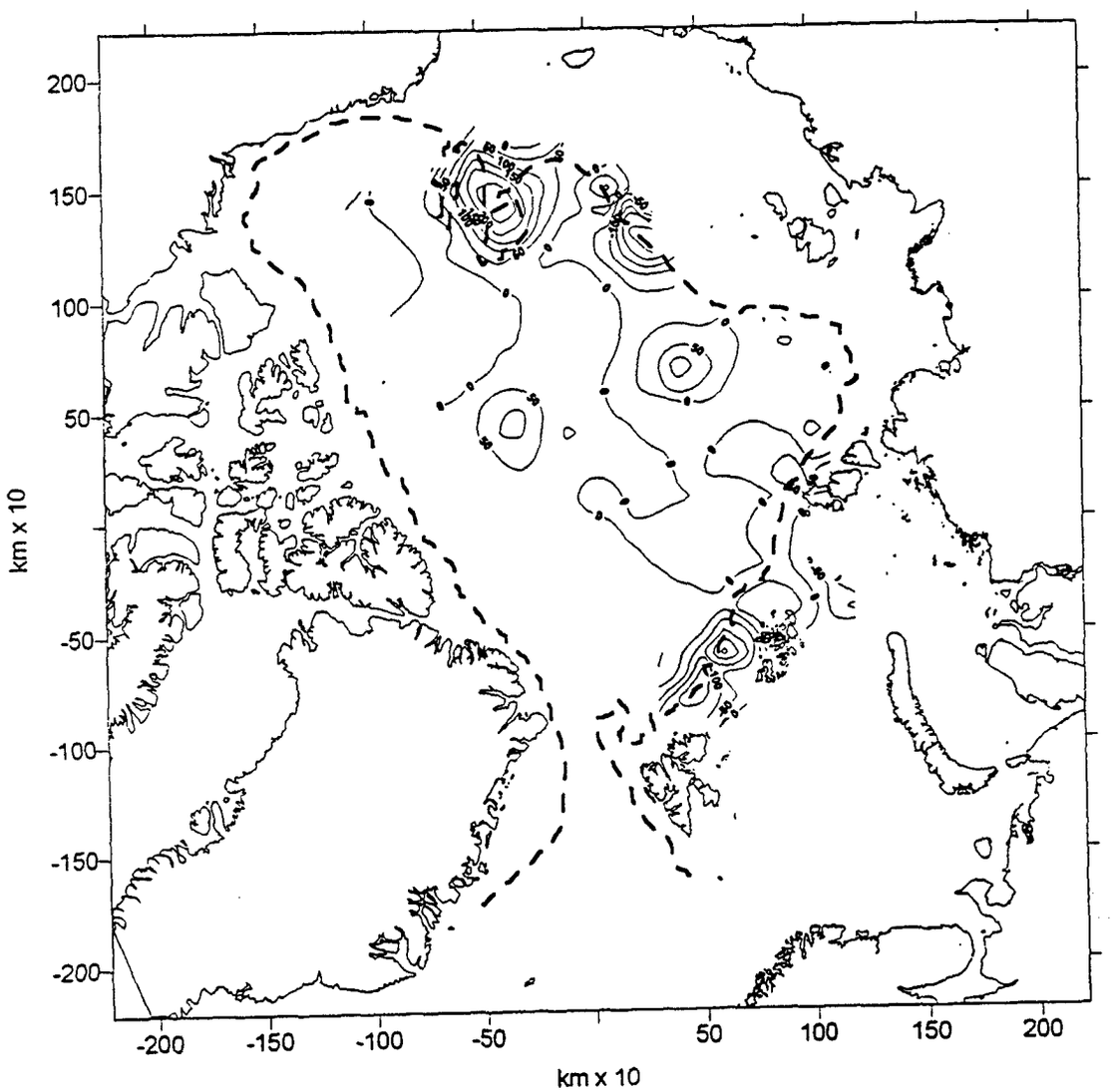

Fig. 33. Anomalies in the depth of the lower boundary of Atlantic water for 1978. The dashed line denotes the 1000 m isobath.

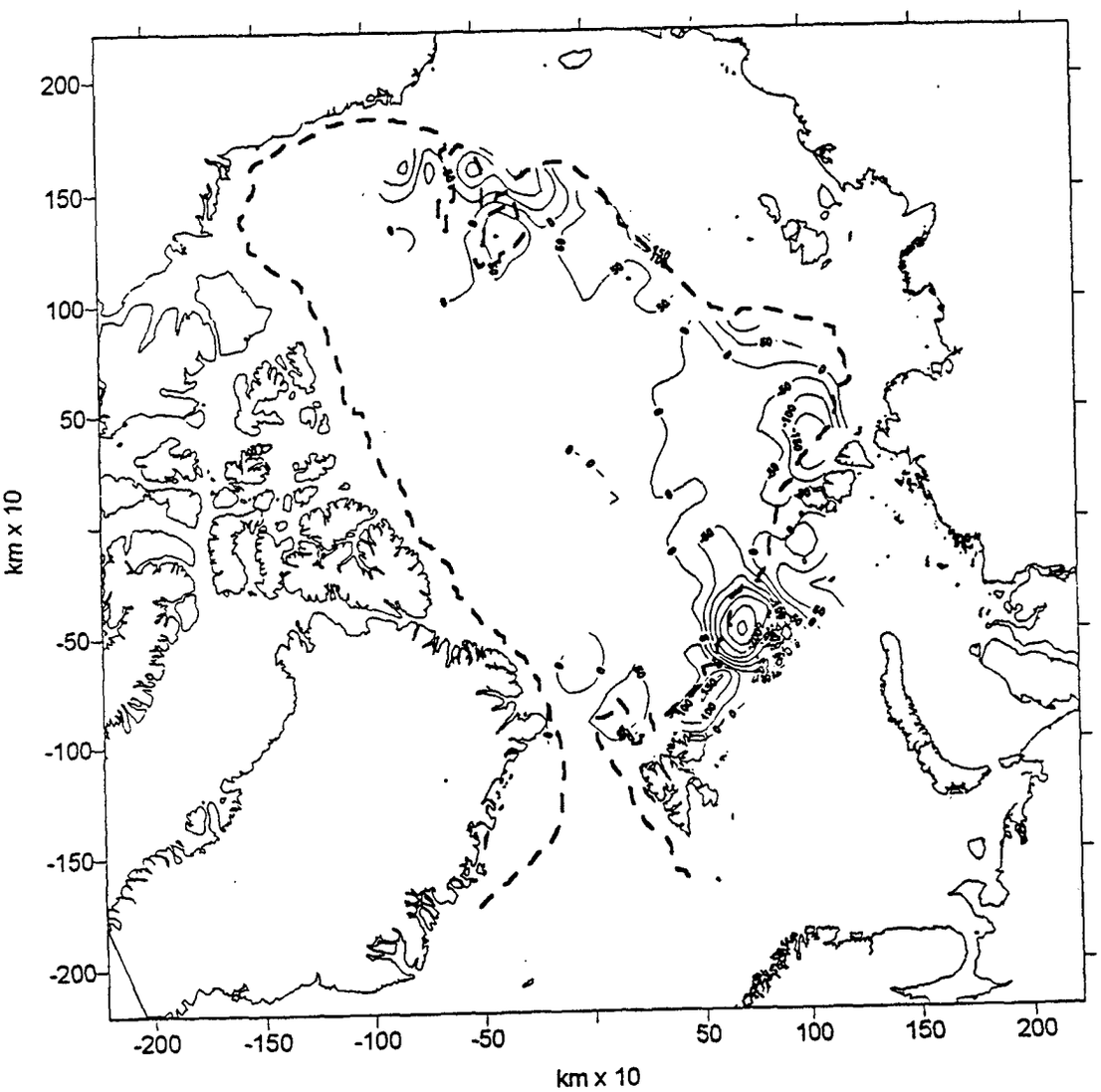

Fig. 34. Anomalies in the depth of the lower boundary of Atlantic water for 1979. The dashed line denotes the 1000 m isobath.

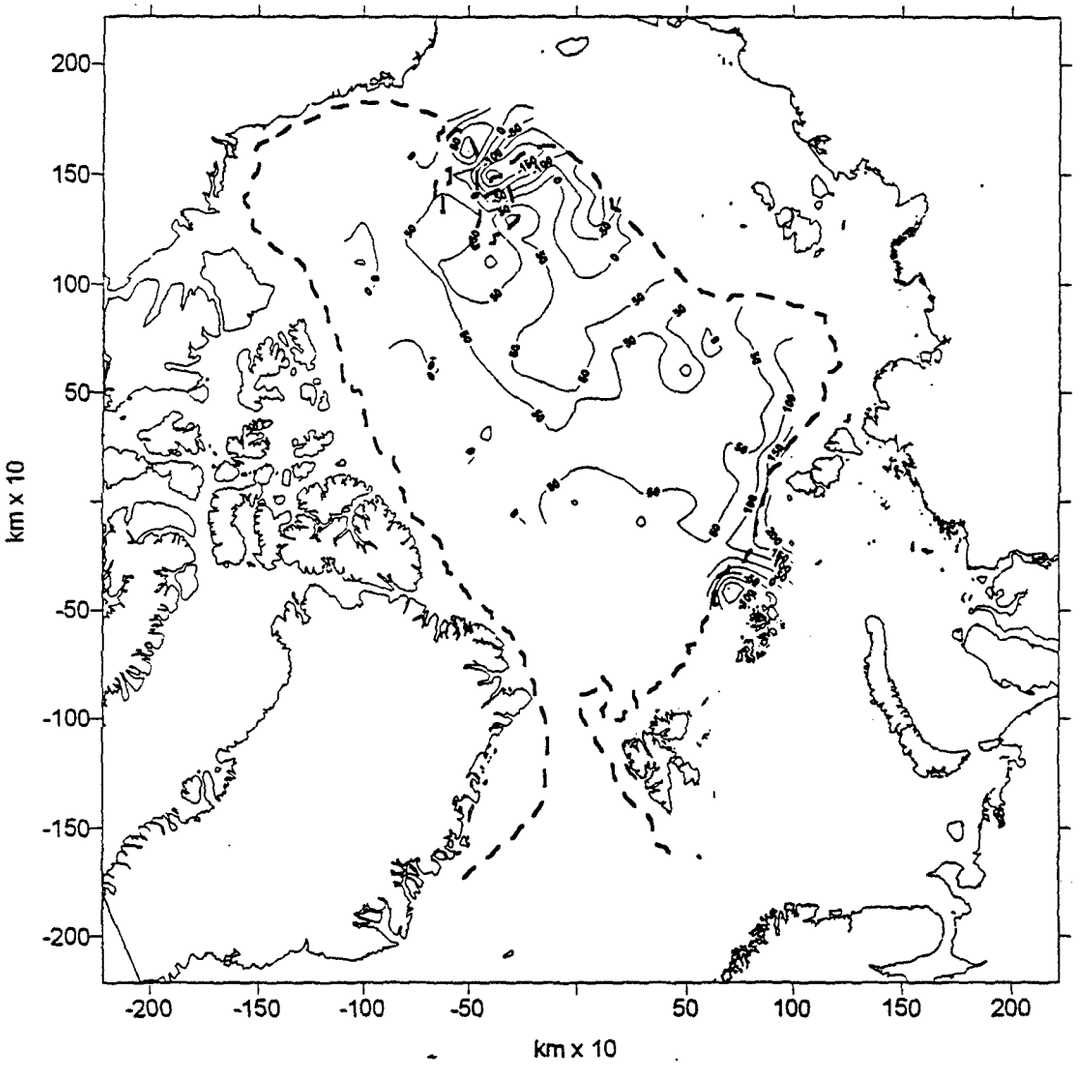

Fig. 35. Anomalies in the thickness of Atlantic water for 1973. The dashed line denotes the 1000 m isobath.

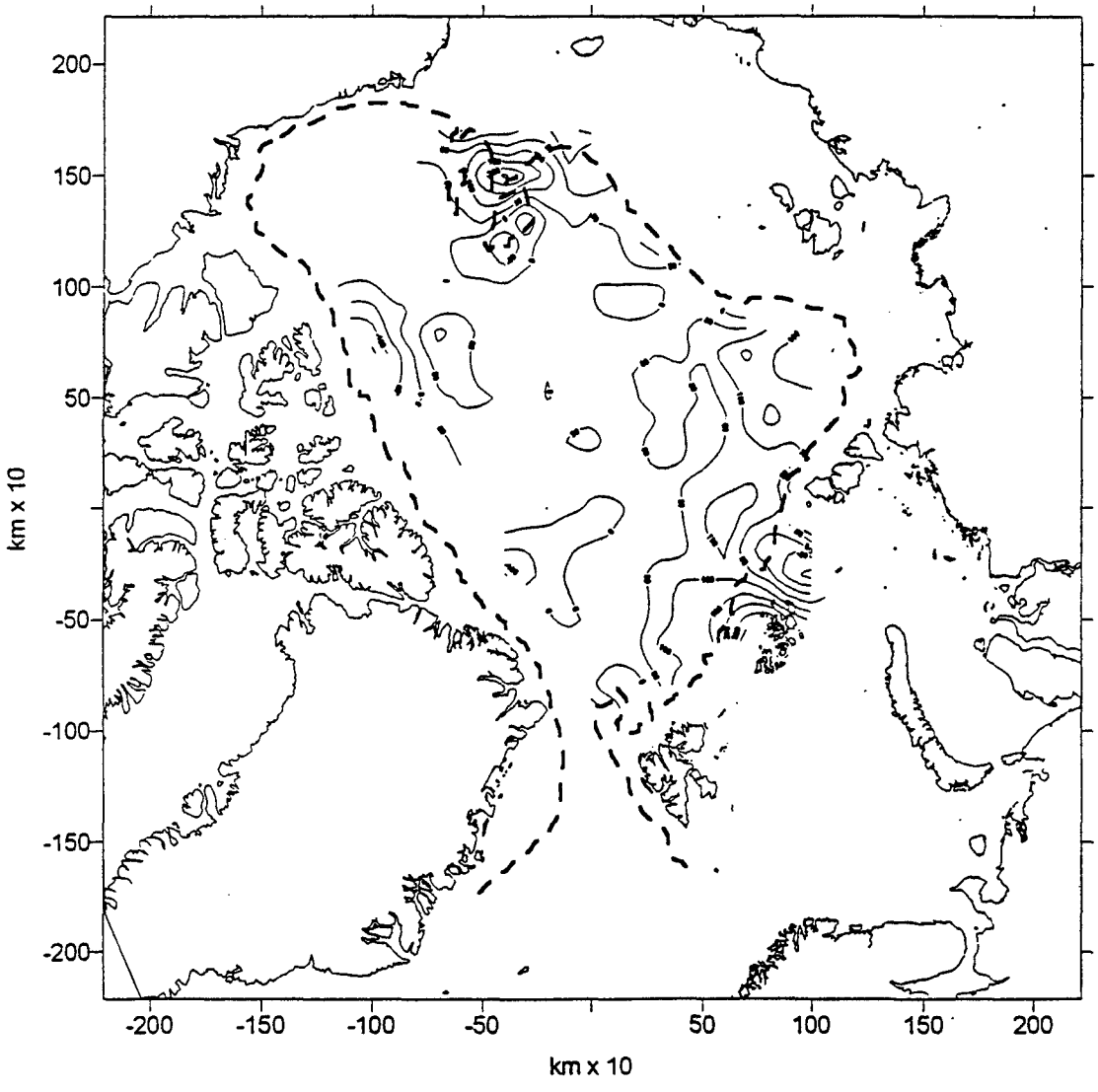

Fig. 36. Anomalies in the thickness of Atlantic water for 1974. The dashed line denotes the 1000 m isobath

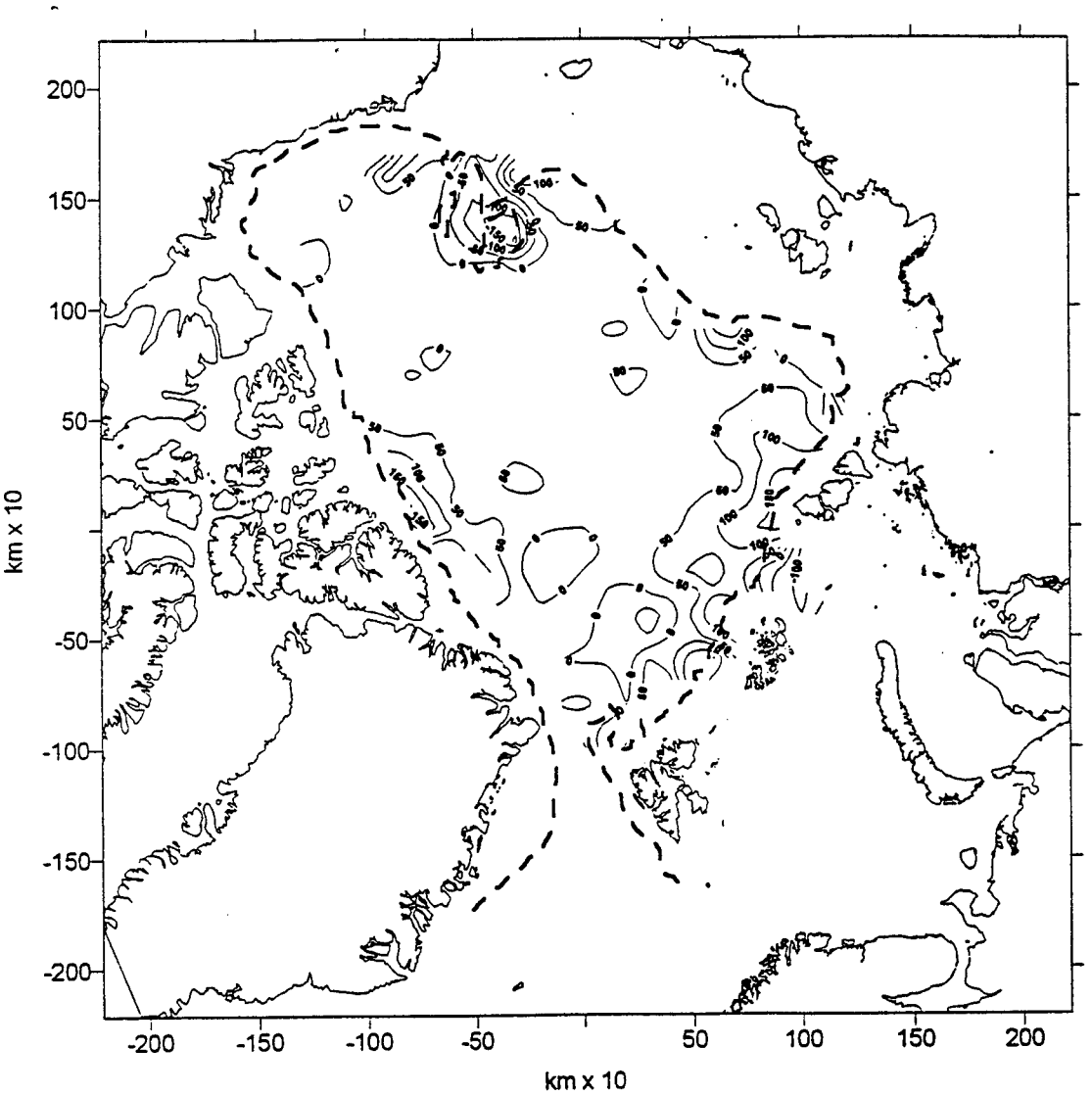

Fig. 37. Anomalies in the thickness of Atlantic water for 1975. The dashed line denotes the 1000 m isobath

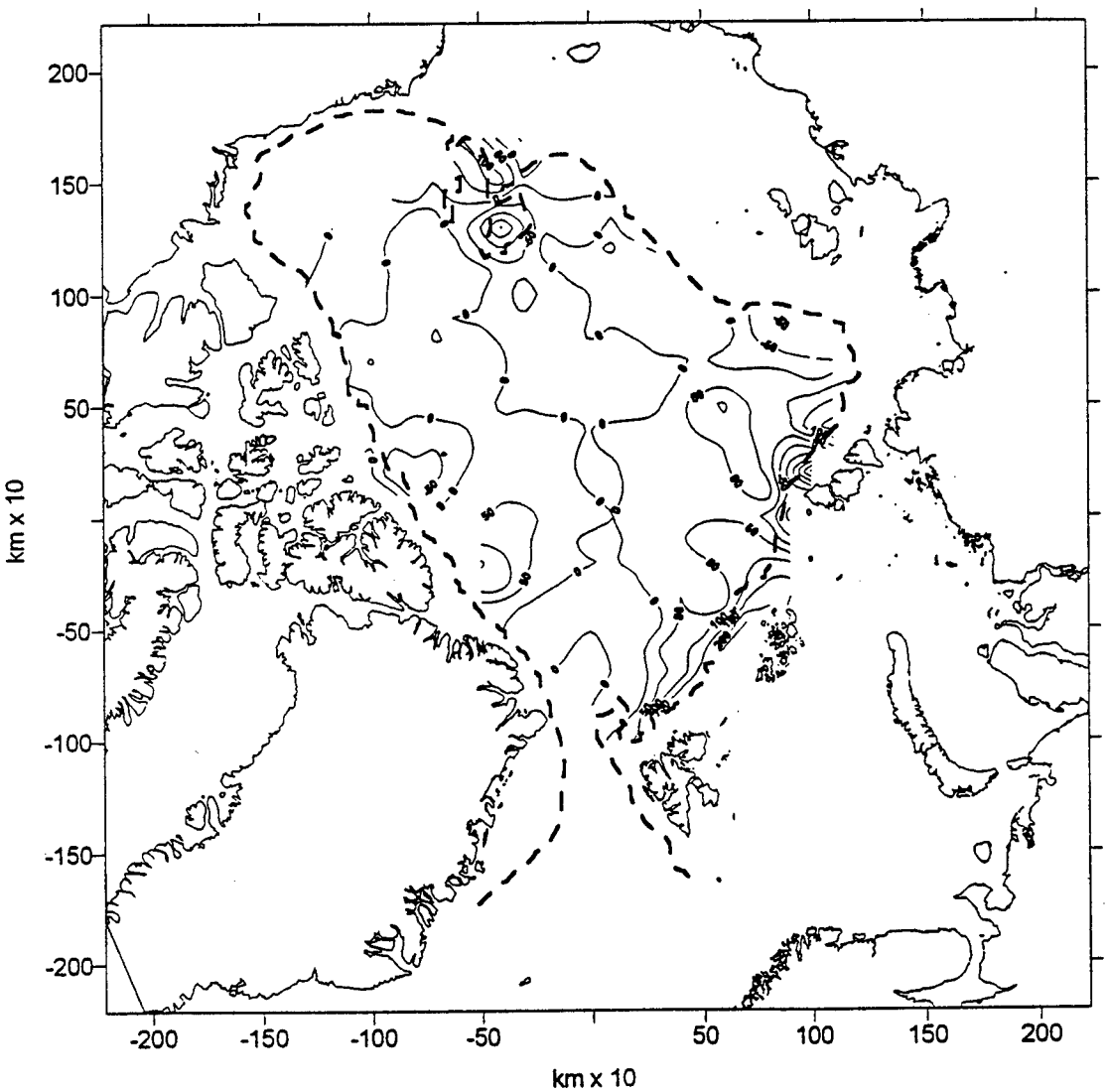

Fig. 38. Anomalies in the thickness of Atlantic water for 1976. The dashed line denotes the 1000 m isobath

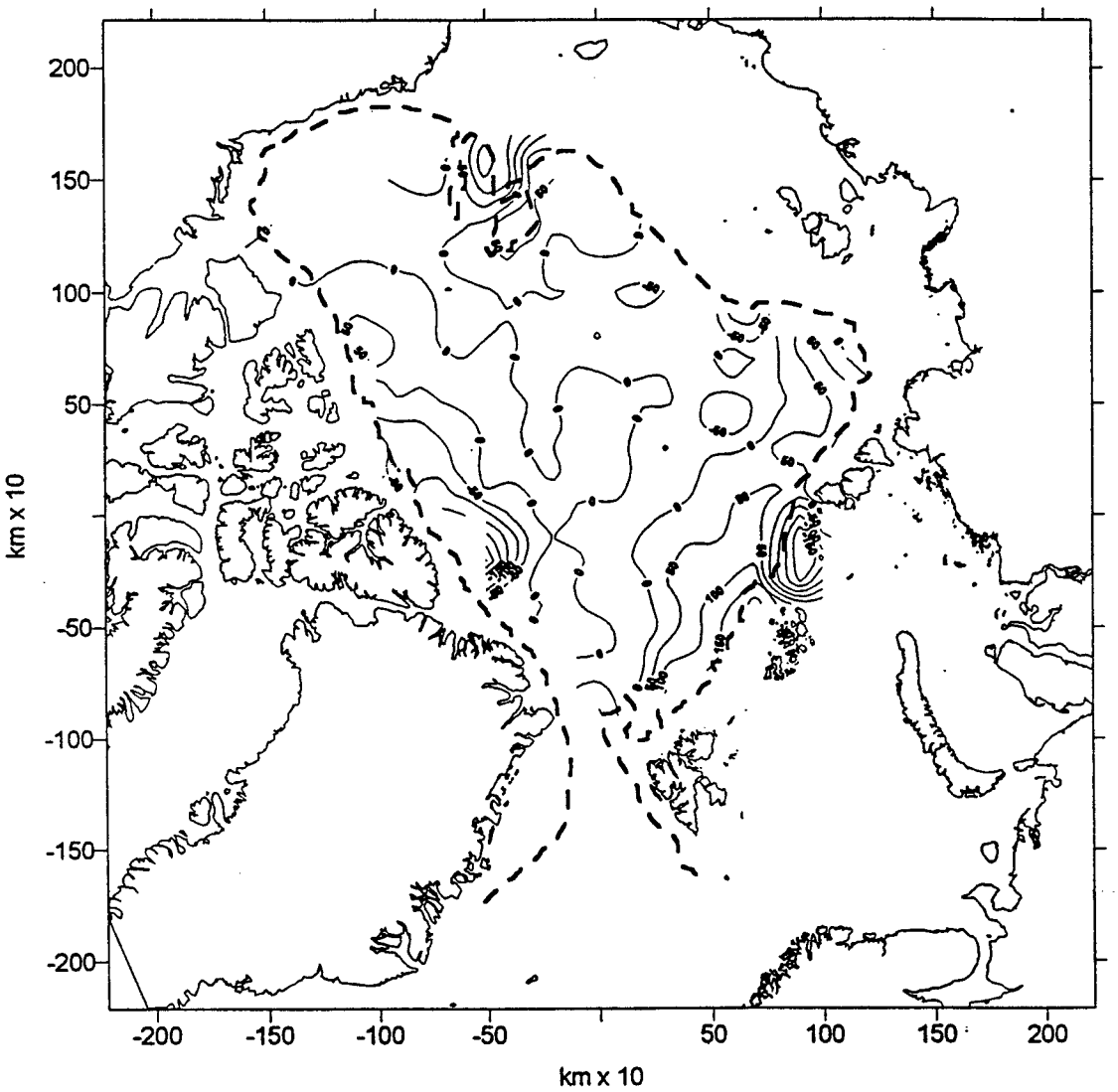

Fig. 39. Anomalies in the thickness of Atlantic water for 1977. The dashed line denotes the 1000 m isobath

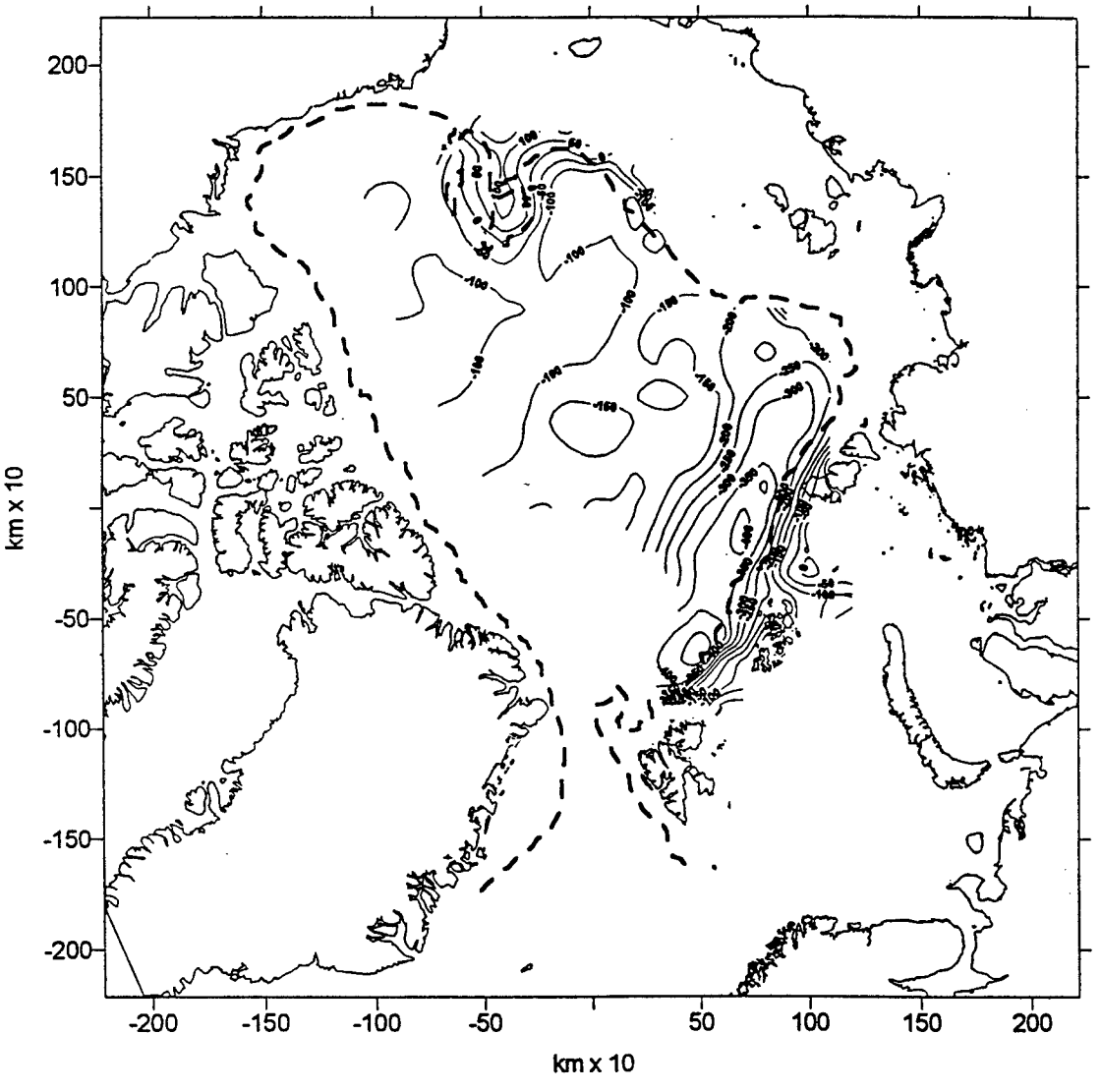

Fig. 40. Anomalies in the thickness of Atlantic water for 1978. The dashed line denotes the 1000 m isobath

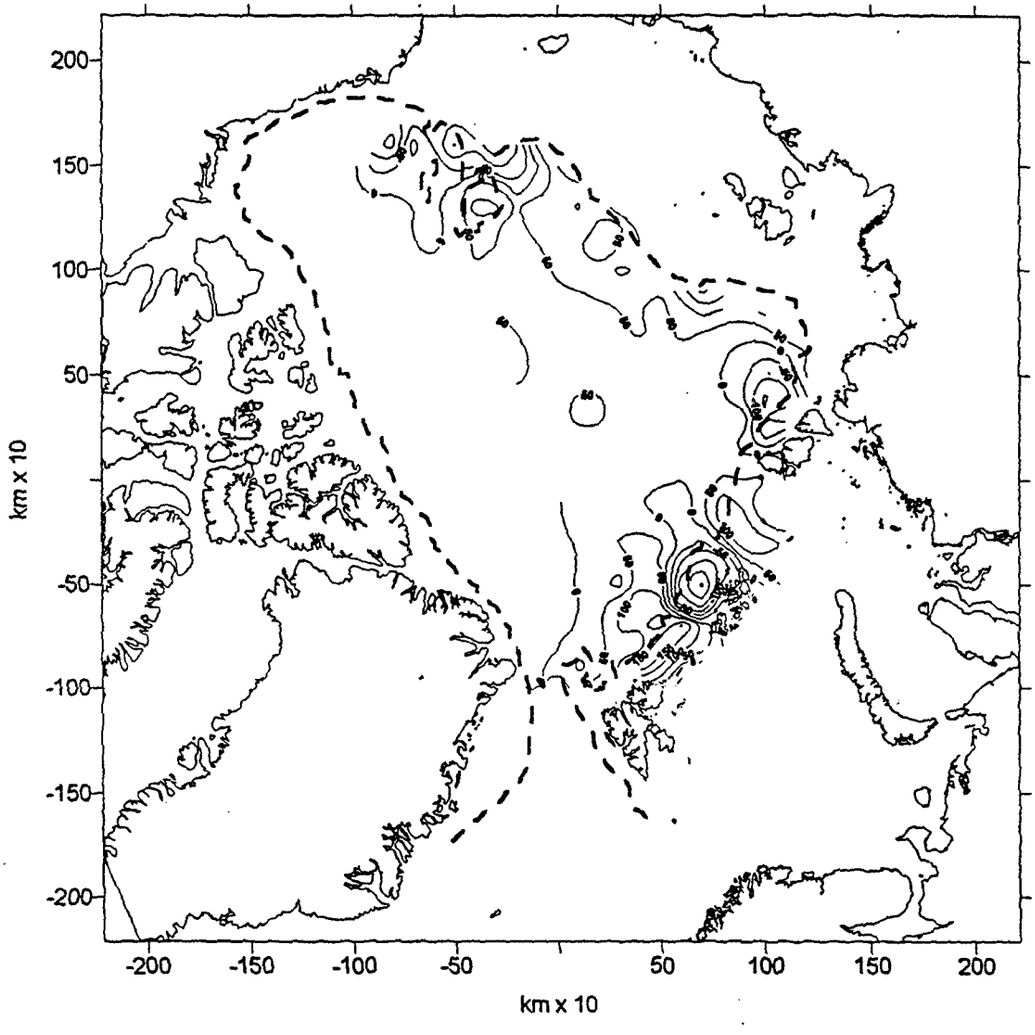

Fig. 41. Anomalies in the thickness of Atlantic water for 1979. The dashed line denotes the 1000 m isobath

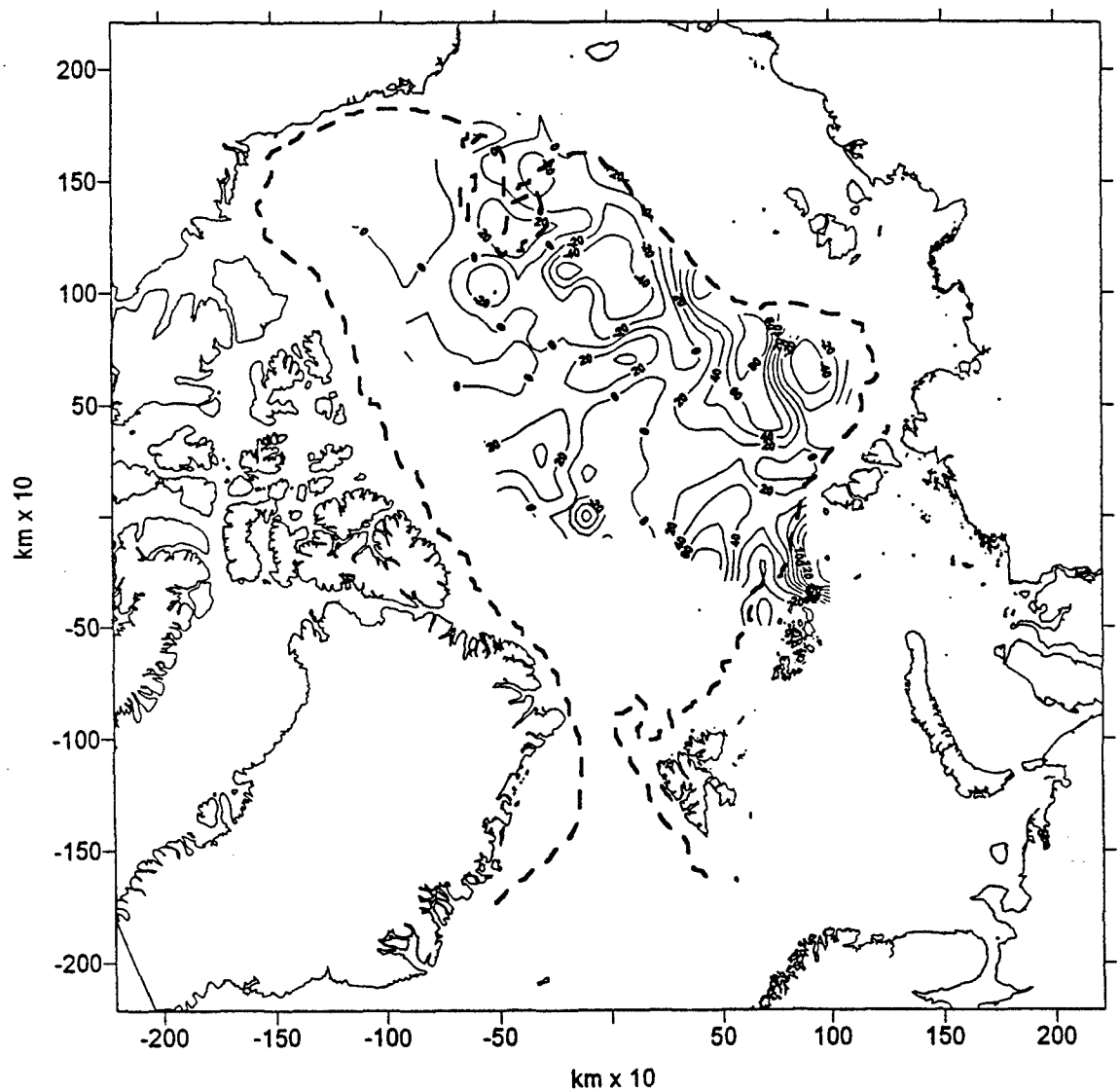

Fig. 42. Anomalies in the depth of the maximum temperature of Atlantic water for 1973. The dashed line denotes the 1000 m isobath.

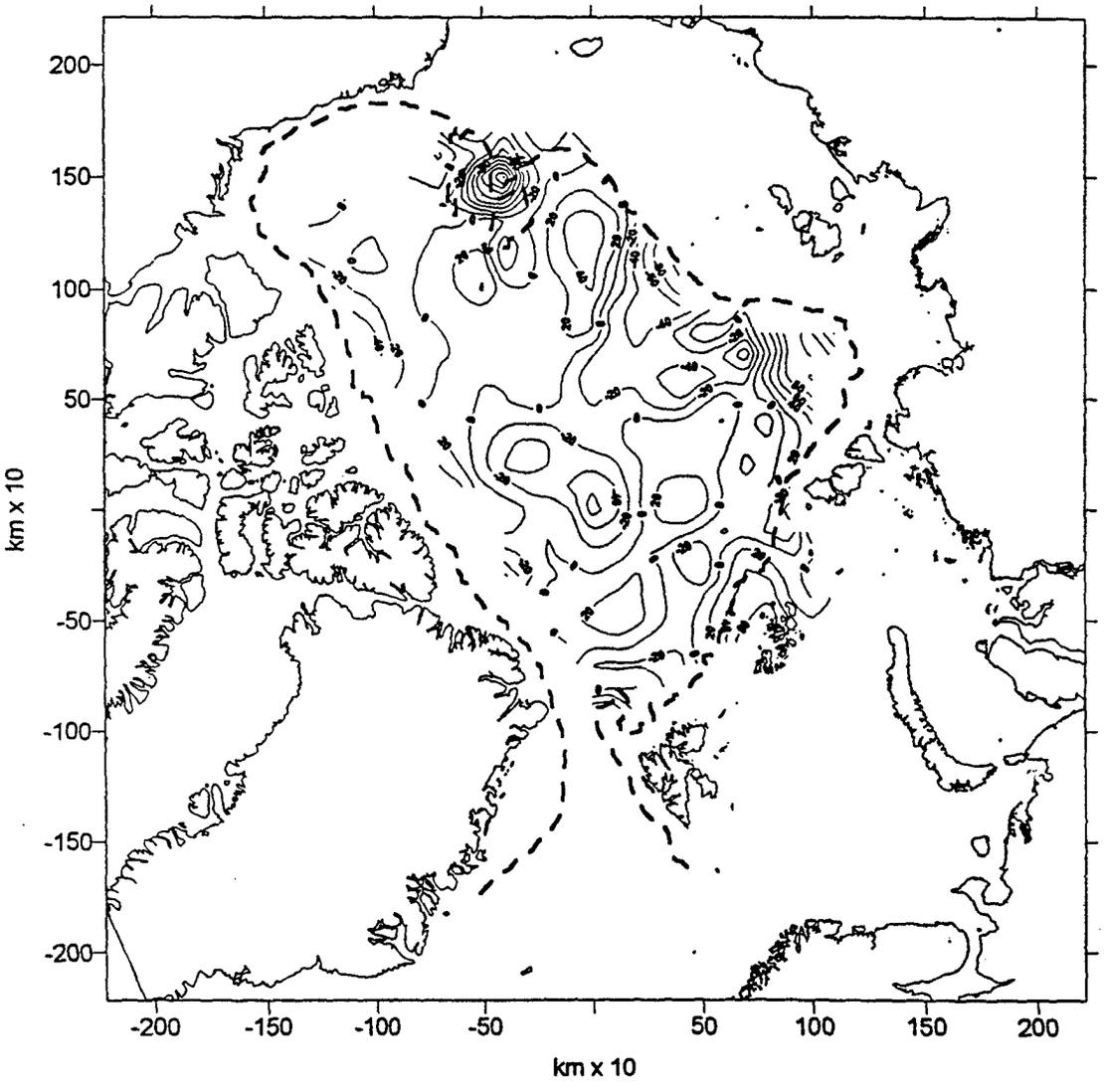

Fig. 43. Anomalies in the depth of the maximum temperature of Atlantic water for 1974. The dashed line denotes the 1000 m isobath

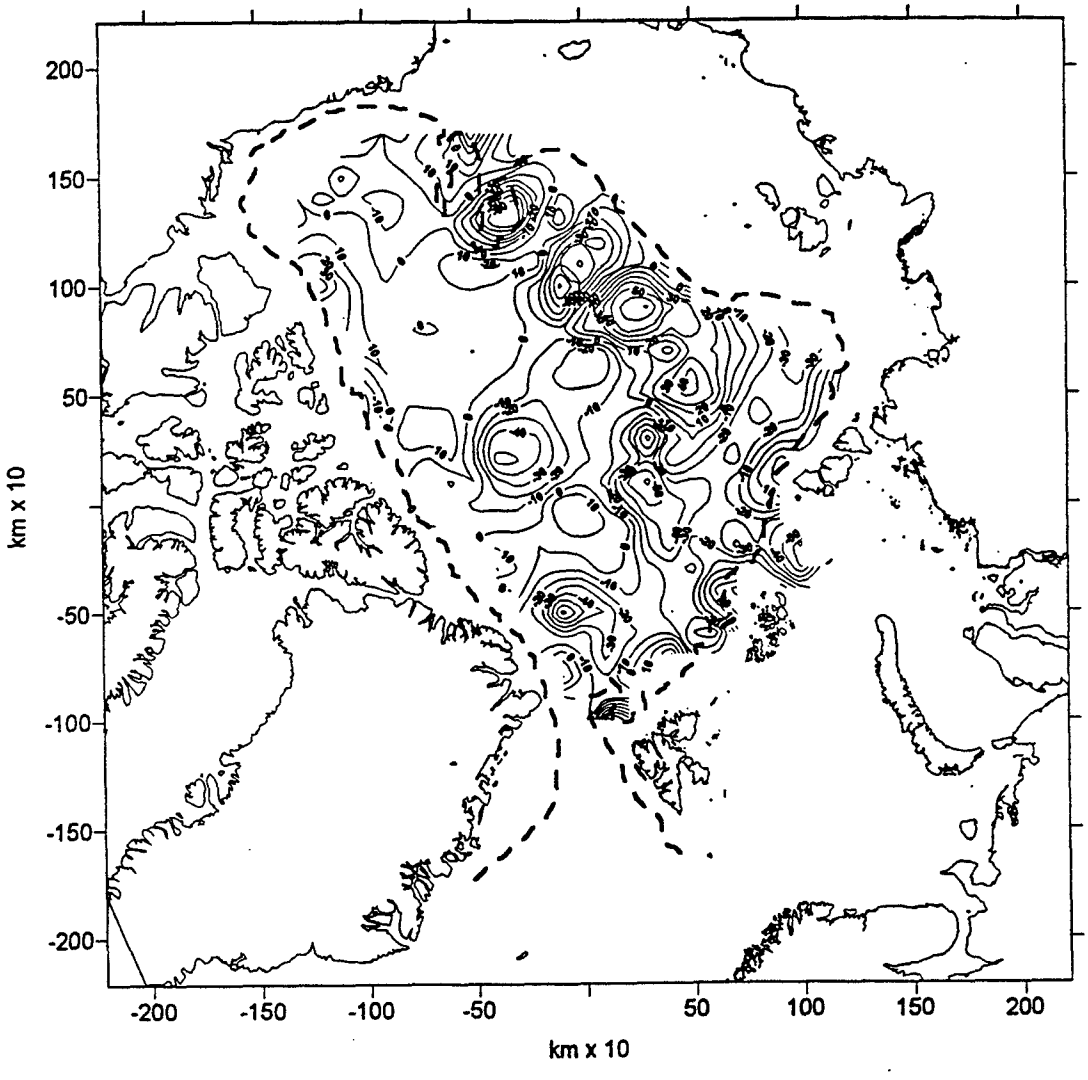

Fig. 44. Anomalies in the depth of the maximum temperature of Atlantic water for 1975. The dashed line denotes the 1000 m isobath

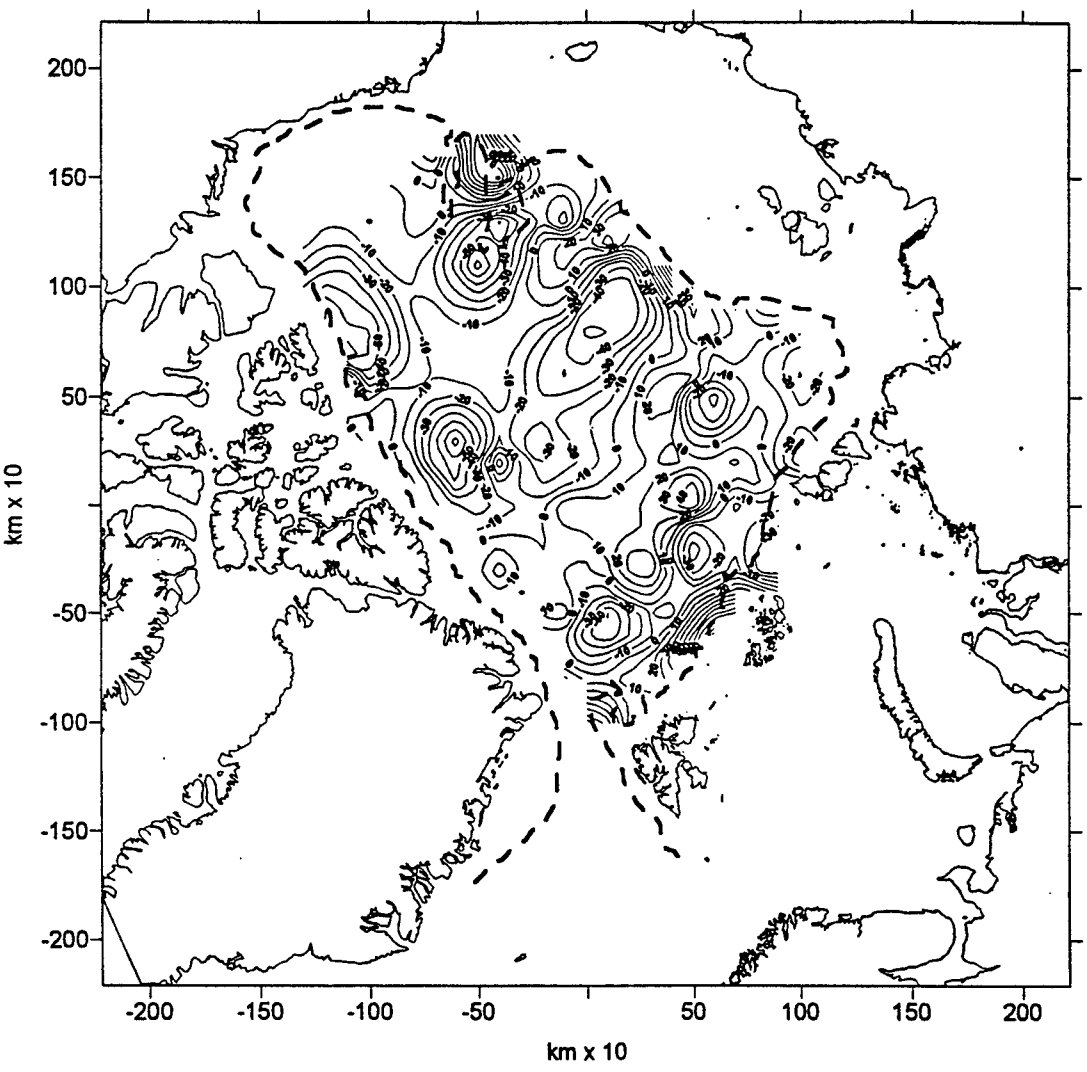

Fig. 45. Anomalies in the depth of the maximum temperature of Atlantic water for 1976. The dashed line denotes the 1000 m isobath

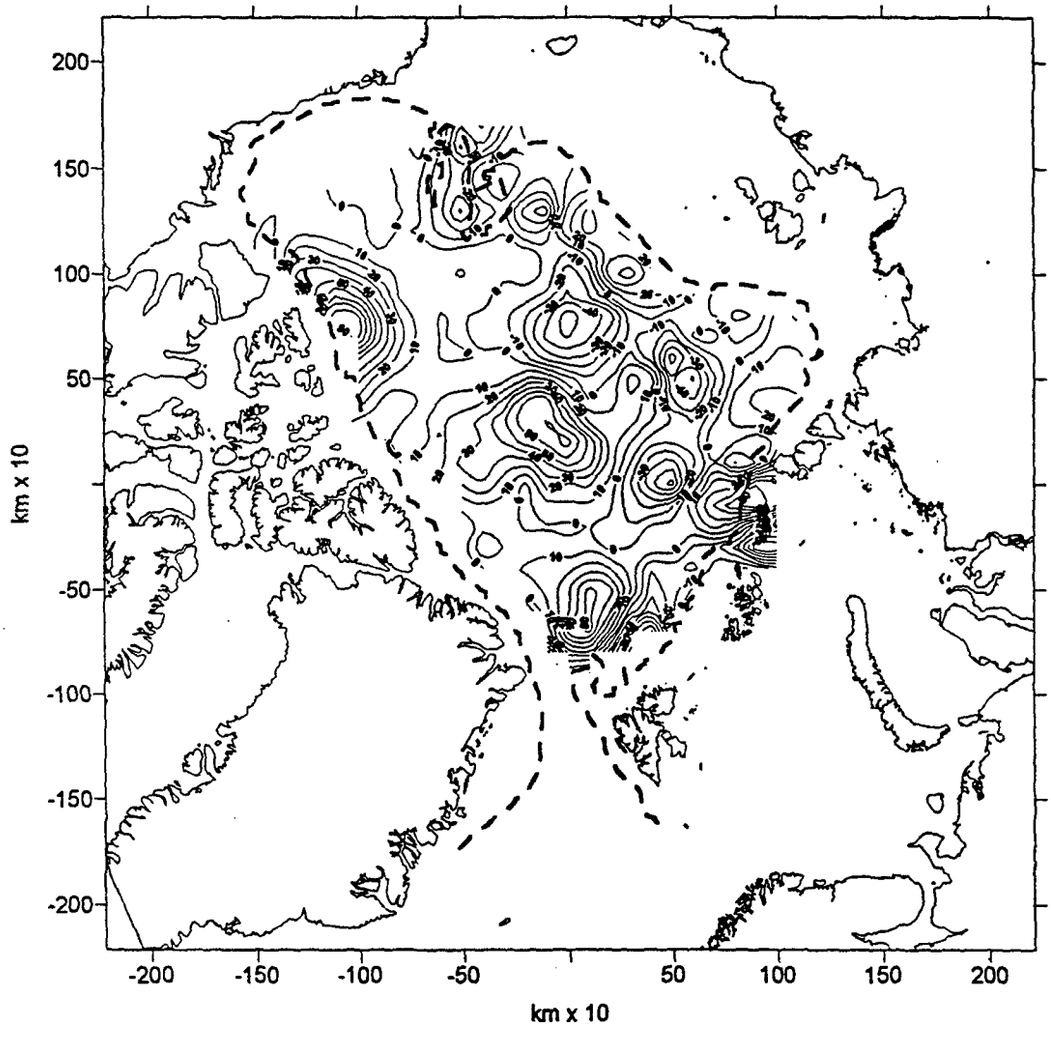

Fig. 46. Anomalies in the depth of the maximum temperature of Atlantic water for 1977. The dashed line denotes the 1000 m isobath

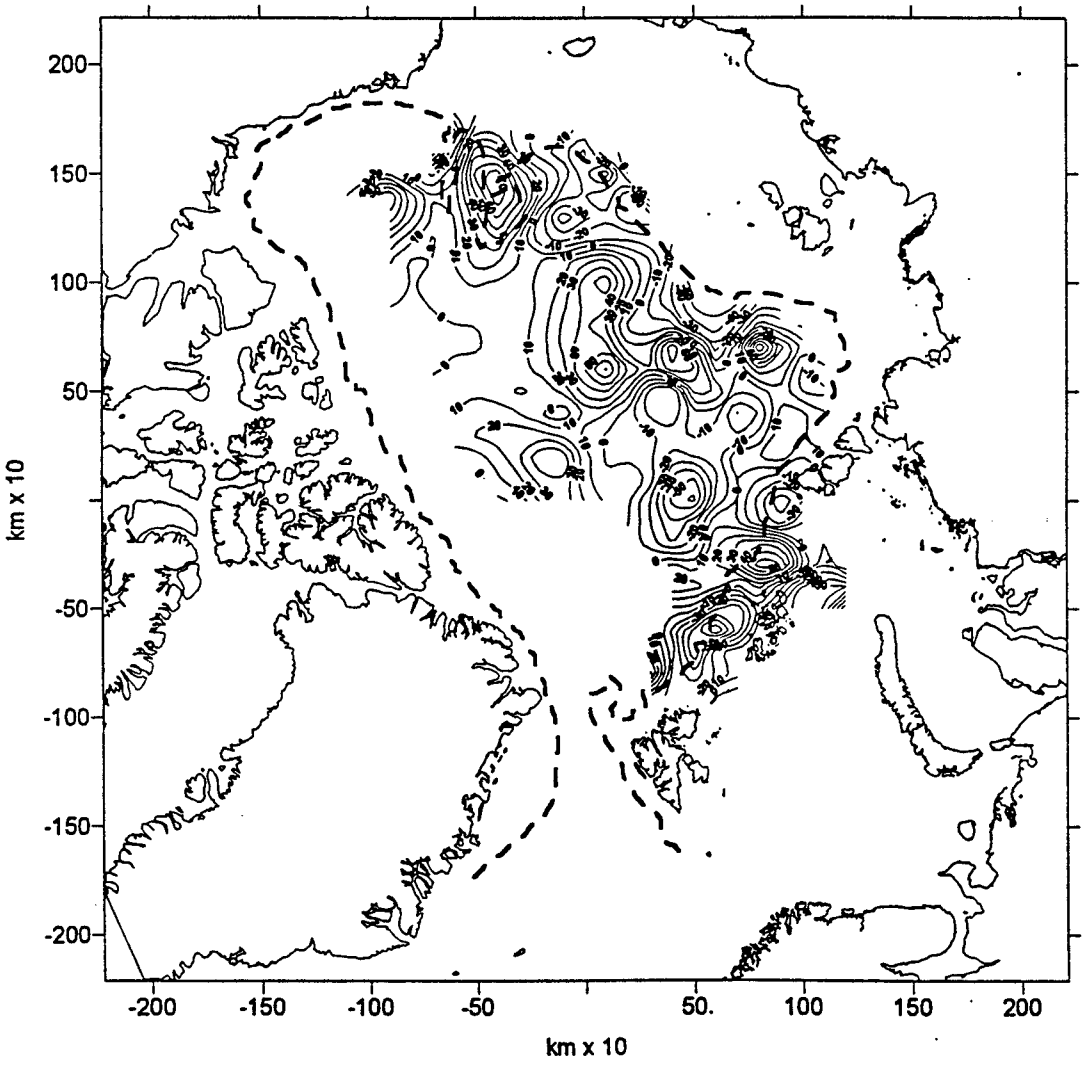

Fig. 47. Anomalies in the depth of the maximum temperature of Atlantic water for 1978. The dashed line denotes the 1000 m isobath

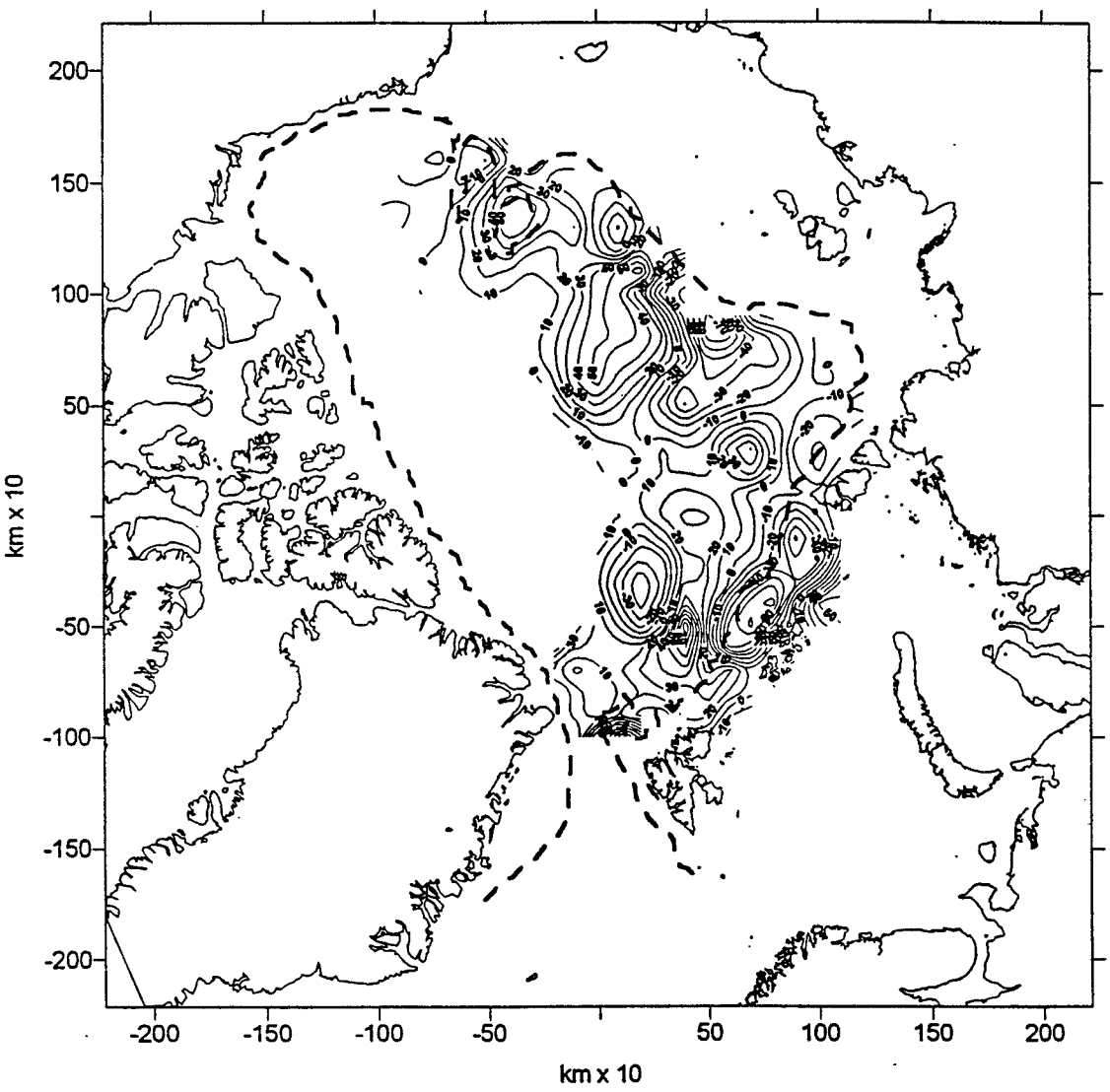

Fig. 48. Anomalies in the depth of the maximum temperature of Atlantic water for 1979. The dashed line denotes the 1000 m isobath

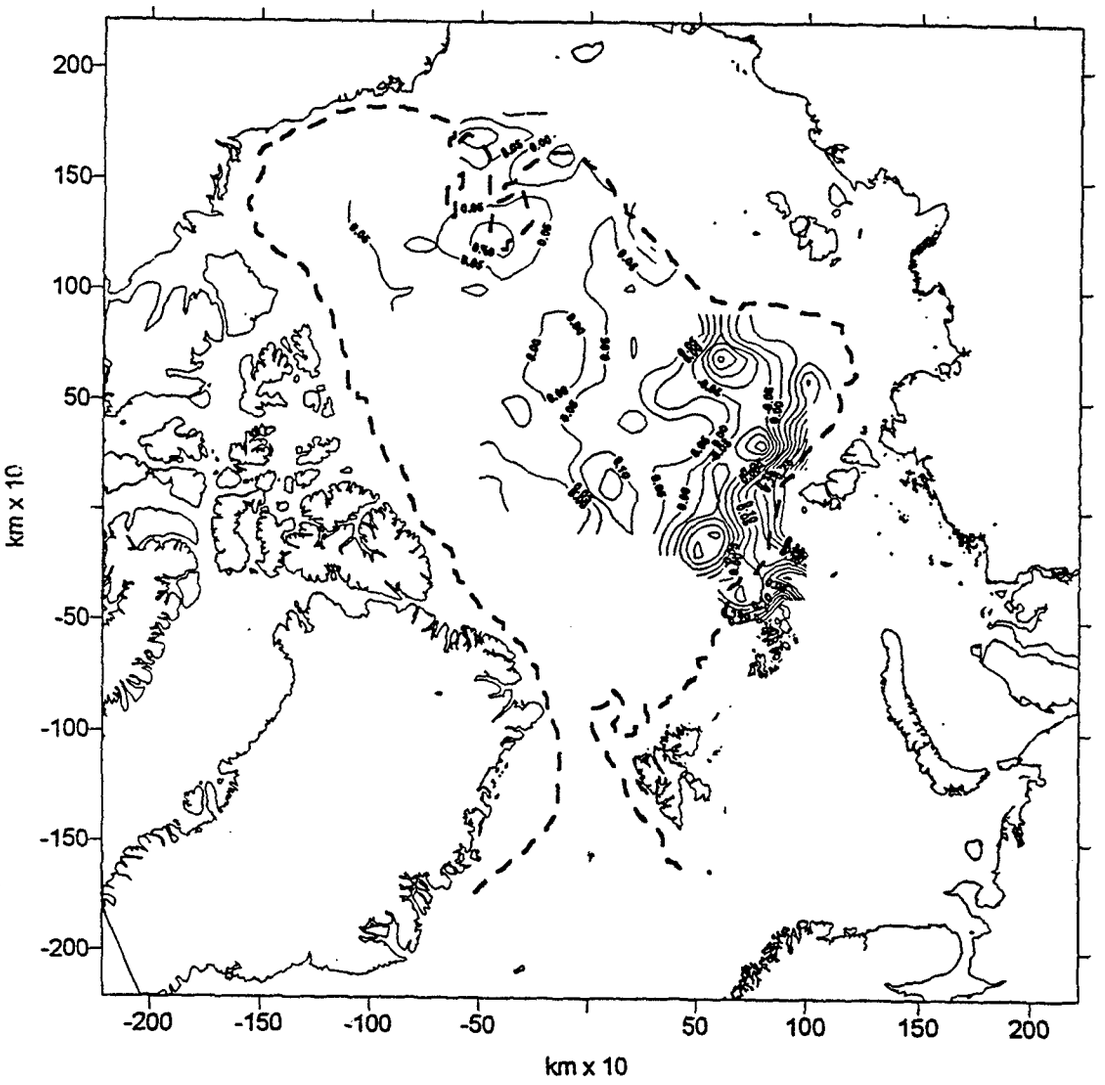

Fig. 49. Anomalies in the maximum temperature of Atlantic water for 1973. The dashed line denotes the 1000 m isobath.

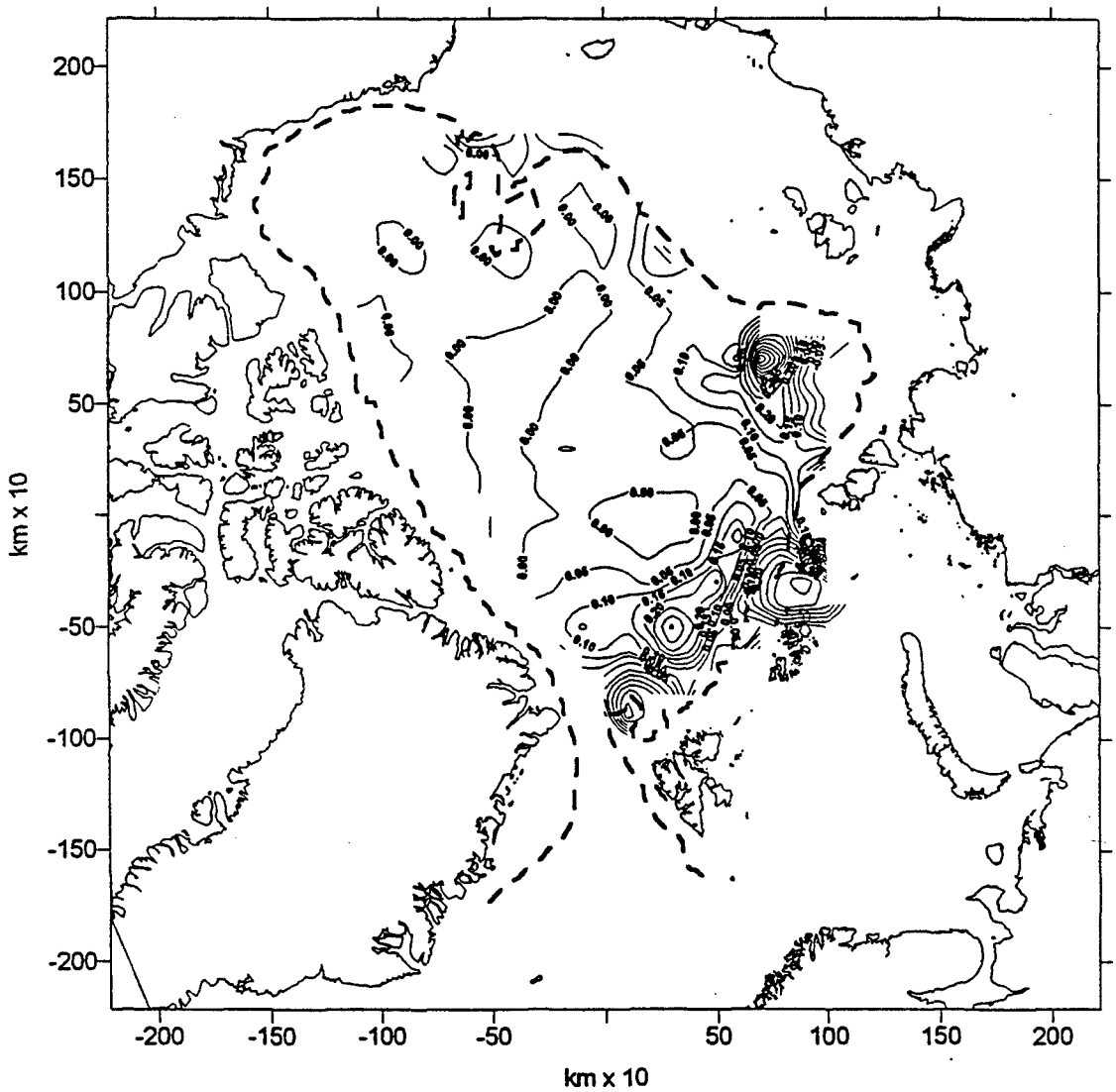

Fig. 50. Anomalies in the maximum temperature of Atlantic water for 1974. The dashed line denotes the 1000 m isobath.

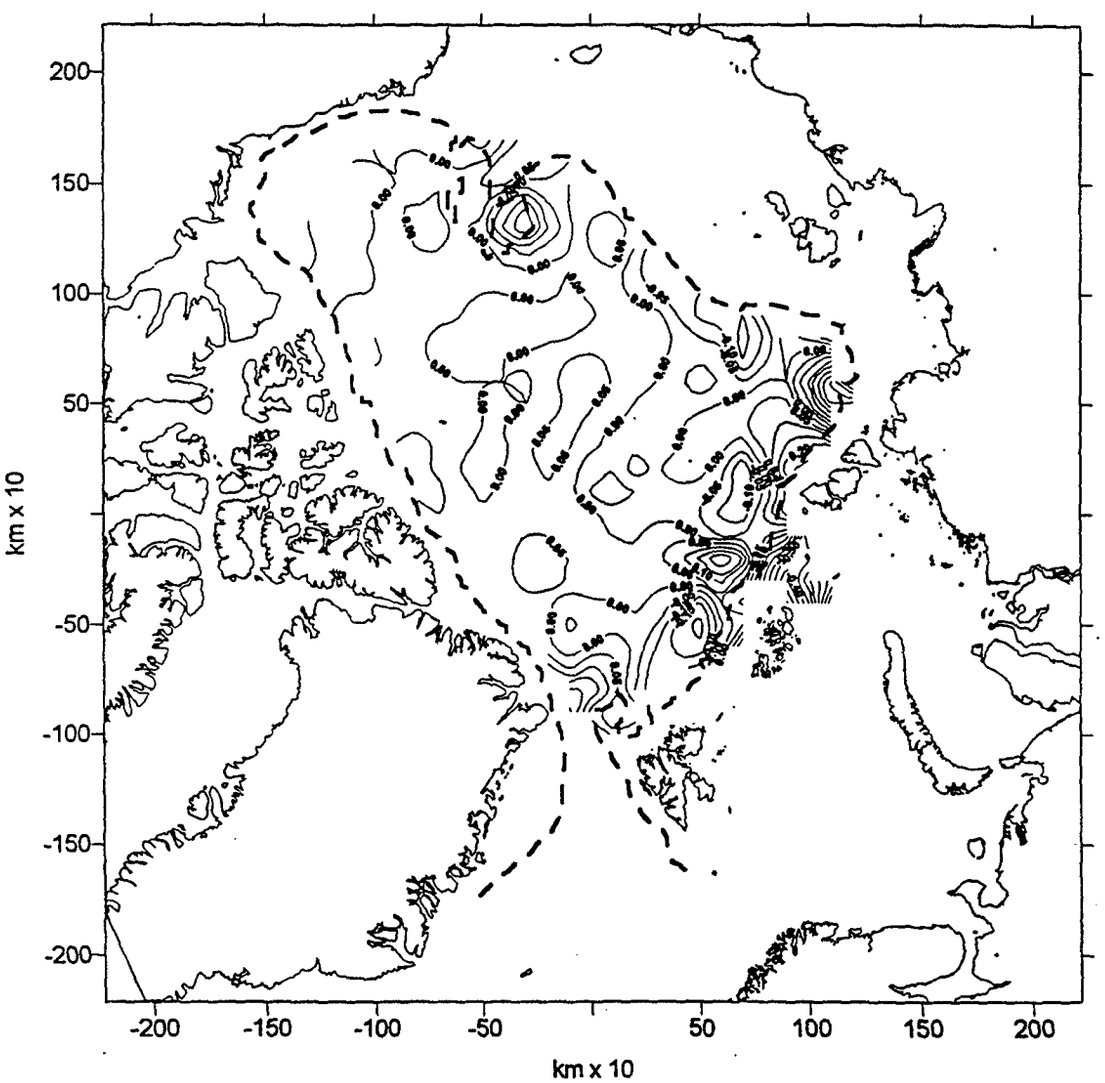

Fig. 51. Anomalies in the maximum temperature of Atlantic water for 1975. The dashed line denotes the 1000 m isobath.

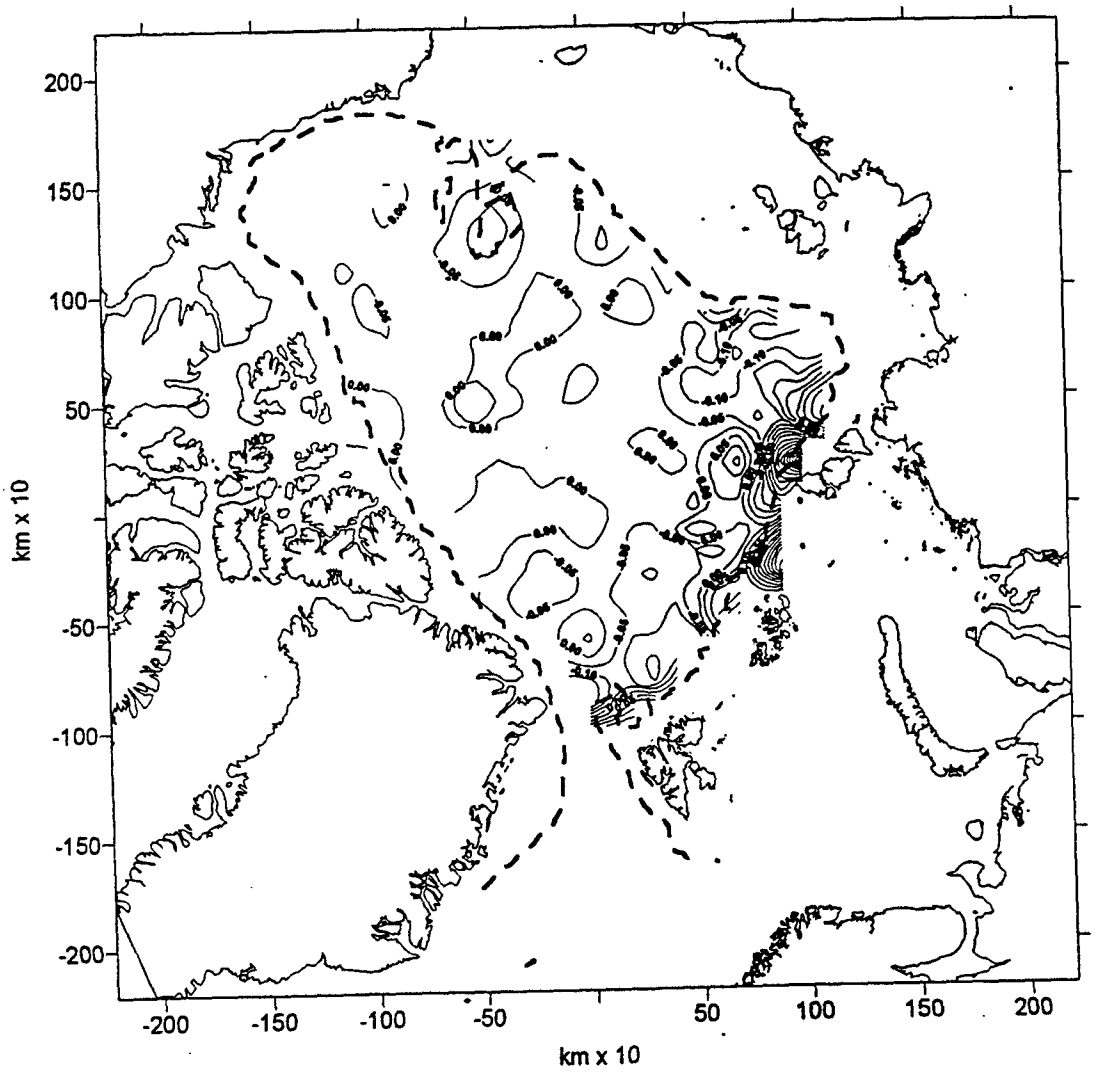

Fig. 52. Anomalies in the maximum temperature of Atlantic water for 1976. The dashed line denotes the 1000 m isobath.

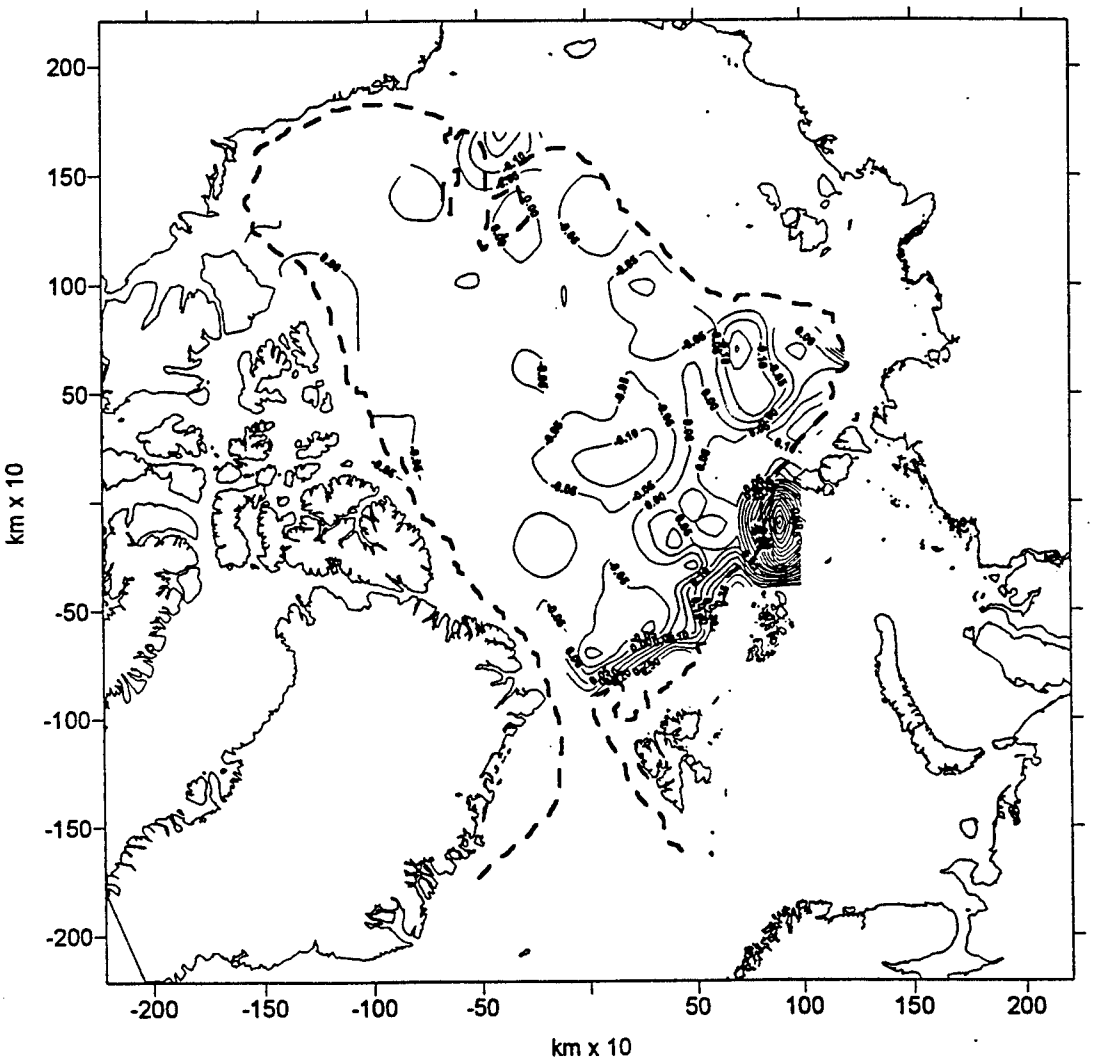

Fig. 53. Anomalies in the maximum temperature of Atlantic water for 1977. The dashed line denotes the 1000 m isobath.

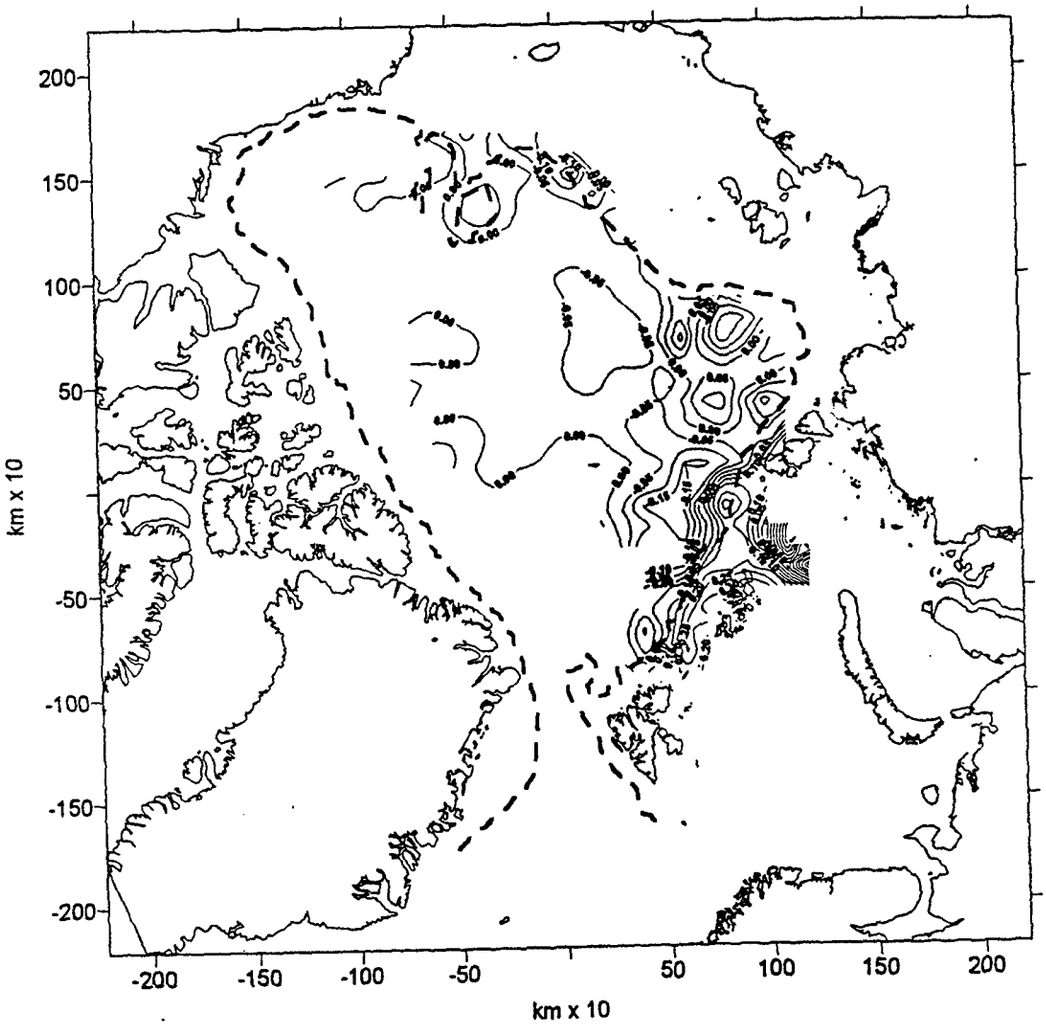

Fig. 54. Anomalies in the maximum temperature of Atlantic water for 1978. The dashed line denotes the 1000 m isobath.

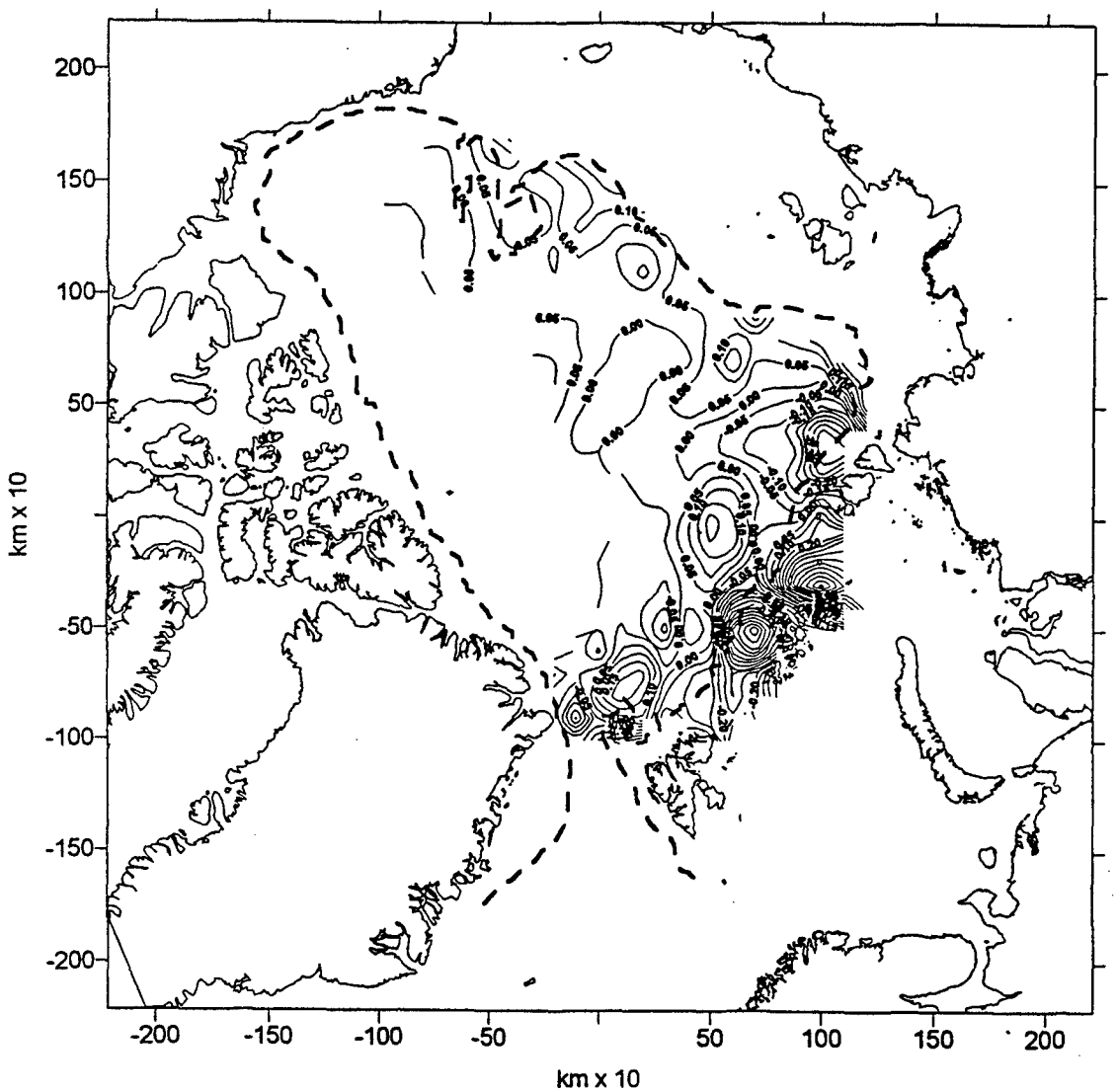

Fig. 55. Anomalies in the maximum temperature of Atlantic water for 1979. The dashed line denotes the 1000 m isobath.

PART II. MODELING OF OCEANOGRAPHIC FIELDS AND CIRCULATION IN THE ARCTIC OCEAN

1. Introduction

During the last decades scientists have become convinced that the interaction between the Arctic Ocean and the atmosphere plays an essential role in World climate variability, and this is one of the reasons why more and more papers have appeared attempting to model this process.

Previously, in the main body of scientific investigations on modelling of the global atmosphere, the Arctic Ocean has been considered as a simple mixed layer. Now, during the last pentad, the subject in many papers on modeling is the Arctic Ocean's surface layer. For brevity we shall mention only five papers, published in the last three years and then present a model and results of preliminary calculations, trying to imitate the effect of the increase of CO2 on the Arctic Ocean climatic characteristics.

There are interesting papers of Sirpa Hakkinen (1993,1995) devoted to an explanation of: The Great Salinity Anomaly (GSA), and Greenland Sea deep water formation under the influence of surface forcing. Her explanation of anomalously large ice transport through the Fram Strait, caused by intensive wind stress, as a source of GSA seems quite realistic. She has also shown that the interannual variability has a memory: deep convection in one year preconditions the following year. The author pays less attention to the problem of sensitivity of results to the chosen parameters.

Three serious investigations (William L. Chapman et. al. 1994, David M. Holland et. al. 1993 and D.Ramsden and G.Fleming 1995) pay quite detailed attention to the sensitivity of models to parameters. The authors of the last two papers tried, also, to imitate the ocean's upper layer's reaction to CO_2 doubling in the atmosphere. David M. Holland et. al. (1993) made numerous numerical experiments using dozens of parameters (some of them are so uncertain that values are in the range of 2 or 3 orders of magnitude) and showed that

the results are very sensitive to many of them, and what is more interesting is that they obtained the opposite reaction of the ocean to the variation of some parameters, compared with the investigations of other scientists. For example, Shine and Crane (1984) "concluded that on an annual basis clouds act to warm the surface and to reduce the ice thickness while our results are opposite".

One of the experiments of D.M.Holland et. al. (1993) and Semtner (1987) may be considered as an analog of the simulation of CO_2 doubling. These two experiments differ drastically: Semtner obtained an ice-free Arctic for the month of September, by increasing the atmospheric temperature by 2^oC while an increase by 5^oC in experiments by Holland et. al. did not lead to an ice-free Arctic, at any time during the seasonal cycle.

William L. Chapman et. al. (1994) chose a set of 13 parameters. They have shown that "interannual variability is a major contributor to the differences of ice thickness and extent over timescales of a decade or less". They discuss also the drawbacks of their modeling. The dependence of their results on parameter values and interdependence of sensitivities to various parameters seems to be convincing.

The last paper chosen by us for review is by D. Ramsden and G. Fleming (1995), in which the authors attempt to model the Arctic reaction to CO_2 doubling. We think that an excess of 10^oC of the atmospheric temperature, which was approved by the authors, is several times larger than it should be. Despite this the authors have shown that "the Arctic ice field appears to act as a regulator of climate change, rather than as an accelerator".

We have to add that none of these papers discuss the results of Arctic deep layer modeling. We have seen also that even very sophisticated Arctic sea-ice models give contradictory results. The validity of the Arctic ice-ocean models still depends on many uncertain parameters, and only some of them are reliable.

For these reasons we decided to attempt to model the whole domain of the Arctic Ocean using the observed temperature T, and salinity S data and to examine, on this basis, whether the results are sensitive to CO_2 doubling. For solving this problem we have, at our disposal, reliable T, S data (Polyakov and Timokhov, 1994). The relaxation of our model to these data would give synthetic "observed" climatic characteristics which are necessary both

for upper sea-ice modeling validation,and for assessment of the ocean's reaction to CO_2 doubling.

2. Basic Equations

The basic features of the model we are developing are as follows. The system of equations and boundary conditions (in common denotations) is:

$$\frac{\partial u}{\partial t}+\frac{u}{R\sin\theta}\frac{\partial u}{\partial \lambda}+\frac{v}{R}\frac{\partial u}{\partial \theta}+w\frac{\partial u}{\partial z}-(l-\frac{uctg\theta}{R})v=-\frac{1}{\rho_0 R\sin\theta}\frac{\partial P}{\partial \lambda}+Du \quad (1)$$

$$\frac{\partial v}{\partial t}+\frac{u}{R\sin\theta}\frac{\partial v}{\partial \lambda}+\frac{v}{R}\frac{\partial v}{\partial \theta}+w\frac{\partial v}{\partial z}+(l-\frac{uctg\theta}{R})u=-\frac{1}{\rho_0 R}\frac{\partial P}{\partial \theta}+Dv \quad (2)$$

$$\frac{\partial P}{\partial z}=\rho g \quad (3)$$

$$\frac{1}{R\sin\theta}\left(\frac{\partial u}{\partial \lambda}+\frac{\partial}{\partial \theta}(v\sin\theta)\right)+\frac{\partial w}{\partial z}=0 \quad (4)$$

$$\frac{\partial T}{\partial t}+\frac{1}{R\sin\theta}\frac{\partial}{\partial \lambda}(uT)+\frac{1}{R\sin\theta}\frac{\partial}{\partial \theta}(vT\sin\theta)+\frac{\partial wT}{\partial z}=D_T T+mix(T) \quad (5)$$

$$\frac{\partial S}{\partial t}+\frac{1}{R\sin\theta}\frac{\partial}{\partial \lambda}(uS)+\frac{1}{R\sin\theta}\frac{\partial}{\partial \theta}(vS\sin\theta)+\frac{\partial wS}{\partial z}=D_S S+mix(S) \quad (6)$$

$$\rho=\rho(T,S), \quad (7)$$

where turbulent exchange of momentum, heat and salt is parameterized, as follows:

$$D_*\varphi=\frac{\partial}{\partial z}\nu_*\frac{\partial \varphi}{\partial z}+\frac{1}{R^2\sin\theta}\left(\frac{1}{\sin\theta}\frac{\partial}{\partial \lambda}\mu_*\frac{\partial}{\partial \lambda}+\frac{\partial}{\partial \theta}\mu_*\sin\theta\frac{\partial \varphi}{\partial \theta}\right).$$

Note, that the coefficients ν,ν_T,ν_S *etc.* may be nonlinear functions of the velocity components and density, as suggested by Pacanowski and Philander, 1981, for vertical mixing, and by Smagorinsky, 1963, for horizontal mixing. The vertical instantaneous adjustment process of temperature and salinity convection in the case of an unstable density profile is described by the *mix(*)* operator, which is essentially a numerical procedure.

Boundary conditions are as follows:
at the upper boundary $z=0$, momentum fluxes due to wind stress and ice dynamics

$$\rho_o\nu(z)\frac{\partial u}{\partial z}=-\tau^{(\lambda)}, \qquad \rho_o\nu(z)\frac{\partial v}{\partial z}=-\tau^{(\theta)}$$

and the linearized kinematic condition

$$w = -\frac{\partial \zeta}{\partial t}$$

are specified.

Here

$$\tau^{(\lambda)} = A\tau_i^{(\lambda)} + (1-A)\tau_a^{(\lambda)}, \qquad \tau^{(\theta)} = A\tau_i^{(\theta)} + (1-A)\tau_a^{(\theta)},$$

the index "i" means ice and "a" means air, "A" is the compactness of the ice, and stresses τ are computed by the commonly used quadratic bulk formulae.

As for temperature and salinity, heat and salt fluxes

$$\mu_T \frac{\partial T}{\partial z} = Q_T, \quad \mu_S \frac{\partial S}{\partial z} = Q_S$$

are specified. At the ice free parts of the boundary, heat and salt fluxes are specified, as usual. The heat flux is composed of long-wave and short-wave radiation components and of latent and sensible heat. If a part of the area is covered by ice, then

$$Q_S = S\frac{\partial h}{\partial t}$$

where h is the mean ice thickness. The water temperature beneath the ice should be set equal to the temperature of the freezing of sea water. In the case of the preliminary adjustment calculations we will fix the temperature and salinity at the upper boundary.

At the bottom $z = H(x,y)$ static

$$u = v = w = 0$$

and heat/salt isolation conditions

$$\nu_T \frac{\partial T}{\partial z} = 0, \quad \mu_S \frac{\partial S}{\partial z} = 0$$

are assumed to be valid.

The side boundary σ should be divided into two parts: the solid boundary and the liquid one. At the solid boundary (i.e. on land), the motionless condition for 2D velocity $(u,v) = (0,0)$ and the heat/salt isolation, are specified. As for the liquid boundary, we usually set some values of velocities u, v and temperature and salinity which are taken either from simplified models or from observations.

The system of equations and boundary conditions should be accompanied by some initial conditions. For climate simulation they are usually assumed to be motionless and of zero sea level elevation.

Because in the Arctic Ocean the geographical coordinate system is not applicable because of the pole, we have to choose some other coordinate frame. There are two ways to overcome this difficulty. The first is to shift the pole to some sufficiently distant location, and the second one is to use a stereographic coordinate system. The last approach produces significant errors far from the pole and the model area cannot be expanded further to the Atlantic and Pacific, so we chose the first way.

3. General description of the numerical procedure.

The numerical procedure is based on the finite element spatial discretization and a modified "leap-frog" time scheme.

Spatial discretization

The spatial discretization is performed by the finite element method (FEM). The finite elements are chosen to be right triangular prisms, with their apices at the intersection of the planes $\lambda = \lambda_i$, $\theta = \theta_j$ and $z = z_k$. Cathetuses of the triangles are parallel to coordinate axes and hypotenuses are directed from south-west to north-east. The approximation of the area we will denote as Ω^h, and the intersection of Ω^h and the plane $z=0$ we will denote as Ω_0^h. Probe (or basis) functions are chosen in the form of tensor products of 2D $\varphi_{i,j}(\lambda,\theta)$ and 1D $\psi_k(z)$ finite linear piecewise functions (so called Courant functions). The components of the vector of solution are searched as a sum

$$\Phi^h = \sum_{i,j,k} \Phi_{i,j,k} \varphi_{i,j} \psi_k$$

Time scheme

As a time scheme, a version of the "leap-frog" scheme with pressure gradients implicitly described is used

$$G\frac{\Psi^{n+1} - \Psi^{n-1}}{2\Delta t} + L^n\Psi^n + C\Psi^n = -\frac{1}{\rho_0}\nabla P^{n+1} + D\Psi^{n-1},$$

where vector $\Psi = (u^h, v^h)$, operator G is the Gram matrix for the probe functions, L^n is the discrete approximation of the advection operator at the n-th time step, C is the approximation of the Coriolis acceleration, ∇ is the discrete 2D gradient operator, D is the discrete operator of the turbulent mixing and Δt is the time step. The Matsuno (a kind of predictor-corrector) scheme is used periodically to filter false numerical oscillations, the same scheme as is used at the very first time step.

Temperature and salinity are calculated by the analogous scheme.

Sea level elevation equation

For the efficiency of the numerical procedure the mass-lumping method is used, wherever it possible. This method leads to the explicit formulae for the velocity, temperature and salinity coefficients with no inversion of the Gram matrix. For example, the velocity coefficients $u_{i,j,k}^{n+1}$, $u_{i,j,k}^{n+1}$ may be determined as follows

$$u_{i,j,k}^{n+1} = -\alpha a_{i,j,k}^{-1} \int_{\Omega^*} \frac{1}{R\sin\theta} \frac{\partial \zeta^h}{\partial \lambda} \varphi_{i,j} \psi_k d\Omega^h + \alpha a_{i,j,k}^{-1} R_{i,j,k}^{(1)},$$

$$v_{i,j,k}^{n+1} = -\alpha a_{i,j,k}^{-1} \int_{\Omega^*} \frac{1}{R} \frac{\partial \zeta^h}{\partial \theta} \varphi_{i,j} \psi_k d\Omega^h + \alpha a_{i,j,k}^{-1} R_{i,j,k}^{(2)},$$

where $a_{i,j,k} = R^2 \sin\theta_j \int_{\Omega^*} \varphi_{i,j} \psi_k d\lambda d\theta dz$, and $R_{i,j,k}^{(1)}, R_{i,j,k}^{(2)}$ are known functions of the density and velocity components at time steps n+1, n and n-1, and α is equal to Δt for the Matsuno time scheme and to $2\Delta t$ for the "leap-frog" scheme.

As an integral function, we use sea surface level (SSL) in the model. The choice of the SSL enables us to solve the problem in any multi-connected area. But most important is the fact that SSL is formed primarily by the density at the upper layers, which is quite the opposite in the case of the total mass transport (Sarkisyan, 1995)

To construct the equation for the SSL the coefficients $u_{i,j,k}^{n+1}$, $v_{i,j,k}^{n+1}$ are substituted into the discrete integral continuity equation

$$-\frac{1}{\Delta t}(\zeta_{i,j}^{n+1} - \zeta_{i,j}^{n}) \int_{\Omega_0^*} \varphi_{i,j} d\Omega_0^h + R \int_{\Omega^*} \left[(u^h)^{n+1} \frac{\partial \varphi_{i,j}}{\partial \lambda} + (v^h)^{n+1} \frac{\partial \varphi_{i,j}}{\partial \theta} \sin\theta \right] dz d\lambda d\theta = \Phi_{i,j},$$

where the right hand side $\Phi_{i,j}$ is due to mass fluxes through the side boundaries. It is easy to show, that for the chosen time scheme the matrix of the algebraic problem for the coefficients $\zeta_{i,j}^{n+1}$ is symmetrical and positively defined. To solve the problem for sea level a combination of the Sequence OverRelaxation method (SOR) and the Conjugate Gradients (CG, with diagonal preconditioner) method, is applied. As a result, in the case of 50 iterations of SOR with the relaxation parameter =1.5 and 80 iterations of CG the mean-square error of the vertical velocity at the ocean surface is about 10^{-9}cms-1.

4. Some aspects of the Arctic area spatial approximation

In the model used for the project we use a special system of coordinates. In this coordinate system the new "North pole" is placed at the equator at 180 longitude. This means that we may use a spherical coordinate system for the polar region. We chose, in the new coordinates, the 1x1 spatial resolution, or approximately 111.2 km mesh size at the North pole. The vertical structure is described by 16 vertical levels: 0, 10, 25, 50, 100, 150, 200, 250, 300, 400, 500, 750, 1000, 2000, 3000 and 4000m. These levels were chosen from analysis of the vertical structure of temperature and salinity at the North pole.

The problem of the area approximation is that for such a comparatively coarse grid it is very difficult to describe narrow passages, for example the Lena Trough. On the other hand, through this zone the warm intermediate Atlantic Water enters the Arctic, forming the specific temperature profile of the basin. We may even say, that the formation of this intermediate water is the main point of the project. The problem of adequate area approximation is extremely important for the model under consideration, where the non-slip condition for velocity at the bottom is specified.

There are two general approaches in dealing with the problem of narrow passages.

1) The mesh refinement in the area of the passage. Usually this is performed by shifting the North pole to some point in Canada, or even in Greenland. This trick was used in the Arctic model by Hakkinen and Mellor (1992) and in the Atlantic-Arctic model by Semjonov (personal communication).
2) If the spatial resolution in the model is almost uniform and about 100km, then the narrow passages should be approximated not simply geometrically, but according to their role in the

water mass formation processes. This means that the principal passages have to be extended to describe the complex system of currents flowing through these passages. According to our understanding, this approach is used in the large-scale model by Semtner, 1987. We will follow this method of area approximation.

5. Choosing turbulent diffusion coefficients

The choice of the turbulent mixture coefficients for momentum depends on the Ekman layer scales. For vertical Ekman layer thickness, D, and for the horizontal one, L, we have

$$D = \pi\left(\frac{2\nu}{l}\right)^{\frac{1}{2}}, \qquad L = \pi\left(\frac{2\mu}{l}\right)^{\frac{1}{2}}.$$

To describe the vertical Ekman layer on the model grid we have to choose a vertical coefficient ν not less than 40 cm^2s^{-1} and the as for horizontal coefficient, it should be not less than 2.10^8 cm^2s^{-1}. As for temperature and salinity turbulent mixing coefficients we take them according to the demands of the model intercalibration subproject of the "Sections" program, and taking into account the experience of simulations carried out during the last pentad, they are correspondingly: 10 cm^2s^{-1} and 5.10^6 cm^2s^{-1}(Sarkisyan, 1995).

6. Initial temperature and salinity data

Temperature and salinity data were received from the Arctic and Antarctic Research Institute (AARI), in St.Petersburg. This data set was prepared on a 55.6km x 55.6km stereographic grid, and on 25 vertical levels. A general description of the data is presented by Polyakov and Timokhov, 1994. For the purpose of further usage of these data in the numerical model, temperature and salinity were interpolated to a model grid by the cubic spline method. The quality of interpolation was checked by visual control.

As for the quality of the AARI data, we may conclude that this set is the most reliable description of Arctic Ocean climate. The temperature and salinity fields at several depths are presented on Figs. 1-6. At a depth of 300m in the temperature field one can see the strong influence of the Atlantic warm water inflow.

As for gridded temperature and salinity from the last World Atlas, by S. Levitus 1994, for example, they are absolutely unrealistic in the case of the Arctic. A vast area of the Central Arctic is covered by surface waters with a temperature ~ -3^{o}C, which is far below freezing point and is due to instrumental errors.

The obvious drawback of the AARI data, from out point of view, is the very weak influence of the McKenzie river on the salinity field.

7. External forcing parameterization

a) Passages

Passages represent the liquid boundaries where we specify 3D temperature, salinity and velocity. In the model we adopted the following mass transports through the passages:

Bering Passage	+0.6 Sv
Denmark Passage	-6.3 Sv
Norwegian Sea area	+6.0 Sv
Nares Passage	-0.3 Sv

The sign "+" means inflow. These transports are the same as in the model by Hakkinen and Mellor, 1992. Following these authors, we specified barotropic velocities at the Norwegian Sea liquid boundary so that the velocity inflow is concentrated in the vicinity of the Scandinavian coast. At all other liquid boundaries the mass transport was distributed uniformly over the cross-section of the passage.

The problem of choosing the velocity at liquid boundaries is that the velocity should be well correlated with the density field in the vicinity of the boundary, and, besides, the mass transport should be close to observed values. The second problem is as follows: as will be seen from the results of the following calculations, the comparatively low value of the mass transport through the Bering passage, of 0.6 Sv (although there are estimates that the inflow is equal to 1.0 Sv) results in rather high velocities. This is why some modelers prefer to close the Bering Passage entirely, as was done in the Atlantic-Arctic model by G.Semjonov (personal communication).

b) Rivers

We specify rivers as liquid boundaries with a given temperature and salinity, and a velocity equal to zero. Thus, we assume that rivers do not change the mass balance, but rather the heat and salt ones, by turbulent diffusion. Generally speaking, we may treat rivers as normal liquid boundaries and specify flow velocities derived from the known river discharge. But the spatial resolution of the model, and the comparatively small input of river waters into the ocean mass balance, makes it possible to use the simplified description. A similar approach is adopted in large-scale models by Semtner, 1987 and by Mellor and Hakkinen, 1992, where rivers are parametrized as the salinity fluxes.

c) Wind and ice stresses

Winter wind velocity was calculated from the atmospheric pressure presented in the Arctic atlas. To compensate for the oversmoothed pressure data (this especially), the absolute value of the velocity was adopted equal to the geostrophic one, i.e. two times greater than the so-called 10m height wind. Essentially the same procedure was adopted by Ramsden and Fleming, 1995.

Ice dynamics have a strong influence on the dynamics of the Arctic waters. Fortunately for us, if we consider the winter season, we may adopt the approximation that almost all of the ocean is covered by ice (at least in the Central Arctic). On the other hand, ice dynamics far from the coast are approximated by free wind drift. Thus, sea ice may be parameterized by the choice of the turning angle in the formulae for the tangential stress. In the calculations presented here, we assume that the total ice/wind stress is directed strictly along the geostrophic wind.

8. Diagnostic and adjustment calculations in the case of normal CO_2

As a first step in the simulation of the normal state of the Arctic Ocean as derived from the specified temperature and salinity, diagnostic calculations were carried out. During these calculations we adjusted the 3D velocity field to the fixed temperature and salinity. The model was run with a time step of 1.0 hour, for a comparatively short period of 30

days. As may be seen from the kinetic energy time series, this period is quite sufficient to achieve a quasi-stable solution.

The second step is the so called "adjustment calculations". This stage was carried out for the purpose of evaluation of the trend of the model if the surface temperature and salinity are stable. Because of the coarse model grid and its inability to describe the very fine processes of the maintenance of temperature and salinity patterns, we have to separate temperature changes caused by model internal variability and by real variability in the Arctic.

The 3D velocity field obtained from 190 days adjustment calculations is rather close to the diagnostic one. The main features at the surface (fig. 7) are the Norwegian current, Transpolar transport and the Beaufort Sea anticyclonic gyre. The most interesting feature of the velocity pattern at the 250-500m levels (fig. 8) is the inflow of the Atlantic Water through the narrow Lena Trough. After the adjustment, this current became more intensive. The general structure of the velocity field is similar to the transport pattern by Rudels. The longer integration leads to unrealistic smoothing of the T and S in the region of the Central Arctic. To simulate processes of the thermohaline structure maintenance we have to choose a very fine spatial resolution, and to incorporate into the model a very sophisticated turbulence closure scheme.

9. Imitation of the CO_2 doubling

We parameterized the "greenhouse" effect by changing the sea surface temperature and salinity. The necessary change was estimated from a paper by Ramsden and Fleming, 1995 (hereafter RF).

Some criticism of the CCC atmospheric model, used by RF, may be caused by the very large warming of the atmosphere in the Central Arctic, up to 10^{o}C. One other drawback of the simulation is that the upper surface temperature and salinity fields are obviously oversmoothed - there is almost no river influence on the salinity field, and so on. Apparently this is a consequence of the spatial coarseness of the model, and the quality of the external forcing parameters. In addition, (this taken directly from the paper) we have no possibility to estimate changes in the circulation pattern and T, S at the depth of the Atlantic Water inflow.

So we propose a methodology combining the comparatively detailed temperature and salinity fields of AARI and the sea surface T, S changes estimated by RF.

The procedure of the new surface temperature and salinity construction may be described as a sequence of several steps:

1. The evaluation of the change of the ice edge location. According to results by RF, the main change of the sea ice extent is in the area of the GIN Sea. The displacement of the ice edge is on average 300km, a little more at Greenland.
2. The approximate location of the ice edge is associated with an isotherm of minus $1^{o}C$. So, for the construction of the new temperature field we shifted the $-1^{o}C$ isotherm to the new ice edge location, received after step 1.
3. The temperature in the initially ice-free area is made $3^{o}C$ higher.
4. The temperature in the area of the completely melted ice is linearly interpolated from $-1^{o}C$ to the temperature specified at step 3.
5. The surface salinity in the area initially covered by the ice is modified by the formula

$$S_{NEW} = S_{OLD} - 0.07\ {}^{o}/_{oo}$$

The increment of $0.07\ {}^{o}/_{oo}$ is chosen according to RF. The new temperature and salinity at the surface of the ocean are presented in Figs. 9, 10.

10. Calculations with surface temperature and salinity, corresponding to the CO_2 doubling.

The general methodology of these calculations is the same as for ordinary adjustment calculations. All the coefficients of turbulent mixing are the same. The model was integrated for a period of 190 days. The velocity pattern is almost unchanged. A comparison of the ordinary adjusted fields of T and S and the fields received during the imitation of the CO_2 doubling will be made in the following section. We have to note, that in the experiment, the temperature and salinity were disturbed only at the upper boundary, and were unchanged beneath the surface at the liquid boundaries. So we have to examine T and S disturbances about one hundred kilometers away from the liquid boundaries, and the boundary in the region of the Norwegian Sea, in particular. In any case, according to the proposed

methodology at this boundary both the temperature and salinity variations will be equal to zero.

11. Discussion

Most attention, in the project, was paid to the estimates of the sensitivity of the model to the upper surface temperature and salinity variations. The main variations in the ocean temperature occur in the GIN Sea area. As for the salinity changes, they are due to ice melting in the regions of the marginal ice zone and the Central Arctic. So the question arises about the possibility of the remote response of the deep ocean layers. This response may be caused by advection by the 3D velocity field, or by some wave mechanism. As the magnitude of the current velocity in the Arctic is comparatively small, one can expect a significant effect of advection by currents, only on long time scales. But any primitive equation numerical model, during the long period of integration, tends to spoil the initial observed data by oversmoothing. This is why we stopped the integration at 190 days - even then the inflow of Atlantic Water into the Central Arctic was noticeably stopped.

To extract the signal, we will analyze the differences in the temperature and salinity corresponding to normal and doubled CO_2 (figs. 11-18).

A strong signal is detected at the 100m depth (figs. 13, 14). The amplitude of the signal is not spatially uniform, as may be expected from the purely vertical diffusive redistribution of the temperature and salinity. The most significant changes occur in the region of the Norwegian current off Scandinavia. Temperature changes here are up to $2.5^{o}C$, while the mean changes in the GIN sea area are ~ $1^{o}C$. Salinity variations have the same spatial structure and the amplitude of the changes is about 0.04 $^{o}/_{oo}$. Generally speaking, this distribution of the signal may be associated with two processes.

1. Given that the maximal and minimal of T, S variations are correlated with jet currents, one may expect that the first mechanism is horizontal advection by the mean currents.
2. Given that extrema of the T, S variations are strongly correlated with the downwelling zones (fig. 19) it is quite natural to suggest that the signal is transported by the vertical convection process.

At the 300m depth the most significant changes of temperature (up to 1.5°C and salinity (up to 0.05 $^{o}/_{oo}$) also are in the region of the Norwegian current. Over the major part of the area, salinity changed little (about minus 0.005 $^{o}/_{oo}$). This negative change may be explained by vertical turbulent mixing. On the other hand, temperature changes in the same area are positive, although are less than 0.2°C. These variations cannot be explained by diffusion because at a depth of 300-400m the temperature vertical profile has a maximum. Thus, we have to assume some dynamical mechanism in the transport of the signal. It is interesting to note, that at the 300m depth there is an area of comparatively strong salinity change (about 0.02 $^{o}/_{oo}$) along the Eurasian continental slope. Taking into account the location of the area of these changes we may associate them with advection or, even more possible, with some wave mechanism. Although we have no strict evidence, we may expect that this signal transport is due to baroclinic coast-trapped Kelvin waves.

In any case we may conclude that the model manifests not a purely diffusive response to the surface temperature and salinity variations, but a dynamic one. This fact makes us optimistic about applying the model in investigations of the Arctic Ocean sensitivity to the variability of the external forcing components (wind, mass transport through the passages, etc.)

The second, and very interesting result, is that our estimates of the Arctic Ocean response to the surface T and S variations shows, that in the Atlantic Water layer the most noticeable signal is the salinity change about 0.01 $^{o}/_{oo}$ - 0.03 $^{o}/_{oo}$ along the Eurasian continental slope. As for temperature changes, we obtained almost no response to applied forcing in the same region.

REFERENCES

Chapman W.L., W.G. Weach, K.P. Bowman, G. Sacks and J. Walsh, 1994. Arctic sea ice variability: Model sensitivity and a multidecadal simulation. J. Geophys. Res., V. 99, NC1, 919-935.

Hakkinen S., G.L.Mellor, 1992. Modeling the seasonal variability of the coupled Arctic ice-ocean system. J.Geophys.Res., v. 97, pp.20,285-20,304.

Hakkinen S., 1995. Simulated interannual variability of the Greenland Sea deep water formation and its connection to surface forcing. J. Geophys. Res., v. 100, N C3, 4761-4770.

Holland D.M., L. Mysak, D.K.Manak and J.M.Oberhuber, 1993. Sensitivity study of a dynamic thermodynamic sea ice model. J. Geophys. Res., v. 98, N C2, 2561-2586.

Pacanowski R.C., S.G.H.Philander, 1981. Parameterization of vertical mixing in numerical models of tropical oceans. J.Phys.Oceanogr., v. 11, N 11, 1443-1451.

Polyakov I.V., L.A.Timokhov, 1994. Mean temperature and salinity fields of the Arctic Ocean. Meteorol. I Gidrologia, N 7, pp.68-75 (in Russian).

Ramsden D., G.Fleming, 1995. Use of a coupled ice-ocean model to investigate the sensitivity of the Arctic ice cover to doubling atmospheric CO2. v. 100, N C4, pp. 6817-6828.

Sarkisyan A.S. 1995. Analysis of model calibration results of the Atlantic O cean climatic characteristics calculation. Journal of Marine Systems, v. 6, pp.47-66.

Semtner A.J., 1987. A numerical study of sea ice and ocean circulation in the Arctic. J. Phys. Oceanogr., v.17, 1077-1099.

Smagorinsky J.S., 1963. General circulation experiments with primitive equations. I: The basic experiment. Mon.Wea.Rev., v. 91, 99-164.

MARINE SCIENCE INTERNATIONAL CORPORATION

VARIABILITY OF THE ARCTIC BASIN OCEANOGRAPHIC FIELDS

K.D. Sabinin

FIGURES
PART 11

Initial temperature at the surface

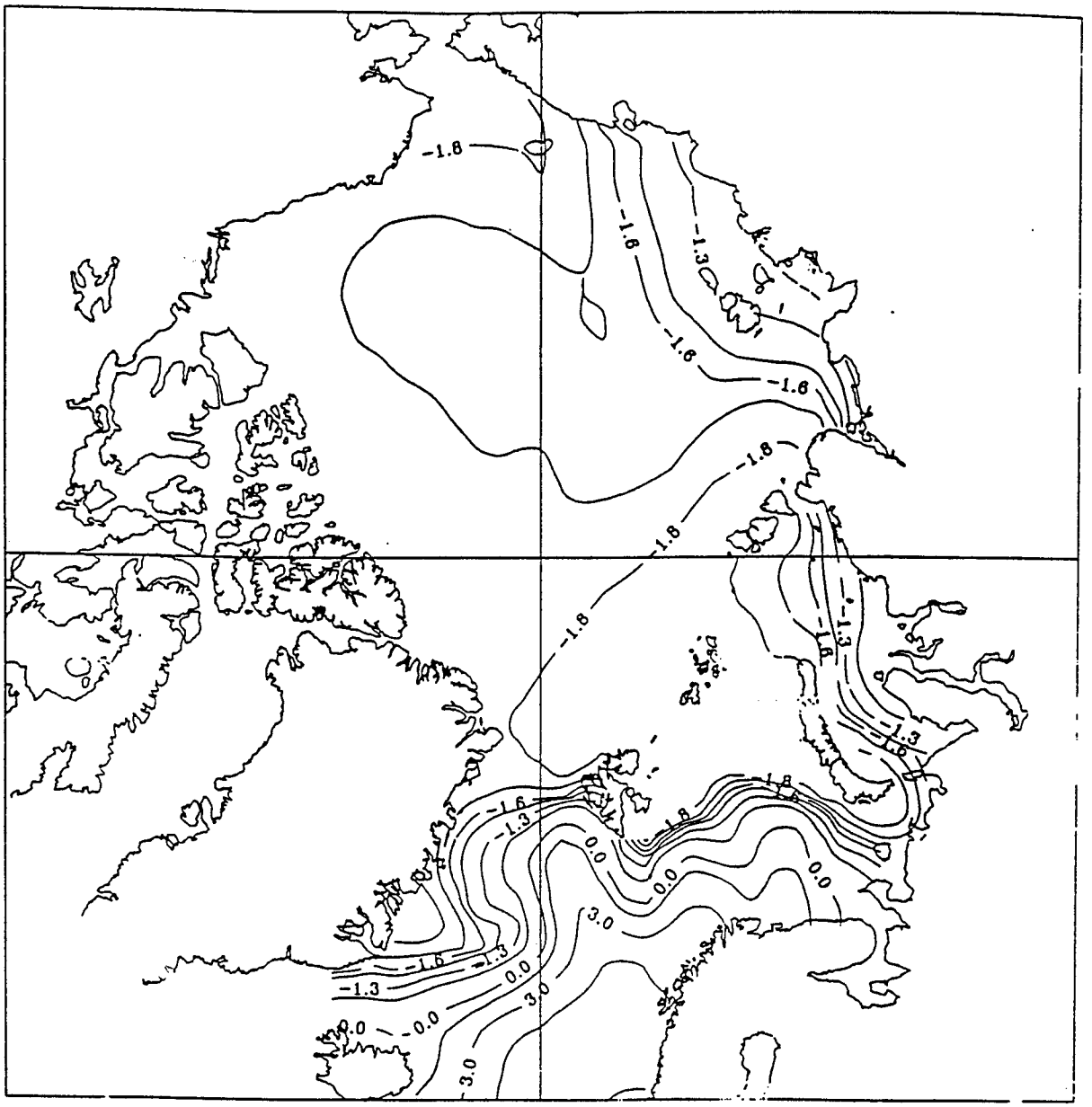

Fig. 1. Initial temperature at the ocean surface

Initial salinity at 0m.

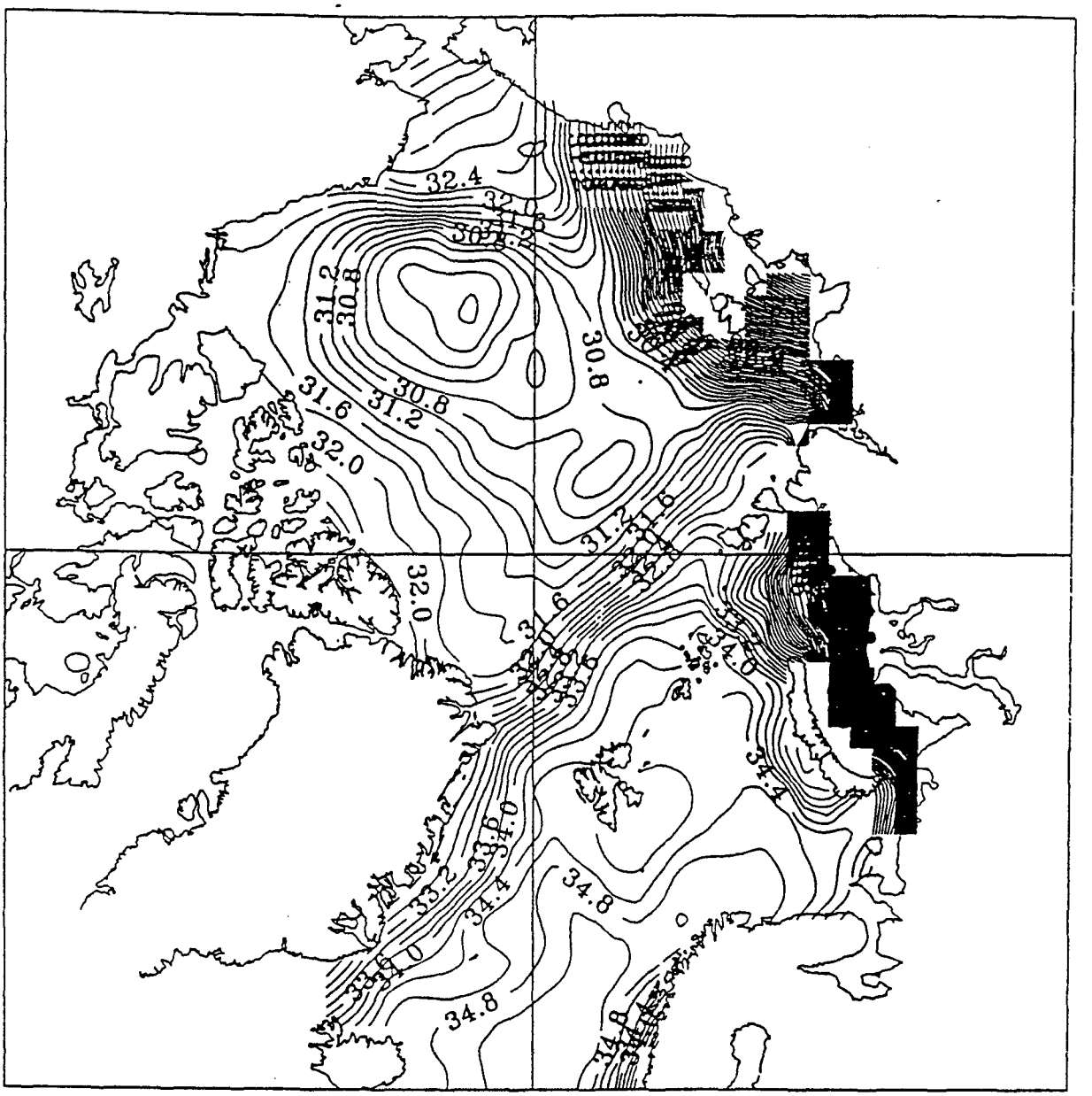

Fig.2. Initial salinity at the ocean surface. The contour interval is $0.2^{0}/_{oo}$.

Initial temperature at 100m.

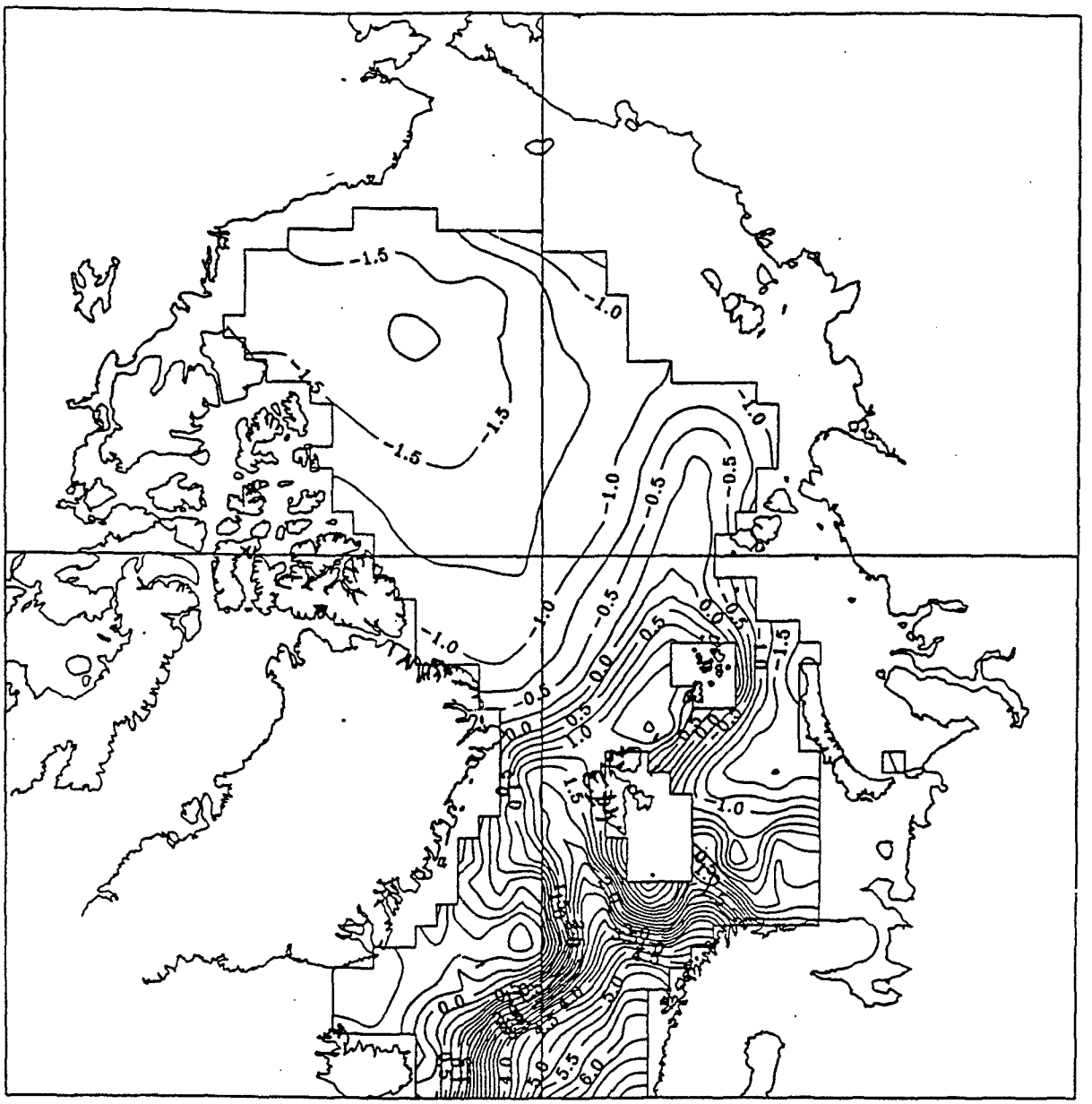

Fig. 3. Initial temperature at the 100m depth.
The contour interval is 0.25^{0}C.

Initial salinity at 100m.

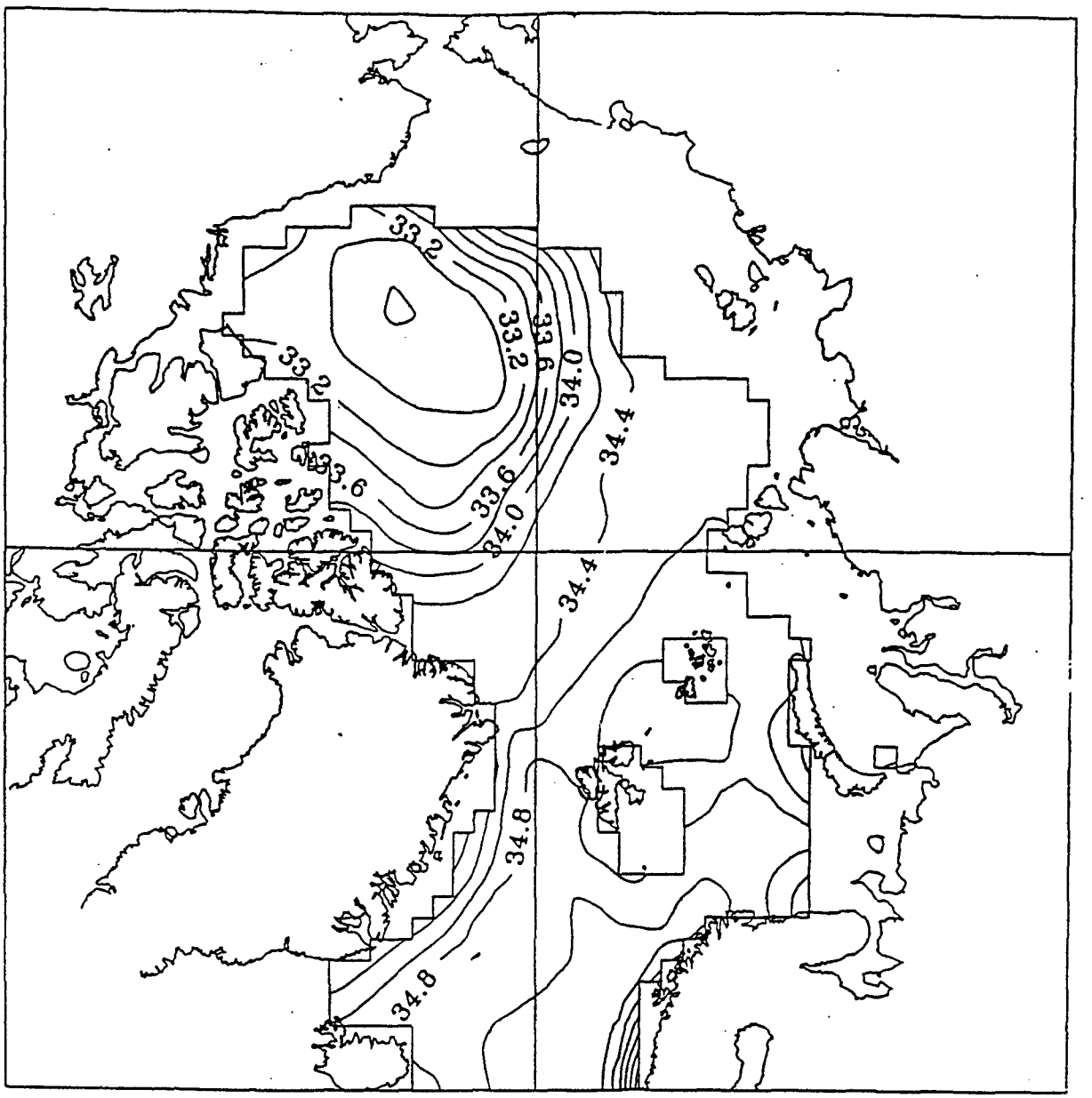

Fig. 4. Initial salinity at the 100m depth.
The contour interval is $0.2^{o}/oo$.

Initial temperature at 300m.

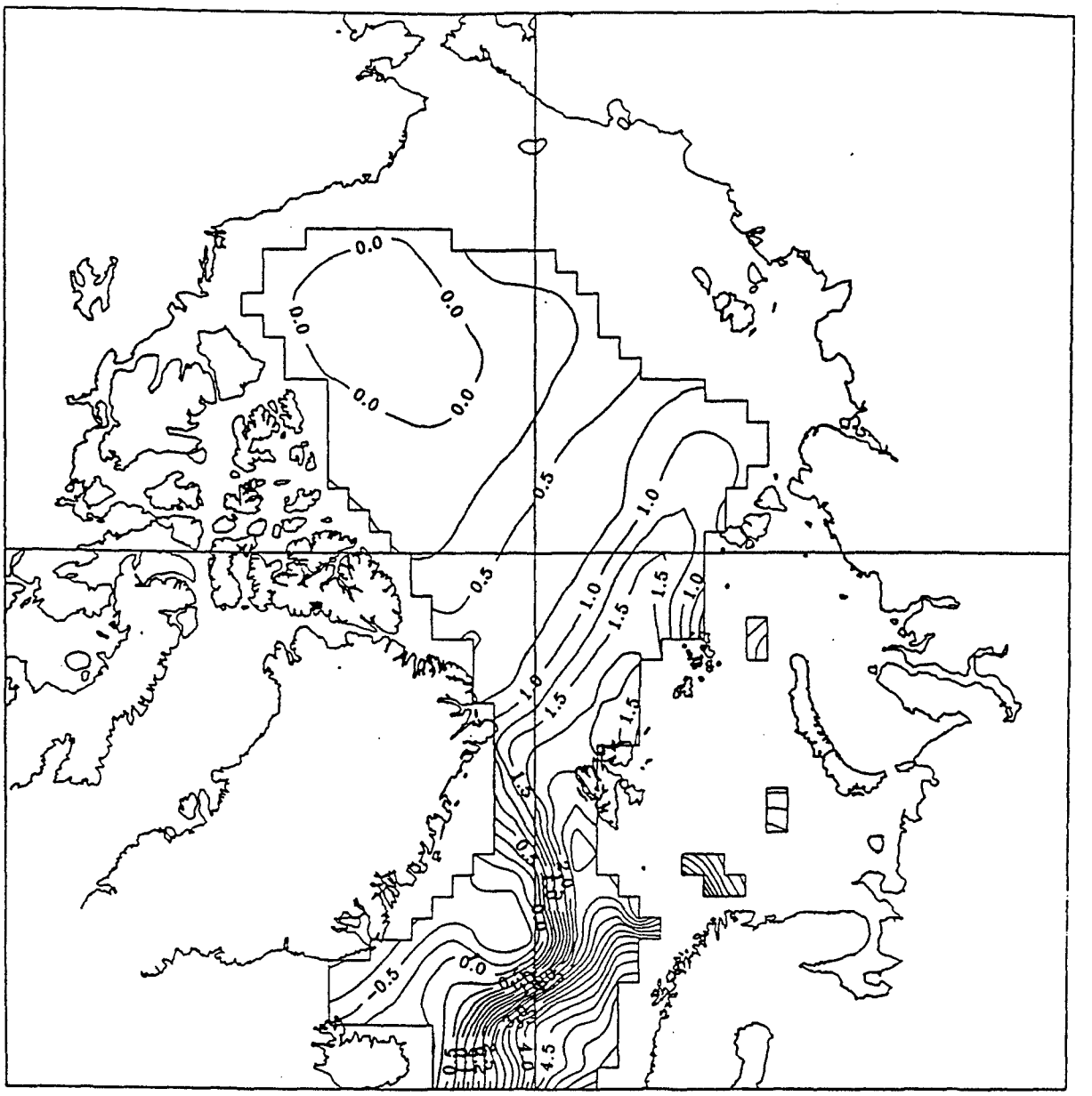

Fig. 5. Initial temperature at the 300m depth.
The contour interval is 0.25^{o}C.

Initial salinity at 300m.

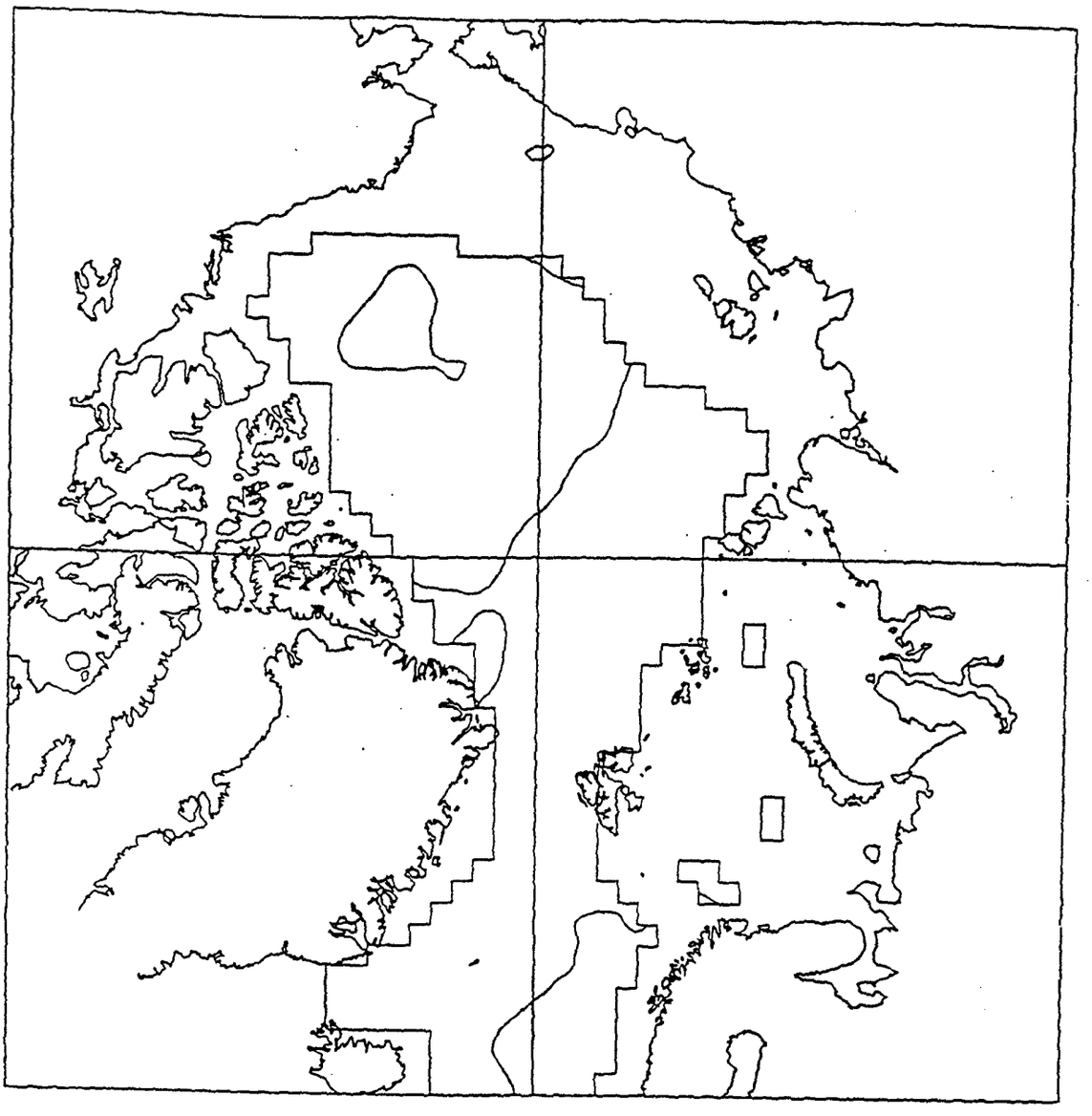

Fig. 6. Initial salinity at the 300m depth. The contour interval is 0.2 $^{0}/_{00}$. Only the 35$^{0}/_{00}$ isohala is presented.

Velocity at the 10m depth. Winter. Adjustment 190 days.

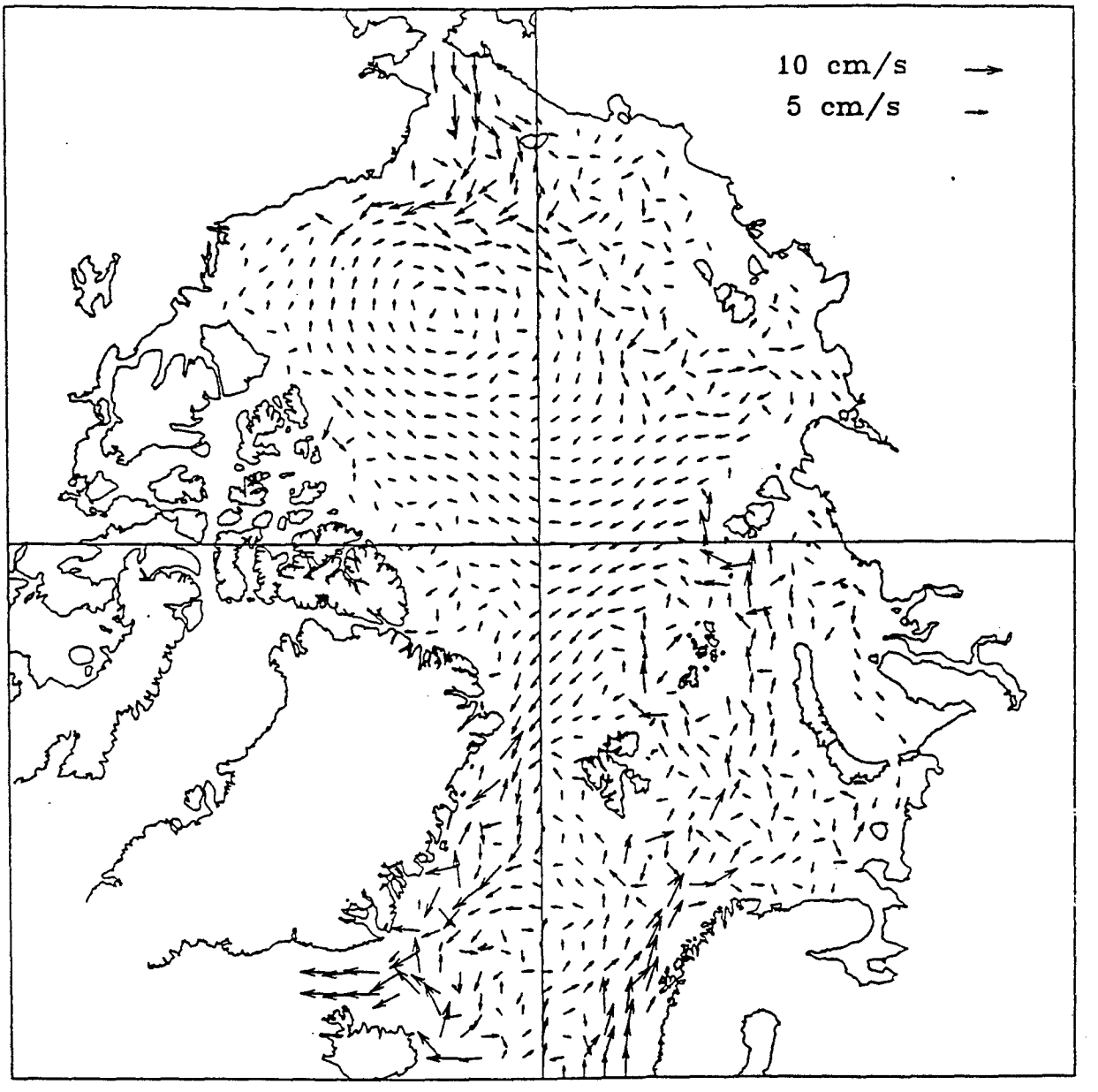

Fig. 7. Velocity at the 10m depth, obtained after 190 days of adjustment calculations. Velocities higher than 10cm/s are truncated.

Velocity at the 500m depth. Winter. Adjustment 190 days.

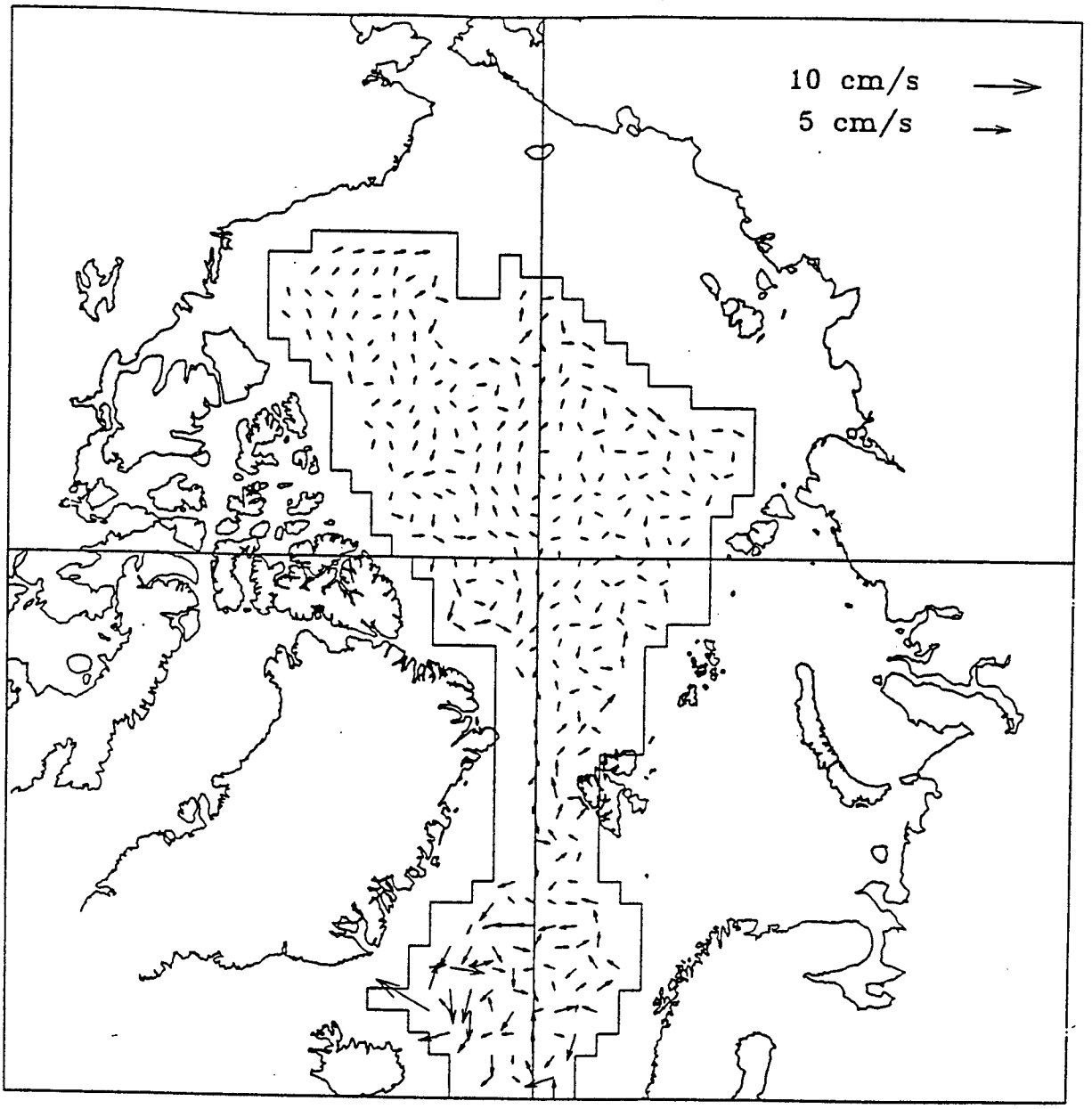

Fig. 8. Winter velocity at the 500m depth, obtained after 190 days of adjustment calculations. Velocities higher than 10cm/s are truncated.

New surface temperature.

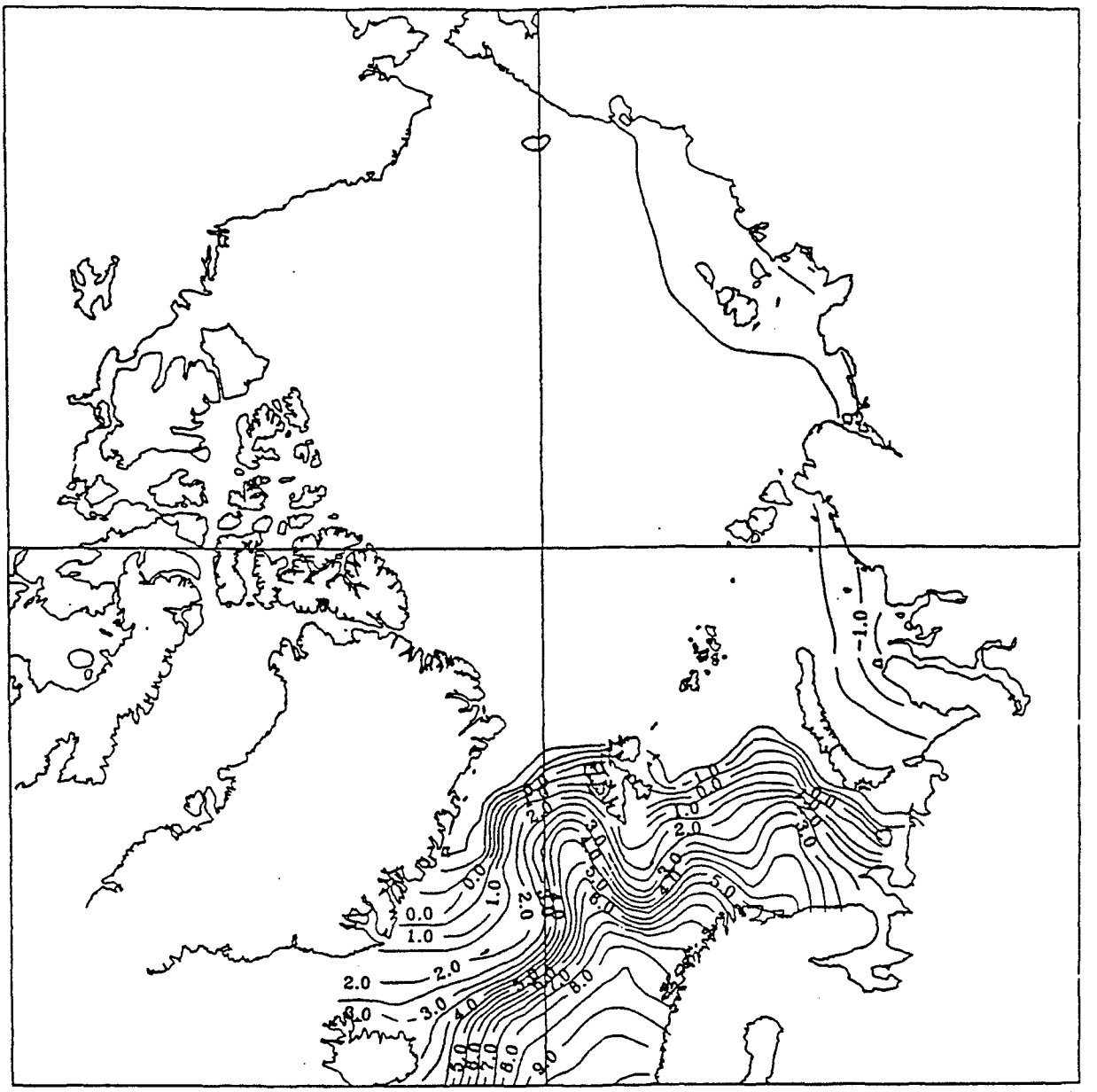

Fig. 9. New temperature at the ocean surface.
The contour interval is 0.5^{0}C.

Salinity at the surface, CO_2 Doubling.

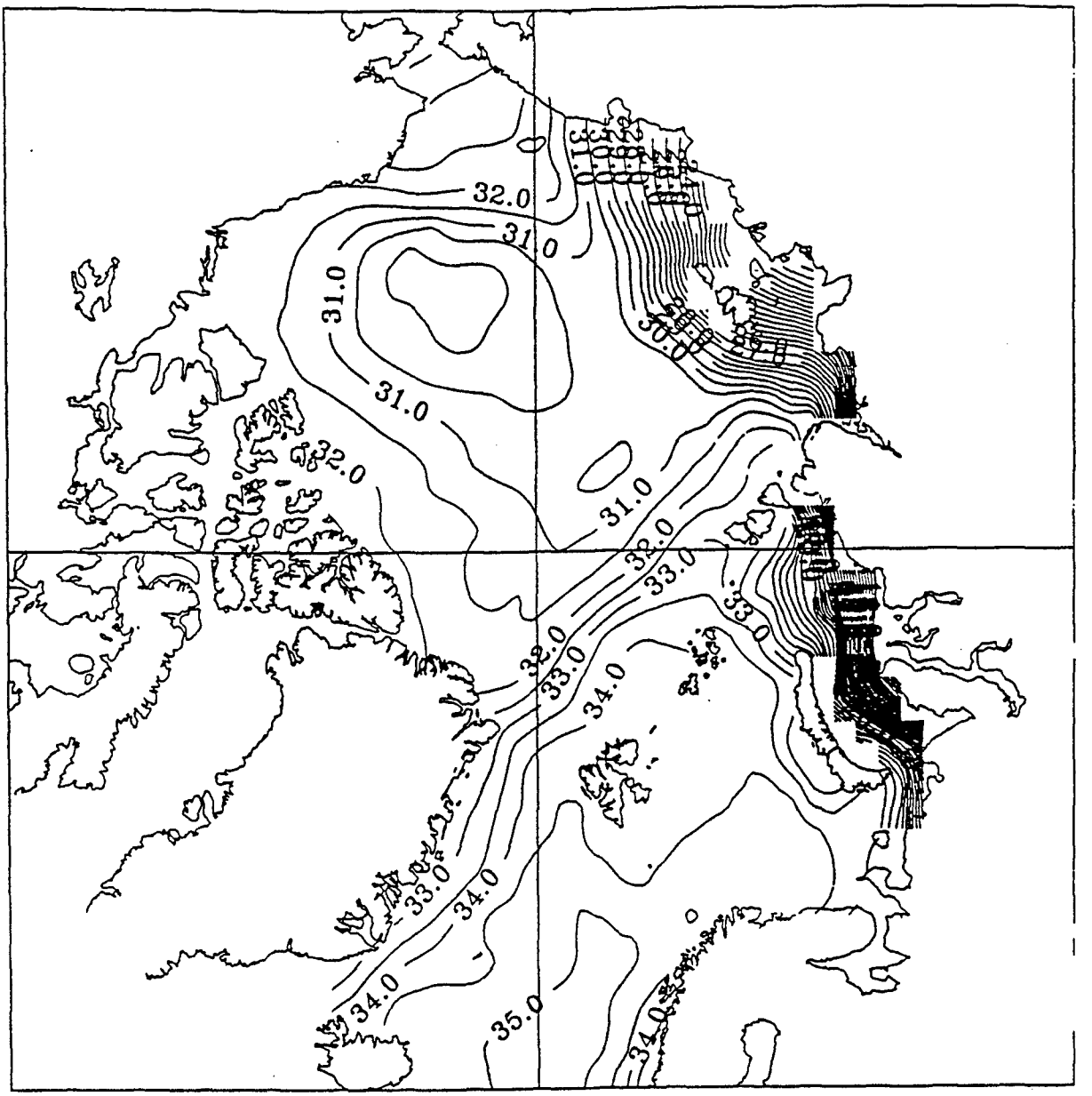

Fig. 10. New salinity at the ocean surface.
The contour interval is 0.5 $^{o}/_{oo}$.

Temperature Differences. CO_2 Doubling - Normal CO_2 at 50m.

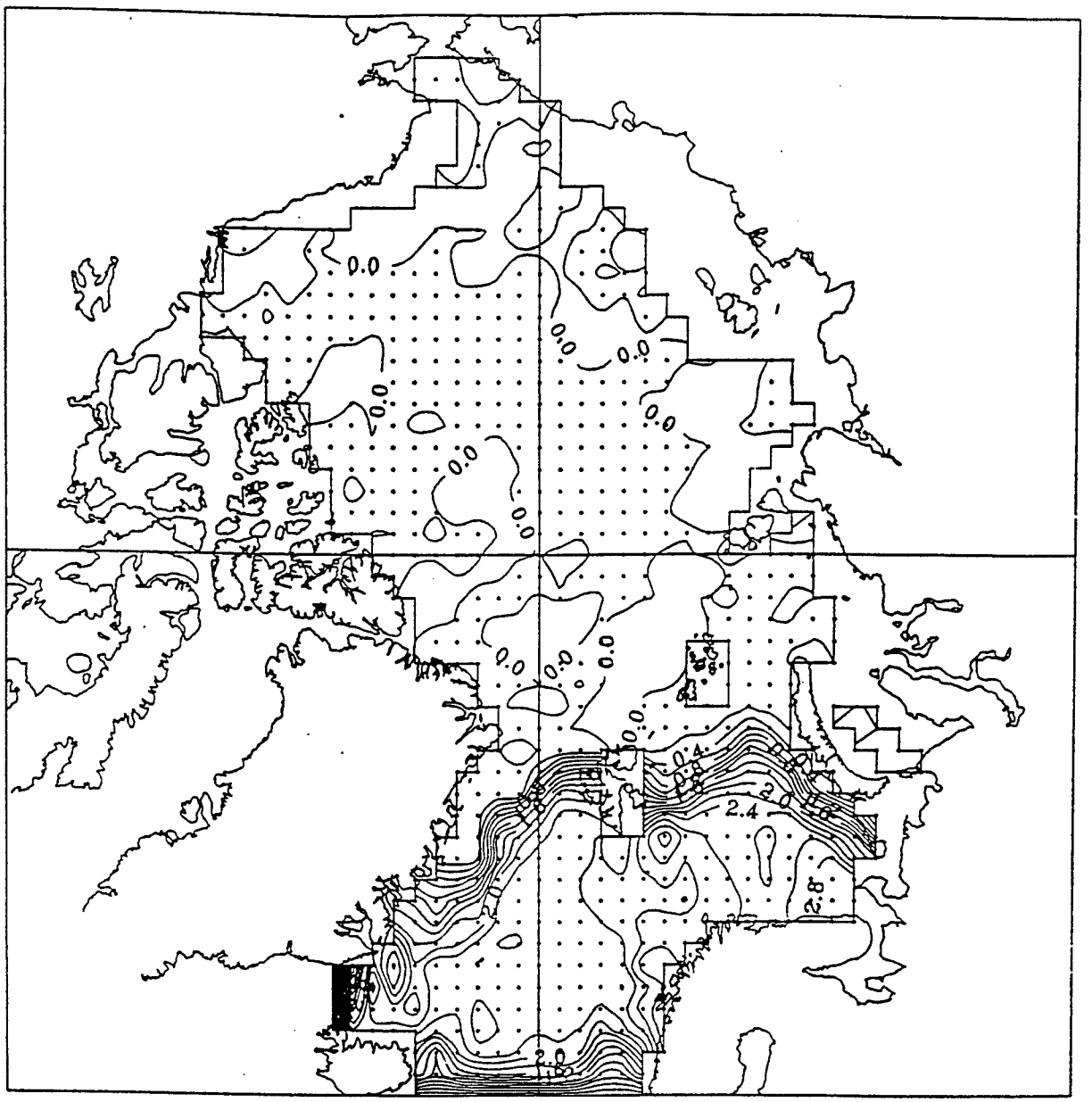

Fig.11. Temperature differences between CO_2 doubling and normal CO_2, at a depth of 50m. The contour interval is 0.2°C. The areas of positive changes (warming) are shaded.

Salinity Differences. CO_2 Doubling- Normal CO_2 at 50m.

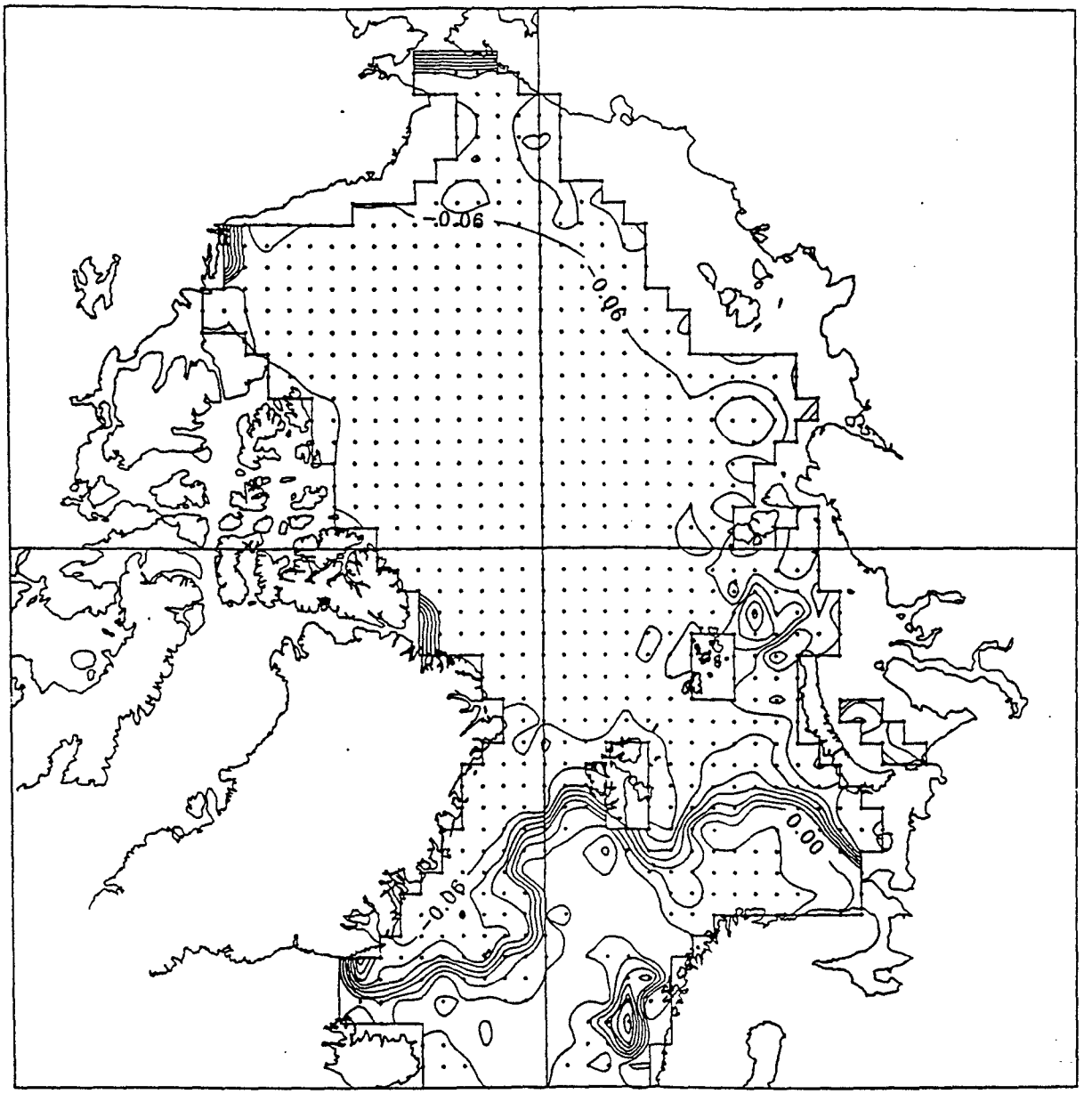

Fig. 12. Salinity differences between CO_2 doubling and normal CO_2 at a depth of 50m. The contour interval is 0.01 $^{o}/_{oo}$. The areas of negative changes (freshening) are shaded.

Temperature differences. CO_2 Doubling - Normal CO_2 at 100m.

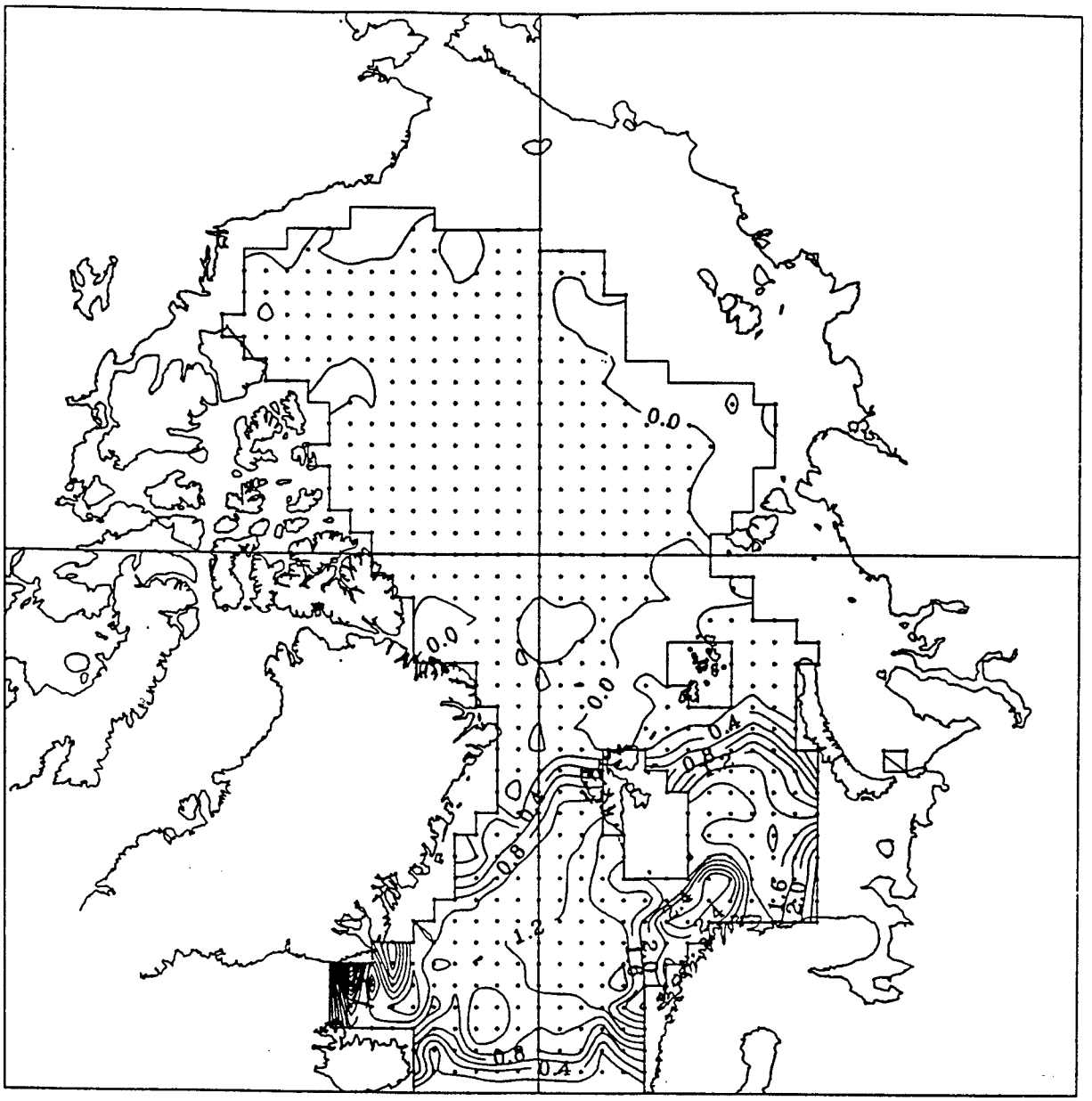

Fig.13. Temperature differences between CO_2 doubling and normal CO_2, at a depth of 100m. The contour interval is 0.2^0C. The areas of positive changes (warming) are shaded.

Salinity Differences. CO_2 Doubling - Normal CO_2 at 100m.

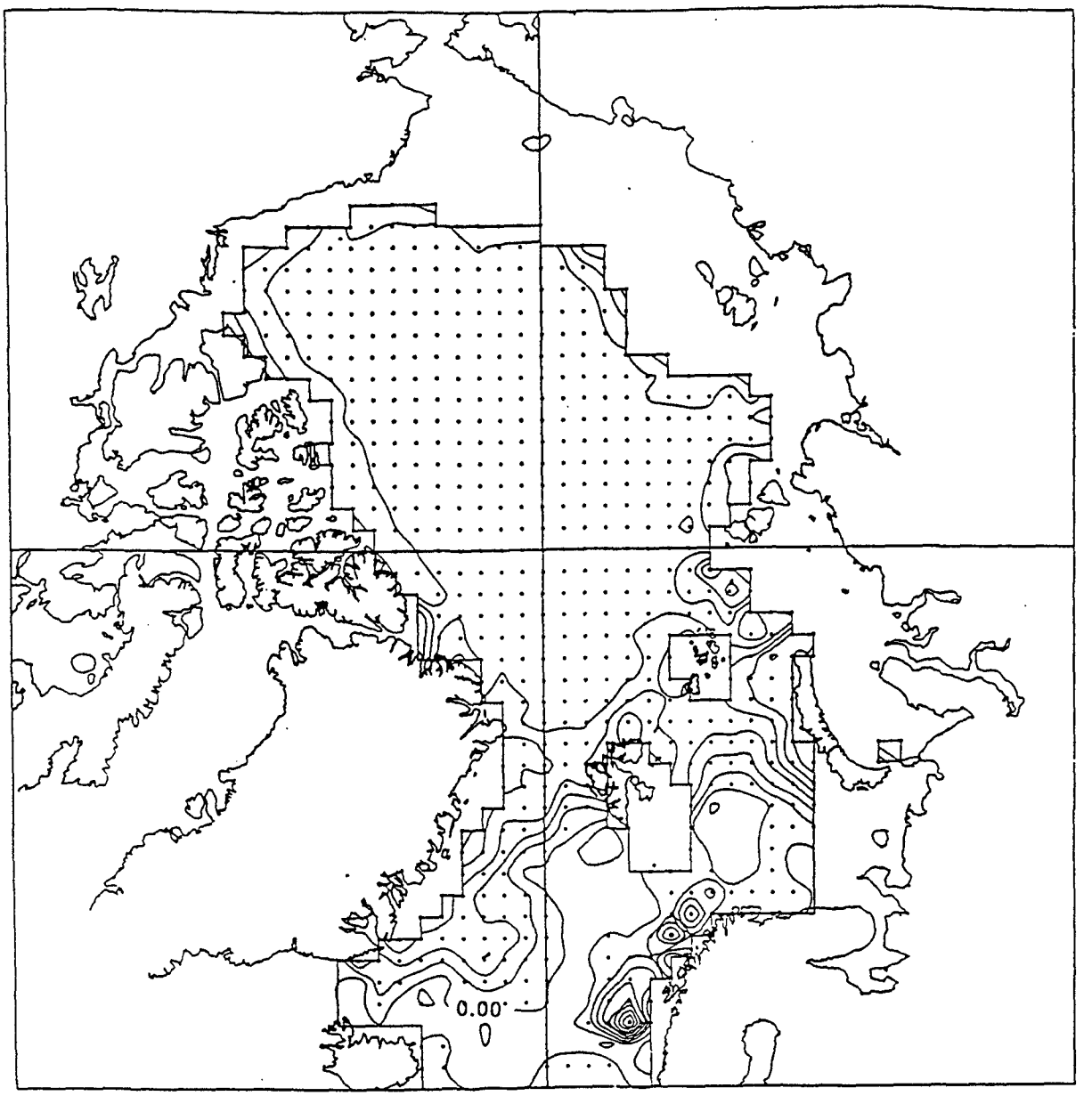

Fig. 14. Salinity differences between CO2 doubling and normal CO2, at a depth of 100m. The contour interval is $0.01^0/_{00}$. The areas of negative changes (freshening) are shaded.

Temperature Differences. CO_2 Doubling - Normal CO_2 at 300m.

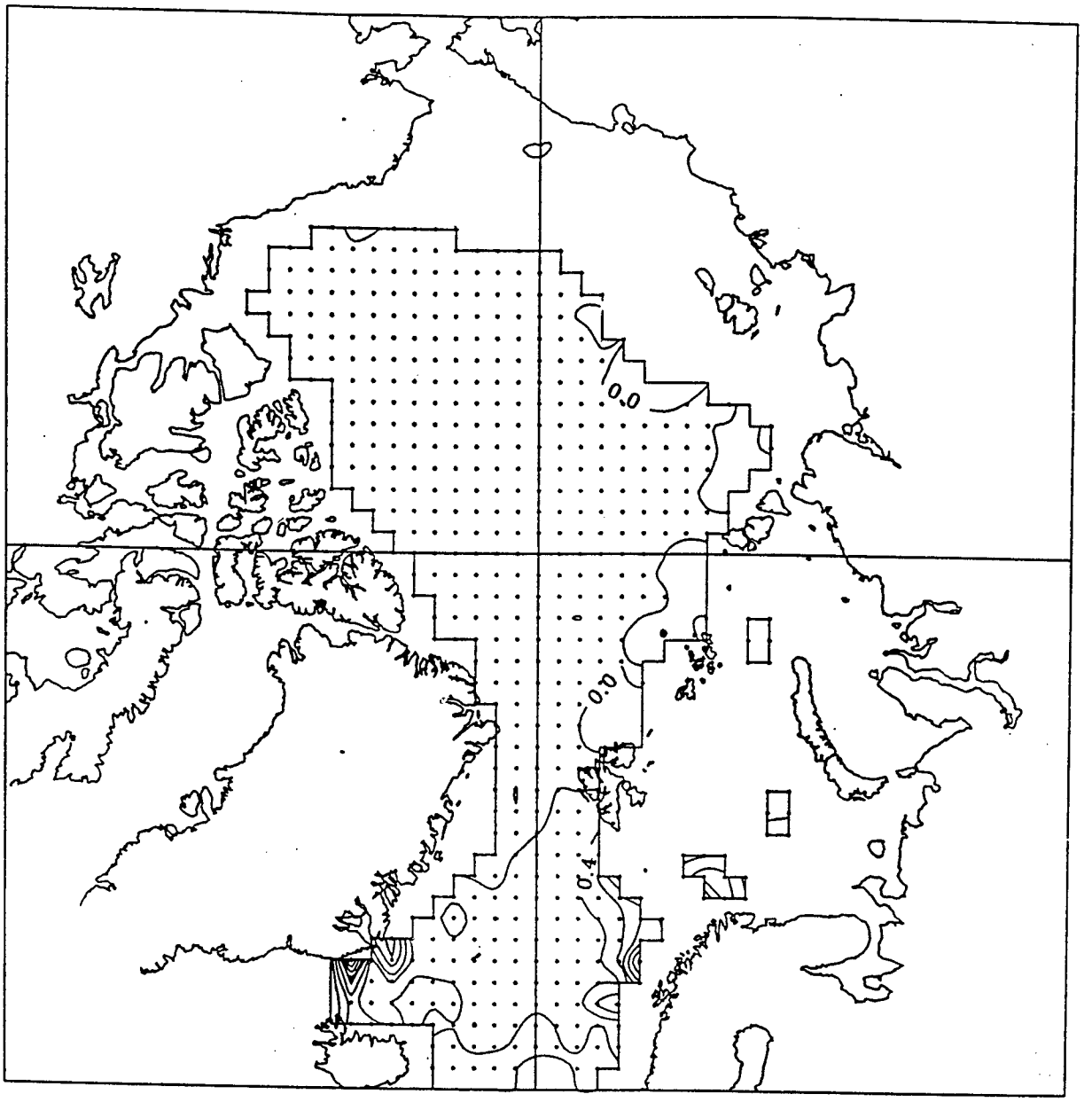

Fig. 15. Temperature differences between CO_2 doubling and normal CO_2, at a depth of 300m. The contour interval is 0.2°C. The areas of positive changes (warming) are shaded.

Salinity Differences. CO_2 Doubling - Normal CO_2 at 300m.

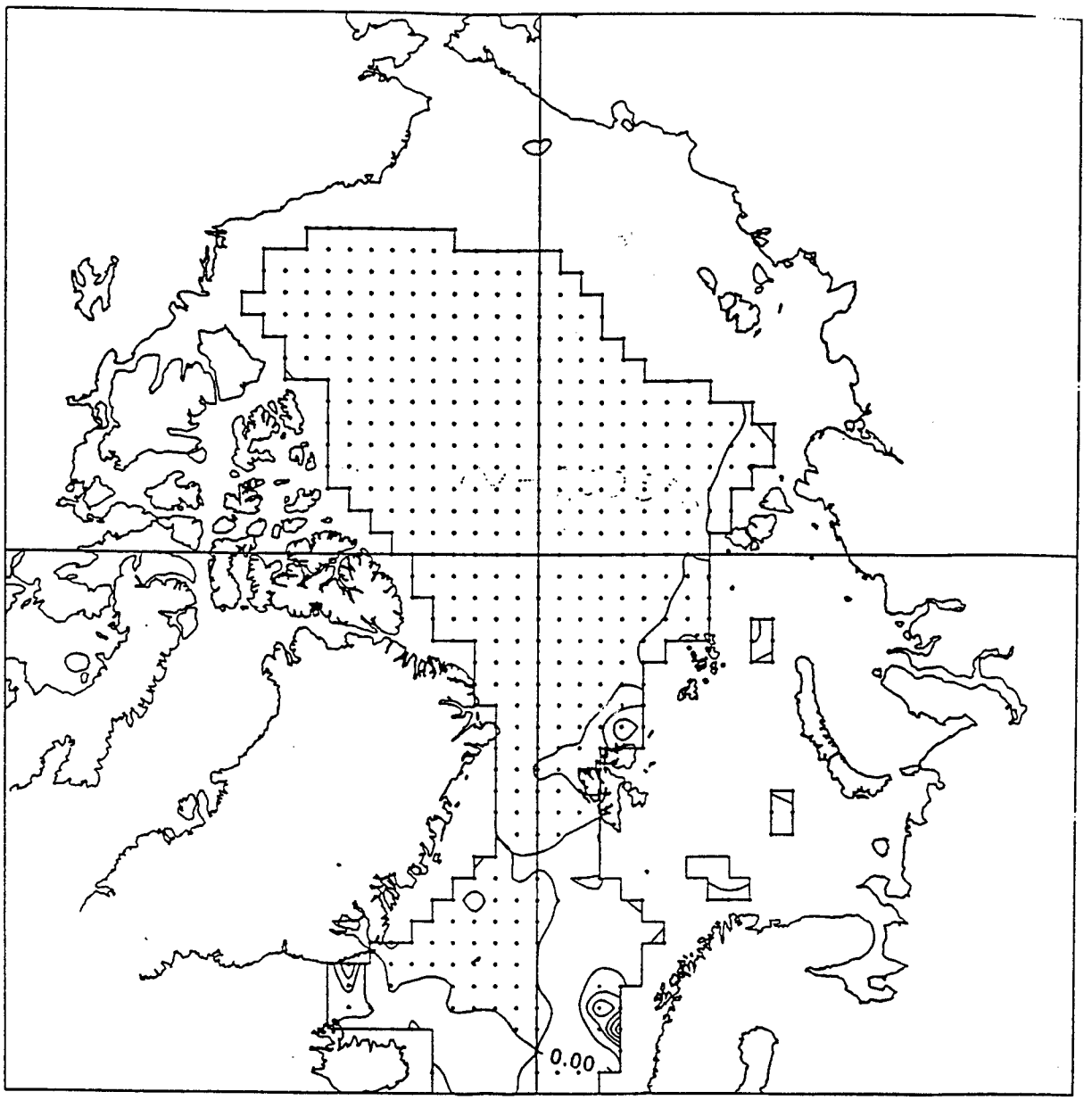

Fig. 16. Salinity differences between CO2 doubling and normal CO2, at a depth of 300m. The contour interval is $0.01^{o}/_{oo}$. The areas of negative changes (freshening) are shaded.

Temperature Differences. CO_2 Doubling - Normal CO_2 at 500m.

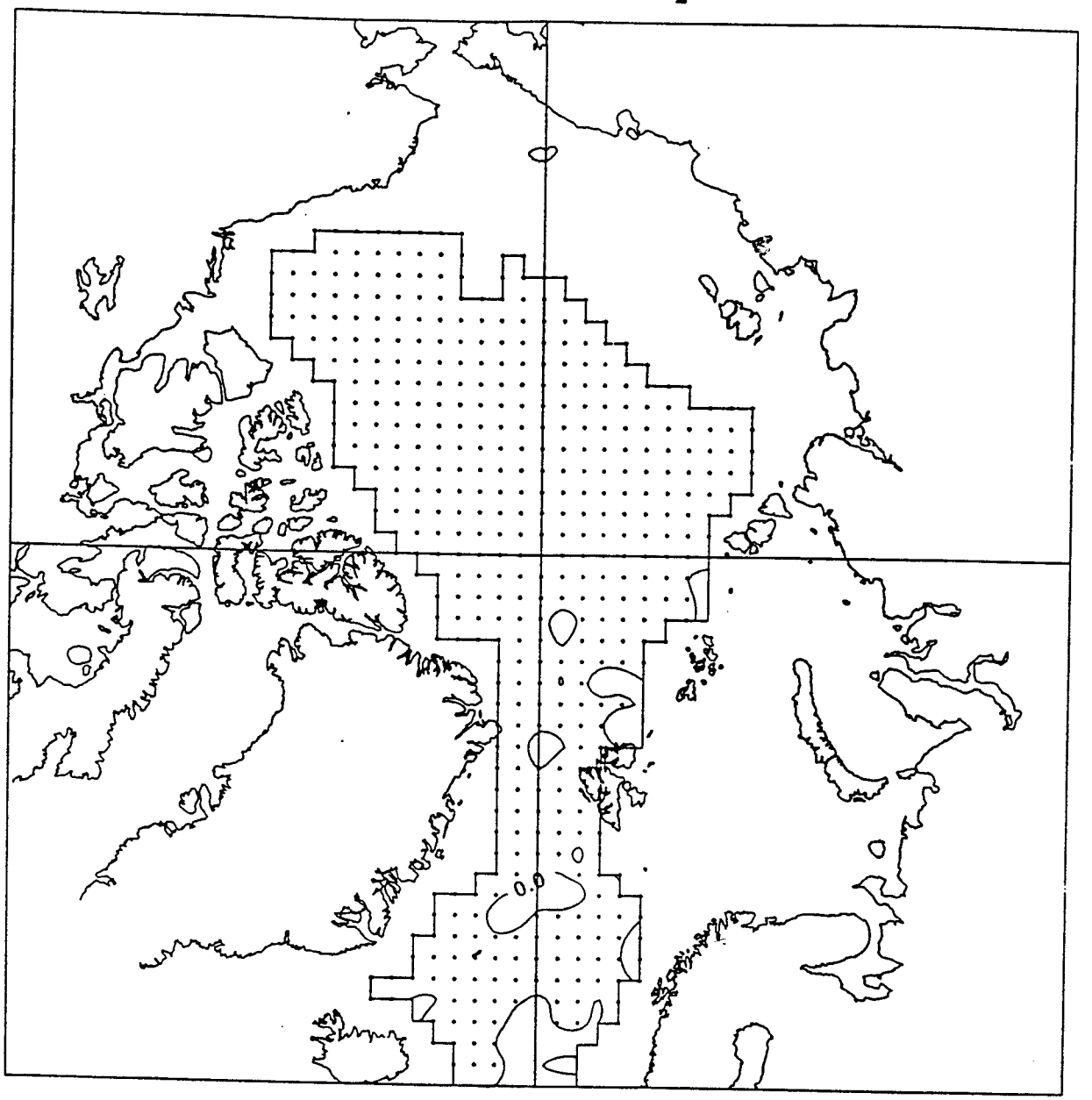

Fig. 17. Temperature differences between CO_2 doubling and normal CO_2, at a depth of 500m. The contour interval is 0.2°C. The areas of positive changes (warming) are shaded.

Salinity Differences. CO_2 Doubling - Normal CO_2 at 500m.

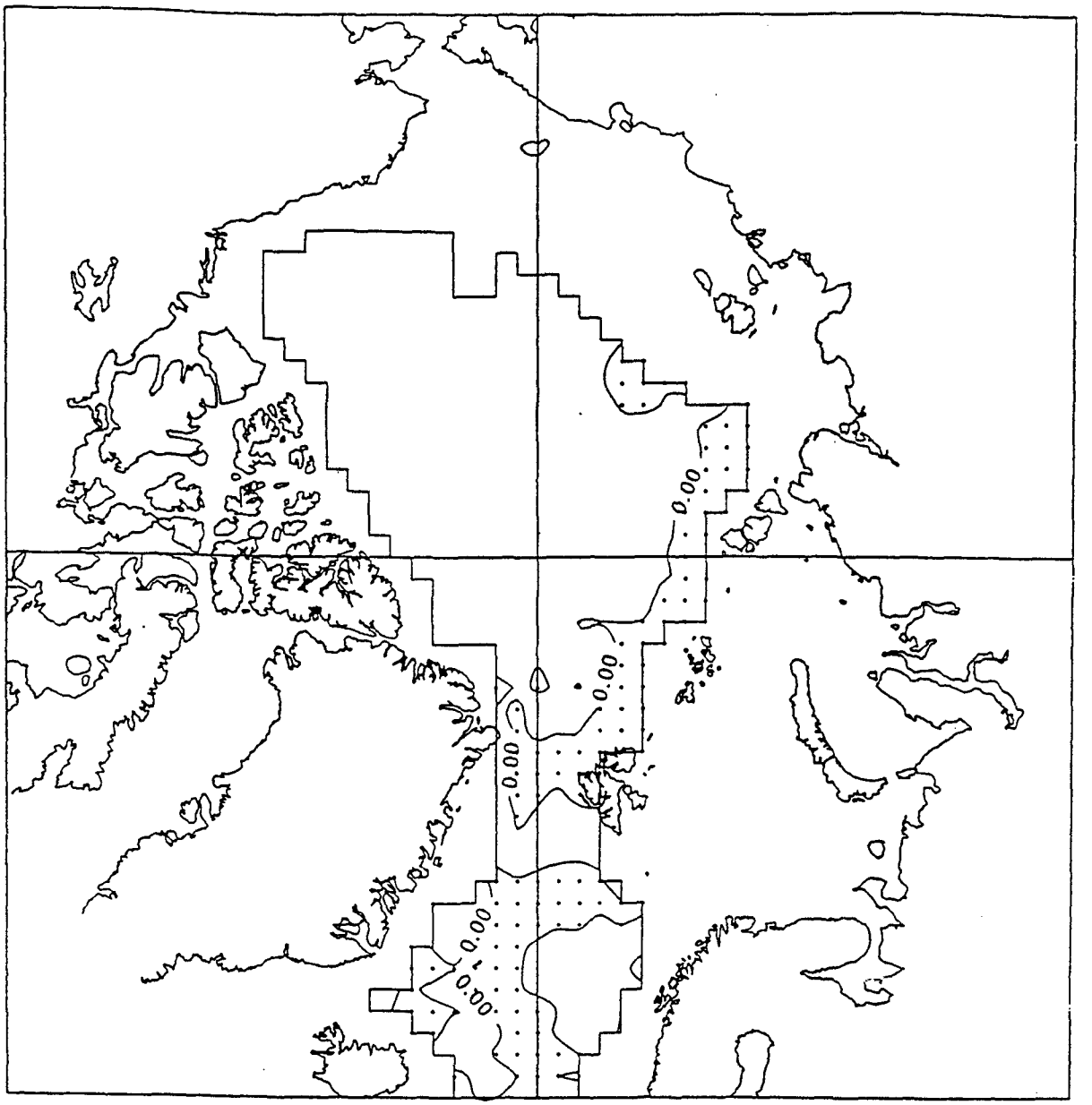

Fig. 18. Salinity differences between CO2 doubling and normal CO2, at a depth of 500m. The contour interval is $0.01^{0}/_{00}$. The areas of negative changes (freshening) are shaded.

Vertical velocity at 100m.

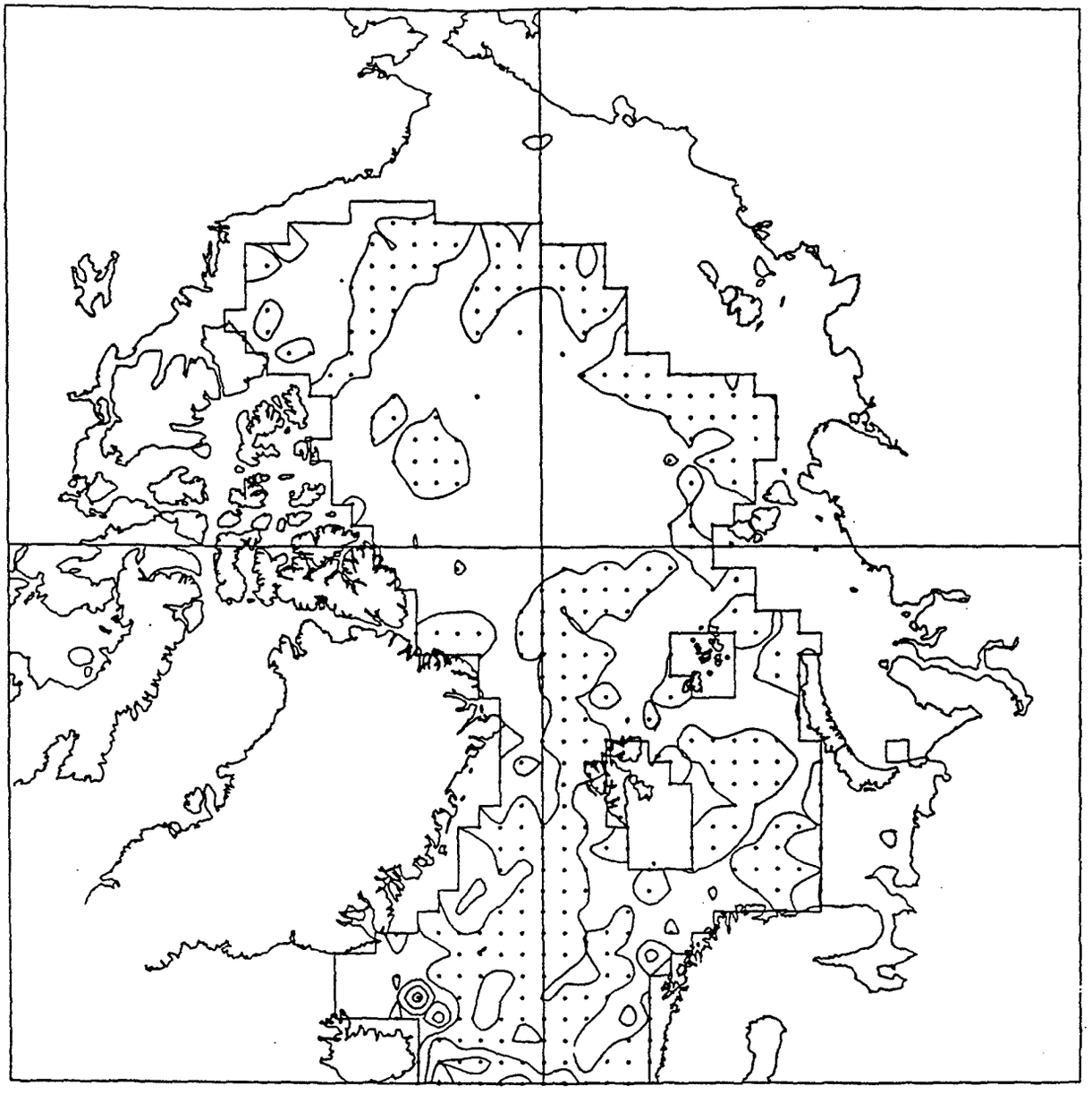

Fig.19. Winter vertical velocity at a depth of 100m, obtained after 190 days of adjustment calculations. Upwelling zones are shaded. The contour interval is 0.001cm/s.

CONCLUSION

Detailed analysis of the data obtained in the Soviet High-latitudinal expeditions "Sever" in 1973-1979 has revealed some specific features in interannual variability of oceanographic fields in different regions of the Arctic Basin. The largest variability is observed in the upper 500-m layer of the Basin where high gradients of temperature and salinity exist. The extreme temperature variability can reach 3 - 3.5 K degrees, as is found at the continental slope in the Franz-Joseph-Land region, where intrusions of cold shelf waters into the Atlantic layer occur. Temperature variability in central regions of the Arctic Basin is smaller, but significant variability takes place in the upper 100-m layer in areas of the Pacific water distribution. Strong variability in the Beaufort Sea is connected with mesoscale processes in flaw polynyas and at the continental slope. Generally, the continental slope all around the Arctic Basin is the place where the variability intensifies due to intrusions, convection and other mesoscale processes.The variability of salinity has its maximum in the upper 100-m layer and can exceed 1 ppt everywhere in the Arctic Basin.

Special attention was paid to the Atlantic Water (AW) layer in the Arctic Basin, because this layer seems to be the main object of the acoustic thermometry of the Arctic Ocean. The variability of different characteristics of this layer (depths of boundaries and thickness of the layer, depth and temperature of the layer's core) was analyzed. In 1973-1975 a small (about 50 m) increase in the AW thickness, as well as a rise in the upper boundary was observed throughout much of the Arctic Basin. A significant decrease of 100-150 m in the AW thickness was observed in 1978 over much of the Basin, and in the Nansen abyssal plain the AW thickness was even 250-400 m less than on average. The largest variability of the AW maximum (core) temperature was observed in the Nansen abyssal plain where temperature anomalies can be more than 0.3 K whereas in the remaining Arctic Basin they seldom exceed 0.05 K. In general, maps of the AW parameters' anomalies reveal a patchy distribution of the anomalies with obvious intensification in the Euroasian part of the Basin, especially at the continental slope of the Basin. Some intensification is observed also at the

Chuckchi Rise. The most interesting feature of the AW temperature interannual variability is a hint at a two-year periodicity in the Nansen abyssal plain.

A significant step was made in numerical modeling of the Arctic Ocean. A more realistic model of the Arctic Ocean circulation was obtained, and an estimation of the impact of the greenhouse effect on the Arctic Ocean climate was made. This estimation was fulfilled for the "CO^2, doubling" scenario. It shows that the most significant "signal" of the greenhouse effect is in freshening of the upper Arctic Basin. Although some shortcomings of the model still exist (an unrealistic high coefficient of diffusion resulting in an overly deep penetration of the freshening, and insufficient duration of the model integration which is not enough for detection of the AW layer warming in the Arctic Basin) it has revealed some characteristic features of Arctic Ocean response to greenhouse warming. The modeling shows the importance of the salinity "signal", especially at the continental slope in the Eurasian sub-basin of the Arctic Ocean.

Thus, salinity monitoring of this region seems to be very important not only from the point of view of the natural variability study but also for detecting the greenhouse effect in the Arctic Ocean. It is worthwhile to investigate the possibilities of monitoring the salinity of the upper Arctic Basin, using acoustics, in the framework of the ACOUS program.